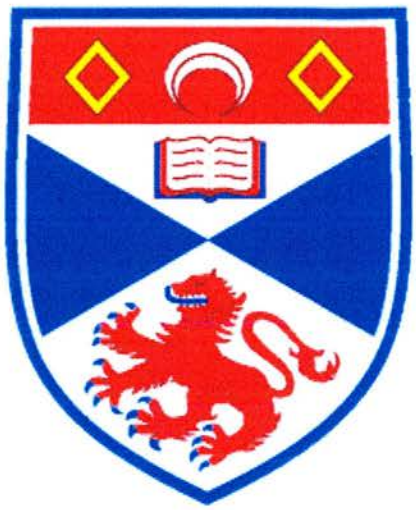

Crystalline Polymer Electrolytes

A Thesis presented for the degree of
Doctor of Philosophy
in the Faculty of Science of the University of St. Andrews
by Edward John Staunton

August 2005

School of Chemistry
St. Andrews

Declaration

I, Edward John Staunton, hereby certify that this thesis, which is approximately 24, 500 words in length, has been written by me, that it is the record of work carried out by me and that it has not been submitted in any previous application for a higher degree.

Date. 10/08/05 Signature of Candidate

I was admitted as a research student in October 2001 and as a candidate for the degree of Doctor of Philosophy in September 2002; the higher study for which this is a record was carried out in the University of St. Andrews between 2001 and 2004

Date. 10/08/05 Signature of Candidate.

Certification

I hereby certify that the candidate has fulfilled the conditions of the Resolution and Regulations appropriate for the degree of Doctor of Philosophy in the University of St. Andrews and that the candidate is qualified to submit this thesis in application for that degree.

Date. 15/8/05 Signature of Supervisor

Library Declaration

In submitting this thesis to the University of St. Andrews I understand that I am giving permission for it to be made available for use in accordance with the regulations of the University Library for the time being in Force, subject to any copyright vested in the work not being affected thereby. I also understand that the title and the abstract will be published, and that a copy of the work of the work may be made and supplied to any *bona fide* library or research worker.

Date. 10/08/05 Signature of Candidate.

For Geraldine,

The most kind, considerate and loyal person I will ever know.

Aspirat primo fortuna labori

- Virgil

Our scientific power has outrun our spiritual power. We have guided missiles and misguided men.

- Martin Luther King, Jr.

Acknowledgements

I would like to thank Professor Peter Bruce for the guidance he has offered me throughout the course of my PhD. His ideas have inspired the work that is presented in this thesis.

I would also like to thank Dr. Yuri Andreev, his tutelage in the field of powder diffraction and structure solution has been invaluable.

Also, my gratitude goes to Dr Ali Christie who imparted a great deal of knowledge to me on the theoretical and practical aspects of electrochemistry.

I would like to thank all the people I worked with throughout my time at St Andrews, Zlatka Stoeva and Isabelle Martin-Litas who introduced me to the practical aspects of my project, and more recently, Scott Lilley and Chuhong Zhang for their discussions with me on all matters relating to polymer electrolytes and otherwise.

Thanks also to Alex Slawin for single crystal x-ray diffraction characterisation, Catherine Botting for mass spec data, Sylvia Williamson for help with DSC measurements and Melanja Smith for NMR spectra.

Finally I would like to express my appreciation to all people in the PGB group who have made my time at St Andrews so enjoyable.

Contents

Abstract

The research presented in this thesis represents the first detailed investigation of the crystalline conducting media, $P(EO)_6$:$LiXF_6$, X = P, As, Sb. The nature of the ion transport mechanism occurring in these materials has been scrutinised and rationalised by a number of complementary techniques. A correlation between crystallite size and conductivity has been established, larger crystals exhibiting higher levels of conductivity.

Manipulation of these materials has shown that their conductivities can be substantially increased by addition of dopants. This has been shown by doping these 6:1 materials with lithium imide.

By adding different functional groups to the polymer chain ends the materials conductivity can be increased. There is evidence to suggest that the functional groups become conformationally disordered, increasing the conductivity.

A polymorph of these 6 to 1 complexes was identified and its structure solved *ab-initio* from its powder diffraction pattern. This provided evidence that structure was an important factor in how these materials transport ions.

The effects that monodispersed polymers have on crystalline polymer electrolytes has been investigated, their use noticeably changes the dimensions of the unit cell and also affects conductivity.

The crystal structure of $P(EO)_8$:$NaBPh_4$, has been solved by single crystal x-ray diffraction followed by refinement of the model obtained by powder diffraction data. This was the first published example of a polymer electrolyte structure solved by this method and represents the most dilute polymer electrolyte structure ever elucidated.

The first crystal structure of a divalent cation containing polymer electrolyte was elucidated, $P(EO)_4ZnCl_2$. A greater understanding of these divalent cation-containing materials paves the way for a new generation of polymer electrolyte that could exploit the interesting optical and magnetic properties multivalent cations possess.

Finally, the structures that a number of glymes and glycols make with $LiXF_6$ salts have been examined and their structures rationalised.

Chapter 1
Introduction

In 1973, Wright and co-workers[1] reported the discovery that certain alkali metal salts, when dissolved in poly(ethylene oxide), form ionically conducting polymeric materials. The term 'polymer electrolyte' can refer to a number of different materials but in the purest sense of the expression it refers to:

'*A solvent free system where the ionically conducting phase is formed by dissolving salts in a high molecular weight polar polymer matrix*'[2]

They represent a unique class of solid co-ordination compounds that support ionic conductivity in a solid yet flexible membrane. Their considerable potential for applications in a diverse range of all-solid-state devices such as rechargeable lithium ion batteries, flexible electrochromic displays and smart windows[2,3,4,5,6] was first realised by Armand in 1978.

Polyethylene oxide (PEO) has been the most intensively studied host polar polymer matrix for polymer electrolytes and it has served as a prototype for the structural features in most of the more advanced polymer electrolyte hosts.

It consists of $-O-CH_2-CH_2-$ sub-units and is obtained from the ring-opening polymerisation of ethylene oxide. PEO is a linear polymer and the regularity of the unit allows a high degree of crystallinity involving 75-80% of the polymer.

The nature of the bonding between PEO and metal ions is similar to that in the more conventional co-ordination compounds of Pedersen's oxo-crown ethers[7]. The driving force for the formation of the complex is the lowering of the free energy in the

complexed state compared to the free energy in the individual salt and polymer. From equation 1.1 below you can see that there are both enthalpic and entropic aspects to be considered.

$$\Delta G_{T,P} = \Delta H_{T,P} - T\Delta S_{T,P}$$

Equation 1.1. *Gibbs free energy equation*

For formation of a polymer electrolyte from the starting materials of salt and polymer the main enthalpic and entropic changes are:

- A positive enthalpy change due to the lattice energy of the salt
- A negative enthalpy change due to cation solvation
- A positive entropy change due to the break-up of the crystal lattice and the subsequent disordering of the ions in the system.
- A negative entropy change caused by the stiffening of the polymer chains as they co-ordinate to the cation.

A polymer that is capable of strongly coordinating a cation is necessary for polymer electrolyte formation, as the change in free energy in any system must be negative for a process to proceed. Large enthalpy terms often dominate the Gibbs energy equation (equation 1.1) so it is important that the enthalpy term due to cation solvation is large, i.e. the electron donating groups in the polymer backbone form strong bonds with the Lewis acid cation. However at the same time it is worth noting that the bonds between the Lewis bases situated in the polymer backbone and the metal cations must not be too strong as this would inhibit conductivity because the ions would no longer be able

to move through the matrix. Another polymer solvent factor that affects the formation of polymer electrolytes is the ability of the polymer chain to complex the metal ion without excessive strain. It has been found that $-(CH_2-CH_2O)_n-$ provides just the right spacing for maximum solvation whereas $-(CH_2O)_n-$ and $-(CH_2-CH_2-CH_2O)_n-$ are much weaker solvents[8]. The weaker solvents cannot wrap around the cations without excessive strain.

The species of cation being co-ordinated also has an important part to play in polymer electrolyte formation. Its interaction with the Lewis bases along the polymer backbone can be described in terms of the hard/soft acid base (HSAB) principle.
Hard acids are typified by small cations with no valence electrons that can be easily removed or polarised, e.g. ions of alkali, alkaline earth metals such as Mg^{2+}, whereas soft acids are larger cations with several valence electrons that are easily distorted or removed (eg. those with partially filled d-orbitals).

Hard bases can be described as non-polarizable ligands of high electronegativity e.g. oxygen in ethers. Soft bases are the more polarizable e.g. the thio group in thio ethers. The strongest interactions occur when a hard acid is paired with a hard base or a soft acid is paired with a soft base. The solvent can be considered as a macromolecular array of Lewis bases, thus in the case of a polyether the strongest solvation with a polyether would occur with a hard acid such as lithium ion or sodium ion. These strong interactions increase the magnitude of the negative enthalpy term in the Gibbs free energy equation and help to drive the free energy, ΔG, towards an overall negative value.

However, unlike water that has a similar donicity to polyethers, such polyethers cannot solvate anions hence the anion has an important role in whether a salt dissolves in ether solutions. Large anions with delocalised charge have little need for solvation. Hence salts of singly charged polyatomic anions such as $LiCF_3SO_3^-$ or $LiSbF_6$ will dissolve easily in polyethers as the lattice energy will be smaller with these salts compared to salts that contain small highly charged anions such as F^-. The large solvation energy of divalent and trivalent cations can induce polymer electrolyte formation even with Br^- as the counter ion but monovalent species such as K^+ require the larger anions such as I^-.

The potential applications for polymer electrolyte materials include devices such as smart windows, electrochromic displays and ion detectors. However the main application for these materials is undoubtedly rechargeable lithium ion batteries due to the numerous performance and fabrication advantages they offer.

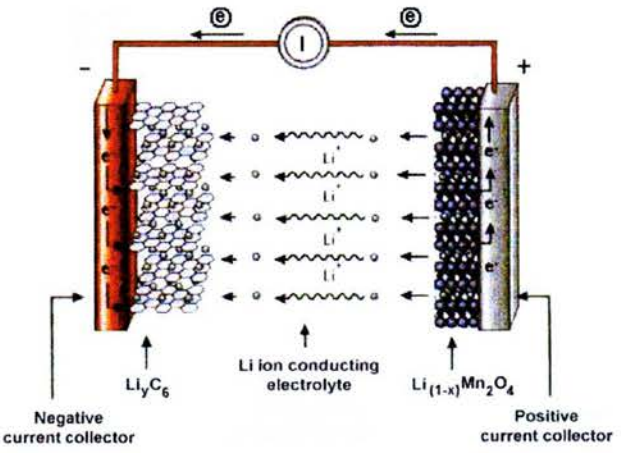

Figure 1.1. *A typical rocking chair cell*

The movement of lithium ions from the positive electrode towards the negative electrode allows electrons to flow through the external circuit thus producing a

current. By applying a current in the opposite direction you can restore the chemical potential of the cell by effectively reversing the motion of the lithium ions.

Lithium battery technology has developed to a stage where high output voltages are now available from lithium metal-free "rocking-chair", or lithium-ion, cells. The use of highly oxidising positive electrodes such as the $Li_{1-x}Mn_2O_4$ spinel, with their high voltages, requires electrolytes that are resistant to oxidation to above 4.5V. Furthermore, the chosen electrolyte must have high conductivity and be compatible with a carbon-based negative electrode down to 0V [5].

As mobile electronics and telecommunications manufacturers strive to reduce the size of the devices that rely on rechargeable batteries, this in turn drives battery manufacturers to produce higher energy density batteries. The production of an all solid-state battery using polymer electrolytes instead of the traditional liquid electrolytes offers several advantages:

1) The polymer electrolyte can be formed into thin films, improving energy density.
2) The solid polymer electrolyte acts as an electrode spacer, eliminating the need for an inert porous spacer.
3) Chemical, electrochemical and photochemical stability
4) Leakage of electrolyte is no longer a problem.
5) Safety

Also due to the mechanical stability of polymer electrolytes they have a major advantage over other solid state electrolytes as they can maintain good electrode-electrolyte contact at all times unlike more brittle solid electrolytes such as β-alumina.

Although polymer electrolytes have conductivities 100 to 1000 times lower than usual ceramic ionic conductors the polymer electrolytes can be drawn into thin films giving high power levels, leading to volumetric power densities equivalent to those of liquid electrolytes or molten salts.

The ion transport mechanism has been shown to involve polymer segmental motion in the amorphous elastomeric phase, irrespective of the coexistence of any stoichiometric crystals of polymer electrolyte. In the conventional theory of ionic conductivity in polymer electrolytes, ions move in a dynamic environment created by the polymer chain motion in the amorphous phase above the glass transition temperature, T_g. The movement of the polymer chains creates free-volume into which the lithium ions can move.

NMR studies conducted by Berthier et al[9] in the early nineteen eighties were important in the adoption of this theory of ion movement through the polymer electrolyte. In this study the decay time of the transverse nuclear magnetism correlation function, T_2, was used to assign the nuclei to crystalline or elastomeric phases. At about the same time it was noticed that the variation of ionic conductivity with temperature for a fully amorphous polymer electrolyte could be more accurately described by a deriviative of the Vogel-Tamman-Fulcher (VTF) equation rather than the simple Arrhenius function[10].

$$\sigma = A\sigma_o \exp[-B/(T-T_0)]$$

Equation 1.2 – *The VTF equation*

In this empirical equation, σ is ionic conductivity, σ_o and A are pre-exponential factors, A contains a $T^{-1/2}$ term, T is temperature and T_o is related to the glass transition temperature.

The VTF behaviour can describe the diffusion of uncharged molecules through disordered materials such as fluids or polymers. The functional form of the equation can be described on the assumption that the ions are transported via a semi random motion of short polymer segments. Typically the polymer motions that are prominent above T_g are crank-shaft torsional moments around the C-C or C-O bonds. And these become more rapid as the temperature is increased (typically this segmental motion occurs at a speed of 1 GHz at room temperature).

The crystalline polymer salt complexes were shown to exhibit inferior conductivity to the amorphous complexes, when the latter were above their glass transition temperatures.

The mindset of researchers was to maximise the amorphous nature of the polymer electrolytes and reduce T_g in order to increase the conductivity of the material. Methods employed to do this include modification of polymer architecture[5], the use of block co-polymers[11], plasticizers[12], large asymmetric anions eg. TFSI[13], nano-composites[14] and super-critical CO_2[15]. However these considerable efforts over the last 20 years have only yielded at best a polymer electrolyte with a conductivity of

$<10^{-4}$ S cm^{-1} at room temperature. To circumvent this, gel electrolytes were introduced in which a liquid electrolyte is effectively immobilised in a high molecular weight polymer matrix. However the conduction mechanism and more significantly the disadvantages of such systems are essentially the same as liquid electrolytes (loss of solvent, mechanical stability etc.).

Despite the notion that crystalline regions within polymer electrolytes are insulators as they lack the necessary chain motion to facilitate ion transport, ceramic materials are known to ionically conduct in the static crystalline state if they have the correct structural attributes. Two examples are sodium β-alumina[16] (discovered by J. T. Kummer of the Ford Motor Company) and lithium lanthanum titanates[17]. These materials by virtue of their structures, have paths through which ions can move (see figure 1.2).

β – alumina has a structure closely related to that of spinel, 50 of the 58 atoms in the unit cell being arranged exactly as in spinel. The large sodium ions are situated exclusively in loosely packed planes between dense spinel blocks together with an equal number of oxygen atoms.

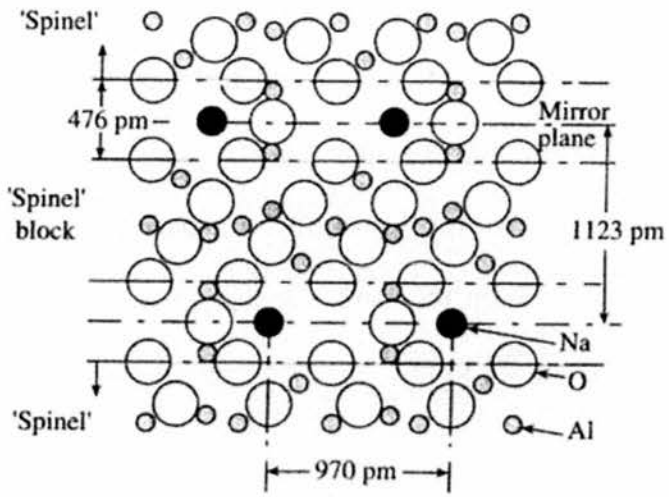

Figure 1.2. *Crystal structure of Na β – alumina. Plane parallel to the c direction*

These planes are 11.23 Å apart, separated by the spinel blocks. The close packed oxygen layers above and below the sodium planes are mirror images of each other and are bound together not only by association with sodium but also by an equal number of Al-O-Al bonds. The structure permits rapid two-dimensional diffusion of sodium within the basal plane.

The most highly lithium ion conducting bulk electrolyte known presently is a perovskite, $Li_{0.34}La_{0.51}TiO_{2.94}$ (LLT). This material exhibits conductivities of 1×10^{-3} S cm^{-1} at room temperature. The high lithium ion conductivity of LLT is considered to be due to the large concentration of A-site vacancies, and the motion of lithium by a vacancy mechanism through the wide square planar bottle neck between the A-sites[18].

This led to the idea that if a crystalline polymer electrolyte were to have a structure where there was a clear path for which the ions could move through the crystals then this material would support ionic conductivity. Essentially, conductivity would be

decoupled from polymer relaxation, as all the co-ordination sites would be already present and aligned in the crystal structure. As such the conductivity would not be limited by the time it takes for chain dynamics to create a suitable co-ordination site in the amorphous phase. This gives the possibility of a material that is cheap and easy to prepare which does not rely on the same conduction mechanism that limits the ionic conductivity to less than 10^{-4} S cm^{-1}.

Recognising from ceramic materials that structure is of utmost important when examining the potential that any material has in allowing diffusion of ions, structural information on the crystalline complexes that form with PEO and lithium salts was key to designing a crystalline conducting polymer electrolyte.

However, polymer electrolytes have poor crystal growth characteristics, as such the structure determination technique of choice, single crystal x-ray diffraction, is not in general applicable to these polymers. Also fibre diffraction gives rise to poor quality data. As a result, powder diffraction has been the main method by which the crystal structures of polymer electrolytes have been established.

The most powerful approach to solving structures *ab-initio* from powder diffraction is *Simulated Annealing* applied to flexible systems, developed by Bruce and Andreev at the University of St. Andrews. This proved capable of solving the structure of $P(EO)_6$:$LiAsF_6$ which, to date, remains the most complicated structure ever solved from its powder diffraction pattern *ab-initio*[19]. On examination of the structure of $P(EO)_6$:$LiAsF_6$ (see figure 1.3) it was seen that it had some important structural properties that would lend themselves to ion movement.

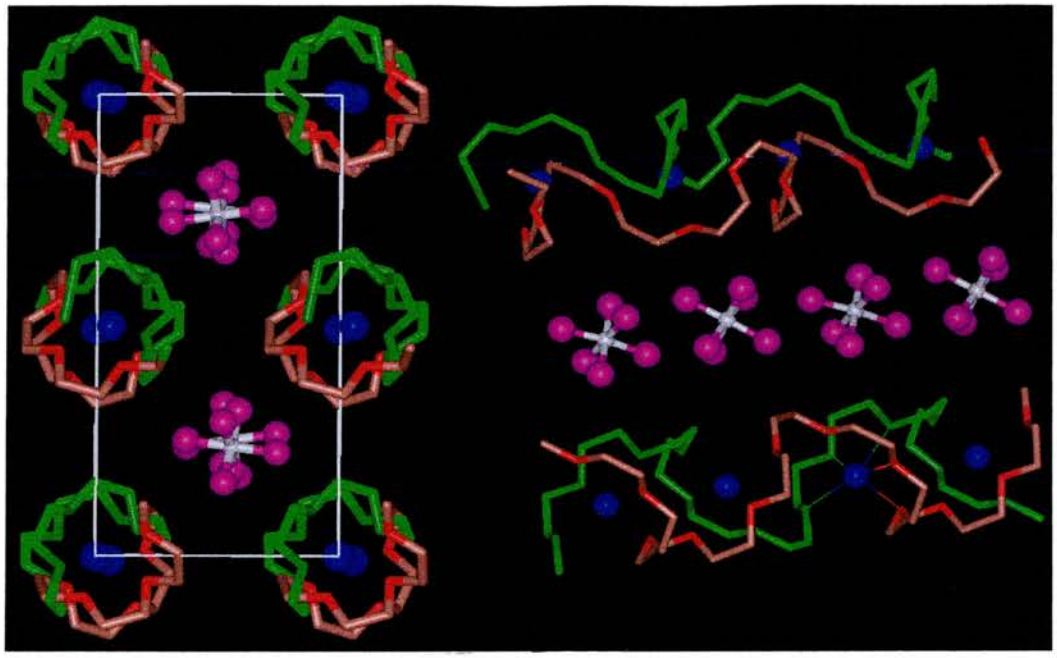

Figure 1.3. *Crystal structure of $P(EO)_6$:$LiAsF_6$..Looking down plane parallel to 'a' direction (left) and perpendicular to 'a' direction (right). Anions (pink & white) lithium ions (blue), carbons in polymer chains (green & orange), oxygens (red)*

First of all, cations were completely dissociated from their anion counterparts. Secondly, the lithium ions exist in tunnels created by two non-helical PEO chains. Within these tunnels a pathway was present that allowed the possibility of movement from co-ordination site to co-ordination by a hopping mechanism. Also, there was a free oxygen that was not involved in co-ordination of the lithium ion (which is formally 5 – coordinate), it is possible that this extra oxygen could be involved in a transitional co-ordination environment when the ions hopped from co-ordination site to co-ordination site[20].

This structure contrasts with other known polymer electrolyte structures. For example anion co-ordination occurs in the structures of P(EO):$NaCF_3SO_3$[21],

$P(EO)_3$:$LiCF_3SO_3$[22] and $P(EO)_4$:KSCN[23] the structures of which are shown in figure 1.4.

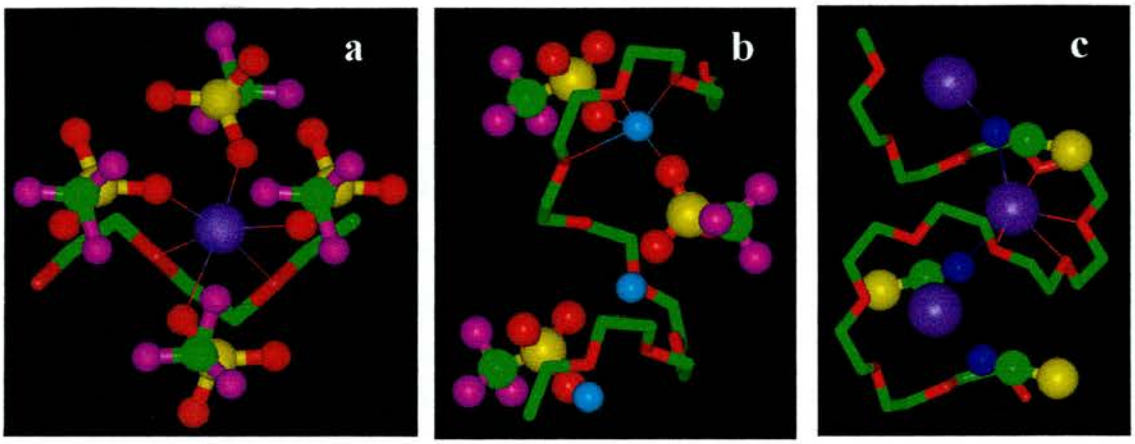

Figure 1.4a *Crystal structure of* $P(EO)_1$*:*$NaCF_3SO_3$. **b** *crystal structure of* $P(EO)_3$*:*$LiCF_3SO_3$ *and* **c** *crystal structure of* $P(EO)_4$*:KSCN.*

These structures, which are insulators, do not have any recognisable ion transport path through the material or spare oxygens to aid migration along the chains. The structure of P(EO):$NaCF_3SO_3$ (see figure1.4a) consists of stretched zig-zag chains. The 6 co-ordinate sodium ions are co-ordinated by 2 ether oxygens from the PEO chain and 4 oxygens from two different triflate anions. The structure of $P(EO)_3$:$LiCF_3SO_3$ (figure 1.4b) consists of helical chains with the cations being co-ordinated, the cation is 5-co-ordinate bonded by 3 oxygens from the PEO chain and 2 oxygen form the triflate anion. Finally the structure of $P(EO)_4$:KSCN (figure 1.4c) which also adopts a helical chain structure but with a fatter helix and the 7 co-ordinate potassium ion bonded by 5 oxygens from the PEO chain and two nitrogen atoms from the SCN^- ions

The crystalline phases of $P(EO)_6$:$LiXF_6$, X = P, As, Sb were shown to ionically conduct[24], the first example of a crystalline polymer electrolyte to exhibit this

phenomenon. Also, not only did these materials conduct but they had a higher conductivity than the comparable amorphous complex of $P(EO)_6$:$LiSbF_6$ (see figure 1.5). As the material showed no evidence of a secondary amorphous phase and the crystalline phase lacks the necessary chain dynamics to allow polymer segmental motion it was concluded that the most likely method of conductivity had to be ion hopping from co-ordination site to co-ordination site through the matrix. This was consistent with the linear Arrhenius plots that would be expected if an ion-hopping conduction mechanism was taking place.

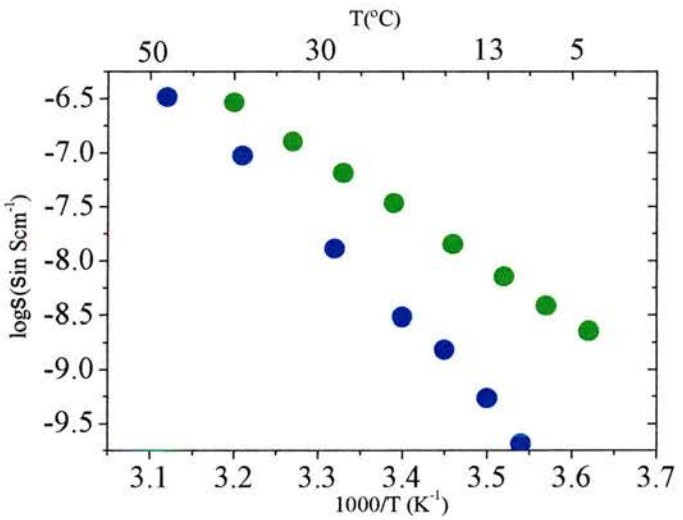

Figure 1.5. *Conductivity vs. 1000/T for crystalline $P(EO)_6LiSbF_6$ (green) and fully amorphous $P(EO)_6LiSbF_6$ (blue).*

A number of other recent papers also support the premise of conduction in the crystalline phase. Golodnitsky et al[25] provide temperature dependant NMR data that indicates that the enhancement of ionic conductivity upon stretching is likely due to structural changes that favour ion transport through the helical PEO structure. Support for this originates from the unexpected anticorrelation between polymer segmental motion and ionic conductivity enhancement.

The same group also provide evidence that stretching at the melting temperature of the PEO results in highly improved orientation of fibres and improved conductivties[26]. They used PXRD data to show that crystalline microphases of aligned helices are preferentially orientated along the stretching direction that are almost absent in the perpendicular plane. Unidirectional lengthwise force applied to the polymer electrolyte caused broadening of the IR bands assigned to hybridised vibrations of the bonds in the PEO helices. They suggest that these effects are indicative of fast ion conduction in the crystalline phase along the direction of the PEO helices.

Other ordered materials have recently been shown to support ionic conductivity [27, 28]. Plastic crystals, which are ordered materials that exhibit a degree of conformational freedom, exhibit enhanced plasticity and support higher levels of diffusivity compared to normal crystals. As such they show high ionic conductivity. Examples of these materials are succinonitrile, doped with lithium imide and substituted pyrrolidinium ion based plastic salts. With these materials, an ordered enviroment is present, however the ability of these materials to undergo dynamic changes within the structured environment allows greater ion movement. This class of ionic conductors has proved useful inspiration in designing crystalline polymer electrolytes with higher levels of conductivity

Although the crystalline phase has been shown to conduct the levels of conductivity exhibited by these materials are still too low to be commercially useful. For these materials to be utilised in lithium ion batteries a room temperature conductivity in excess of around 10^{-4} S/cm[29] and for applications in SMART windows a room temperature conductivity of around 10^{-5} S/cm[7] is necessary.

One goal of this project was to investigate the electrochemical and physical properties of these materials and determine ways in which the conductivity could be increased. By looking at the conduction mechanisms involved in ordered conducting material a number of strategies were developed for increasing the conductivity of these crystalline polymer electrolytes.

The conductivity of ceramic conductors has been shown to be increase when doped with different ionic species. Complexes of $P(EO)_6$:$LiXF_6$ have been doped isovalently (using lithium imide) resulting in large increases in conductivity.

Also the functionality of end groups of the polymer chains were modified using ethoxy ($-OC_2H_5$), benzyl ($-OCH_2C_6H_5$) and neopentoxy ($-OCH_2C(CH_3)_3$) groups in order to introduce defects and conformational disorder within the structure.

Another approach has been to examine the effect of polymer dispersity. This was done by comparing the complexes prepared using a standard polydispersed polymer of Mw 1000 and complexes prepared using monodispersed PEO of 1015 Daltons.

The final objective of the project was to identify new structures of polymer electrolytes. A technique was developed that involved growing crystals using PEO oligomers, which have better crystal growth characteristics than their polymeric counterparts, by obtaining a structural model from these oligomeric complexes and then refining the crystal structure of the polymeric complex from this structural model. This method was used successfully to solve the structures of the first 8:1

complex, $P(EO)_8$:$NaBPh_4$, the most dilute polymer electrolyte structure (in terms of salt) solved to date and also the structure of $P(EO)_4$:$ZnCl_2$, the first crystal structure of a polymer electrolyte containing a divalent cation. Also by growing single crystals of $P(EO)_3$:$LiAsF_6$, I was able to confirm the structure solved from the powder diffraction pattern of this material using 'Simulated Annealing' highlighting the power of the 'Simulated Annealing' structure determination technique developed by Andreev et al[30]

The structure of a group of glyme/glycol based complexes has also been determined, permitting investigation of the chain length on complex structure and the point at which the complexes adopt the structure of the polymers.

---

[1] Fenton, D.E., Parker, J.M., Wright, P.V., *Polymer*, **14**, 589, (1973)

[2] Gray, F. M. *Polymer Electrolytes.* RSC materials monographs. The Royal Society of Chemistry, Cambridge (1997).

[3] Scrosati, B (ed.) *Applications of Electroactive Polymers* (Chapman and Hall, London, 1993)

[4] Bruce, P.G. *Solid State Electrochemistry, (*Cambridge Univ. Press, Cambridge, 1995)

[5] Gray, F. M. *Polymer Electrolytes.* RSC materials monographs. The Royal Society of Chemistry, Cambridge (1997).

[5] Tarascon, J.M. and Armand, M. Issues and challenges facing rechargeable lithium batteries. *Nature* **414**, 359-367 (2001).

[6] Barnes, A., Despotakis, A., Wong, T. C. P., Anderson, A. P., Chambers, B. and Wright, P. V. *Smart Mater. Struct.* 7, 752-758 (1998).-

[7] Pedersen, C.J., *Journal of the American Chemical Society*, **89:26**, 7017-7036 (1967)

[8] Bruce, P.G. and Gray, F., in *Solid State Electrochemistry*, Cambridge University Press, Bruce P.G. (ed.) pg. 122 (1995)

[9] Berthier, C., Gorecki W., Minier, M., Armand M.B., Chabagno J.M., Rigaud P., *Solid State Ionics*, **11**, 91, (1983)

[10] Armand, M.B., Chabagno, J.M., Duclot M.J., in *Fast Ion Transport in Solids*, North Hollands Amsterdam, p131, 1979 and Armand, M.B., Chabagno, J.M., Duclot M.J., *2nd International Conference on Solid Electrolytes*, 1978.

[11] Sadoway, D.R., *Journal of Power Sources,* **129**(1), 1-3 (2004)

[12] Lee, H.S., Yang, X.Q., McBreen, J., Xu, Z.S., Skotheim, T.A., Okamoto, Y., *Journal of the Electrochemical Society*, **141**, (4), 886-889 (1994)

[13] Armand, M., Gorecki, W. and Andreani, R., *Second International Meeting on Polymer Electrolytes* (ed. Scrosati, B.) 91-96 (Elsevier, London)

[14] Croce, F., Appetecchi G.B., Persi, L., *Nature*, **394**, 456-458, 1998

[15] Tominaga, Y., Izumi, Y., Kwak, G.H., Asai, S., & Sumita, M., *Macromolecules*, **36**, 8766-8772 (2003)

[16] Kummer, J.T., *Prog. Solid State Chem.* **7**, 141-175 (1972)

[17] Inaguma, Y., Liquan, C., Itoh, M., Nakamura, T., Uchida, T., Ikuta, H., Wakihara M., *Solid State Commun.*, **86**, 689 (1993)

[18] Stramare, S., Thangadurai, V., Weppner W., *Chem. Mater.*, **15**, 3974-3990, (2003)

[19] MacGlashan, G. S., Andreev, Y. G. and Bruce, P. G. *Nature* **398**, 792-794 (1999).

[20] Brandell, D. Conference proceedings *Molecular Scale Interations in Ion Conducting Polymers*

(2001)

[21] Andreev, Y.G., MacGlashan, G.S. and Bruce, P.G., *Physical Reviews B*, **55**, 12011 – 12017 (1997)

[22] Lightfoot, P., Nowinski, J.L. and Bruce P.G., *Journal of the American Chemical Society*, **116**, 7469-7470, (1994)

[23] Lightfoot, P., Mehta, M.A. and Bruce, P.G., *Science*, **262**, 833-885 (1993)

[24] Gadjourova, Z., Andreev, Y. G., Tunstall, D. P. and Bruce, P. G. *Nature* **412**, 520-523 (2001).

[25] Chung, S.H., Wang, Y., Greenbaum,S.G., Golodnitsky, D. and Peled, E., *Electrochem. Solid-State Lett.*, **2**, 553-555, (1999)

[26] Golodnitsky, D., Livshits, E., Rosenberg, Yu., Lapides, I., Peled, E., *Solid State Ionics*, **147**, 265 – 273 (2002)

[27] Alarco, P.J., Abu-Lebdeh, Y., Abouimrane, A., Armand, M., *Nature Materials*, **3**, 476-480 (2004)

[28] MacFarlane, D.R., Huang J., Forsyth, M., *Nature*, **402** (1999)

[29]Tarascon, J.M. & Armand M., *Nature*, **414**, 359-367 (2001)

[30] Martin-Litas, I., Andreev, Y.G. and Bruce P.G., *Chem. Mater*, **14** (5), 2166 – 2170 (2002)

Chapter 2
Theory

2.1 Powder X-Ray Diffraction[1,2]

X-ray diffraction examines the interaction of fixed wavelength radiation with atoms in molecules. By measuring the diffraction pattern of the radiation by the sample and the variation of intensity with direction, it is possible to calculate the position and identity of atoms in a sample. It is the electrons of an atom that interact with and scatter the X-rays, so every atom has a unique scattering power. Figure 2.1.1 depicts an object and the diffraction pattern it would produce.

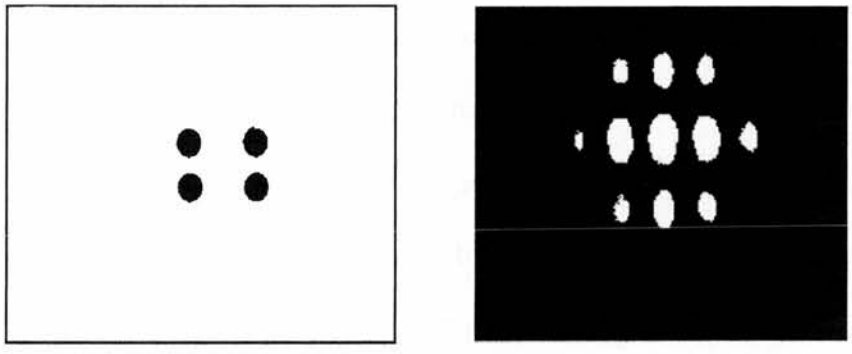

Figure 2.1.1. *An object and the diffraction pattern it would produce*

A crystal is a highly ordered repeating assembly with regularly spaced planes. When X-rays hit the sample, they are diffracted by the atom's electrons according to Bragg's Law. This allows us to predict when a given plane will diffract with constructive interference and this gives an observable x-ray intensity (see figure 2.1.2).

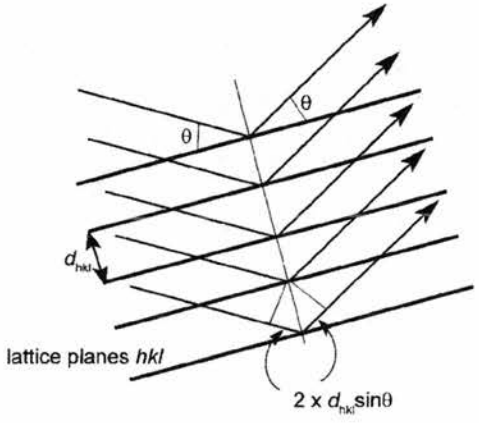

$$n\lambda = 2d\sin\theta$$

Figure 2.1.2. *Bragg's Law and the reflection of x-rays from planes of electrons.*

Where n is an integer, λ is the wavelength of the x-rays produced by the source, d is the interplanar spacing and θ is the angle of diffraction.

A single crystal gives a diffraction pattern with discrete diffracted spots, each in a definitive direction relative to the orientation of the crystal and the incident beam, according to the Bragg equation. A stationary single crystal gives very few reflections. In order to generate the complete diffraction pattern it is necessary to rotate the crystal in the x-ray beam in three dimensions. In the case of a powder where you have very many microcrystalline crystals each of these crystals gives off its own diffraction pattern that are superimposed. As the sample is rotated, any particular reflection will be generated by each of the individual crystals at different times as the Bragg equation is satisfied, assuming equally sized crystals the Bragg angle and the intensity will be the same in each case. However the direction of the diffracted beam will vary, while always being inclined at 2θ to the straight through direction.

On a flat detector perpendicular to the incident beam and on the opposite side of the sample, this set of corresponding reflections from the multiple crystals appear as spots of the same intensity on a circle assuming no preferential orientation has occurred. With an increasing number of crystals more such spots appear, all lying on the same circle.

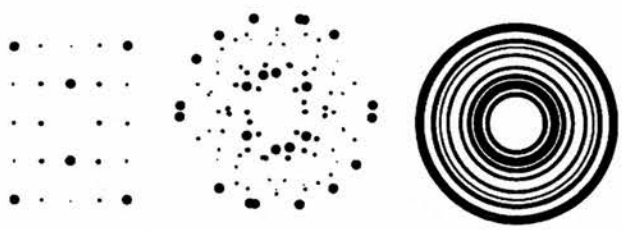

Figure 2.1.3. Diffraction from a single crystal (left) from an aggregate of a small number of crystals (centre) and a powder (right)

Consider Figure 2.1.3. The pattern on the left represents the reflection produced by a single crystal. The diffraction pattern in the middle represents the reflection received when four such crystals are superimposed in random relative orientations. The pattern on the right is what is produced when carrying out a powder x-ray diffraction, ie. the pattern for a very large number of crystals. Each spot on the left diagram has generated a circle on the right one.

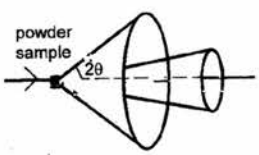

Figure 2.1.4.
Cones of x-rays reflected from a powder sample

The powder diffraction pattern is often measured by an electronic detector that is driven in a circle around the sample under computer control (a powder diffractometer). Intensity is measured as a function of angle, and for each reflection a Bragg angle and intensity is obtained. The effect of using a microcrystalline powder instead of a single crystal is to compress the full three-dimensional diffraction pattern into a one-dimensional pattern (the only geometric variable being θ)

2.1.1 Solving Structures using PXRD Data[3,4]

For relatively simple structures, giving few reflections, there may be little overlap of these in the powder diffraction pattern. In such cases it is easy to assign individual indices and intensities and carry out structure determination as with single crystals. As the structures become more complicated elucidation of the powder x-ray diffraction becomes more complex. Overlapping peaks results in a loss of access to the individual intensities that are crucial to the structure solution. Modern high resolution

instruments have improved greatly the separation of the peaks. However, significant numbers of reflections cannot be resolved by any improvement in the instrumentation.

There are a number of ways powder x-ray diffraction data can be treated in order to elucidate the crystal structure of the material in question. Intensities of individual reflections or groups of reflections can be extracted using equipartitioning or permutation estimates for grouped reflections and then treating these as a single crystal data set which then have direct methods and Patterson methods applied to the data sets. Alternatively, a structural model can be postulated independently from the powder diffraction data, with the suitability of these models assessed by comparison of the PXRD pattern calculated for this model and the actual powder diffraction data of the material. This comparison is often quantified by an agreement factor (R, R_{wp} or χ^2) which considers the whole digitised intensity profile (not just the integrated intensities of individual diffraction maxima) and therefore implicitly takes care of the overlap peaks. This method avoids the problematic step of extracting intensities of overlapping peaks. This method is utilised in the Monte Carlo and simulated annealing methods. The simulated annealing (SA) approach has been used recently with great effect in solving the structures of crystalline polymer electrolytes[5]. A brief description of Monte-Carlo and simulated annealing methods of structural elucidation is given below.

A group of atoms known as the structural fragment (or molecule) is given a random position and orientation within the unit cell to give an initial structure x_i. The structural fragment is then moved randomly within the unit cell and also changes in the internal geometry of the molecule (based on user defined constraints) are used to

generate a trial structure x_{trial}. The trial structure is then compared to the initial structure and it is then accepted or rejected on the basis of the difference Z, between the value of R_{wp} (the weighted profile R factor) for the trial structure and the value of R_{wp} for the initial structure ie.

$$Z = R_{wp}(x_{trial}) - R_{wp}(x_i) \qquad (2.1.1.1)$$

If $Z \leq 0$ or $Z > 0$ with a probability of $e^{-z/s}$ then the trial structure is accepted as the new structure ie.

$$x_{i+1} = x_{trial} \qquad (2.1.1.2)$$

If $Z > 0$ with a probability of $1\text{-}e^{-z/s}$ the trial structure is rejected and the initial structure x_i is adopted ie.

$$x_{i+1} = x_I \qquad (2.1.1.3)$$

S represents an appropriate scaling of Z, and operates in a similar manner to kT in conventional Monte-Carlo simulation techniques. The maximum displacement of the structural fragment and the value of S are chosen so that the optimum number of trial structures are accepted (around 40%). It may however be desirable to change the value of S to explore a larger range of structural space. The above processes are repeated to generate a Markov chain of structures (x_{i+2}, x_{i+3}, x_{i+4}, ...,x_N). This process of accepting and rejecting trial structures according to z values is repeated until the structural fragment has explored an extensive range of structural space. The structure corresponding to the lowest R_{wp} is considered as the starting structural model for the Reitveld refinement.

The simulated annealing technique also involves the Monte-Carlo algorithm to generate a series of structures. The fundamental difference between SA and Monte-Carlo is how the S parameter is handled. In the SA approach the S value is

systematically decreased under the control of an 'annealing schedule'. The initial value of S is chosen so that virtually all trial structures are accepted and as S is decreased, the number of trial structures that are accepted decreases until the best structure solution is obtained.

2.1.2 Extracting Crystallite Sizes and Strains from PXRD Data[6]

The basis of size-strain analysis for the case in which assumed analytical functions are fitted to clusters of diffraction lines has been outlined in Keijser et al (1983). The procedure is based on extraction and analysis of Gaussian, β_G, and Lorentzian, β_L, components of the integral breadth of a single Bragg peak corrected for the instrumental broadening using a reference profile. First of all, the values of Γ (full width at half maximum) and β (integral breadth) calculated as the width of a rectangle that has the same area and height a the line profile (or more simply put, the area of the peak divided by the height) for both the peak for analysis and a reference sample peak (used to correct for instrumental broadening) were measured. From these values the auxiliary parameters β_L and β_G (subscripts L and G denote Lorentzian and Gaussian components of the Voigt profile-shape function) were calculated using equation 2.1.2.1 and 2.1.2.2.

$$\frac{\beta_L}{\beta} = 2.0207 - 0.4803\left(\frac{\Gamma}{\beta}\right) - 1.7756\left(\frac{\Gamma}{\beta}\right)^2 \qquad (2.1.2.1)$$

$$\frac{\beta_G}{\beta} = 0.6420 + 1.4187\left(\frac{\Gamma}{\beta} - \frac{2}{\pi}\right)^{1/2} - 2.2043\left(\frac{\Gamma}{\beta}\right) + 1.8706\left(\frac{\Gamma}{\beta}\right)^2 \qquad (2.1.2.2)$$

β_L and β_G are then corrected for instrumental broadening using equation 2.1.2.3 and 2.1.2.4.

$$\beta_L'' = \beta_L - \beta_L' \qquad (2.1.2.3)$$

$$\{\beta_G''\}^2 = \{\beta_G\}^2 - \{\beta_G'\}^2 \qquad (2.1.2.4)$$

Where β_L' is the Lorentzian component of the integral breadth of the reference profile and β_G' is the Gaussian component of the integral breadth of the reference profile. The corrected Lorentzian and Gaussian components of the integral breadth, β_L'' and β_G'', are then used to calculate the volume-weighted crystallite size and weighted average strain, ε using equations 2.1.2.5 and 2.1.2.6.

$$\langle D \rangle_v = \lambda/(\beta_L''\cos\theta) \qquad (2.1.2.5)$$

$$\varepsilon = \tfrac{1}{4}\beta_G''\cot\theta \qquad (2.1.2.6)$$

2.2. Measuring Electrical Properties of Polymer Electrolytes by AC Impedance[7]

AC impedance techniques are the most widely used methods in determination of electrical conductivity of polymer electrolytes due to the simple cells that are used which use inert blocking electrodes to determine bulk electrolyte properties. However the theory and the equipment required for this technique are more complicated.

From AC impedance data it is possible to gain information about long-range migration of ions and also polarisation phenomena occurring in the cell.

In an AC experiment a sinusoidal voltage is applied across a cell and the sinusoidal current passing through the cell as a result of this perturbation is measured. Two parameters are required to relate current to voltage which is the crucial difference from DC perturbations as this only requires one parameter ie. resistance. One represents the opposition to the flow of charge and is equal to the ratio of the voltage and current maxima, V_{max}/I_{max}, and is analogous to the resistance in DC measurements. The other parameter, θ, is the phase difference between voltage and current see figure (2.2.1).

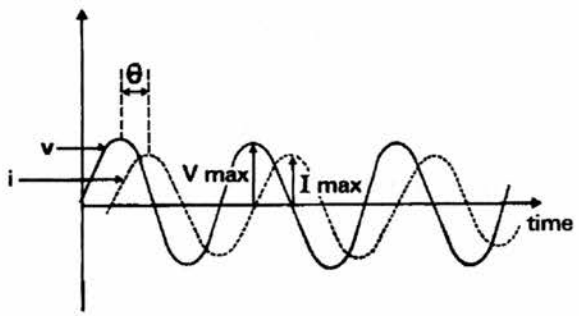

Figure 2.2.1. *Representation of sinusoidal voltage and current, at a given frequency associated with the cell.*

The combination of these two parameters represents the impedance, Z, of the cell. Generally for an electrochemical cell both the magnitude of the impedance $|Z| = V_{max}/I_{max}$ and its phase angle θ are functions of the applied frequency.

The most commonly used a.c. method involves measuring the impedance as a function of the frequency of the applied signal over a wide frequency range, typically 1mHz to 1MHz. Because the impedance is frequency dependant we can extract information about the electrical properties of the cell.

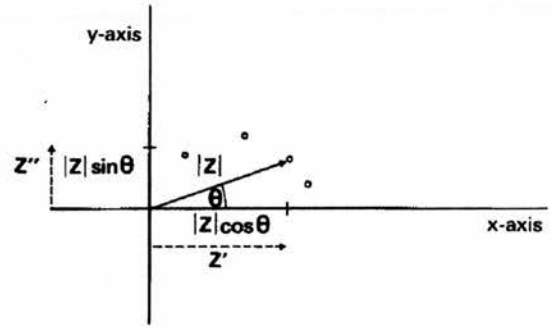

Figure 2.2.2. *A typical phasor diagram*

Cell impedance is a vector quantity and can be represented by a point on a phasor diagram (see figure 2.2.2.). The impedance for each frequency measured is represented by a separate point on the vector diagram.

The distance from the origin to the point represents the magnitude of the impedance and the angle made with the x-axis represents the phase difference between voltage and current. The impedance vector may also be represented by its x and y components, $|Z|\cos\theta$ and $|Z|\sin\theta$. The representation of an impedance on a vector diagram is analogous to the representation of a complex number in the complex plane. Impedance is often represented by a complex number because of this so is often referred to as the complex impedance, represented by the symbol Z^*.

Impedance can therefore be represented in three ways;

1) In terms of its phase, θ, and its magnitude, $|Z|$;

2) In terms of its x and y components, $|Z|\cos\theta$ and $|Z|\sin\theta$.

3) As real and imaginary parts of a complex number, $Z^* = Z' - jZ''$, where j represents the complex number operator $\sqrt{-1}$.

The third way is often the most useful as the laws of complex algebra can be applied to calculate the impedance of circuits knowing the impedance of individual components.

A typical ac experiment consists of determining the complex impedance of the cell as a function of the signal frequency and presenting the results in the form of a complex impedance plot.

2.2.1 AC Response of Cells with Blocking Electrodes Containing Polymer Electrolytes

In a cell with blocking electrodes the mobile species in the electrolyte do not participate in any electrode reactions and 'type 1' polymer electrolytes have only one mobile ionic species. Consider the case of this type of polymer electrolyte sandwiched between two platinum electrodes with a lithium ion conducting polymer electrolyte. Assuming an idealised lithium ion conducting polymer and Platinum electrodes, an a.c. voltage is applied to the cell and the frequency is varied. (The equivalent circuit to the cell is given below in figure 2.2.1.1.)

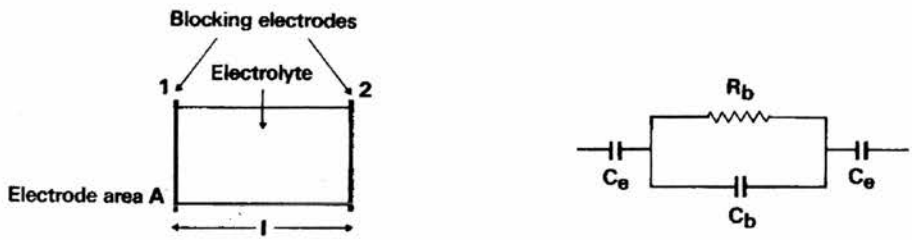

Figure 2.2.1.1 A blocking electrode cell and the equivalent circuit

The electrodes become alternately positively and negatively charged and the alternating field across the electrolyte causes the lithium ion to migrate back and forward in phase with the voltage. The migration of the ion is represented by the resistor R_b. At the same time the polymer chains become polarised in the alternating field, just as they would if the polymer film had no mobile charges present. This dielectric polarisation is represented by a capacitor C_b. As the lithium ions move in the alternating field they are alternatively accumulated and then depleted at each electrode. On each half cycle, ionic charge builds up within the electrolyte near the electrodes, these charges being balanced by an equal and opposite electronic charge on the electrodes. Each electrode is similar to a parallel plate capacitor and can be represented by C_e, this representation is a reasonable approximation when the ion concentration in the electrolyte is high, ie >1 M

Bulk polarisation and ionic migration are physically in parallel hence there representative components R_b and C_b are connected in parallel and both are in series with the electrode capacitance, C_e. Since both electrodes are identical they are combined into one overall capacitance term, $1/C_e = 1/C_{e1} + 1/C_{e2}$. C_b is related to the dielectric constant of the polymer,

$$C_b = \frac{\varepsilon_r \varepsilon_o A}{L} \qquad (2.2.1.1)$$

Where ε_r is the relative permittivity, or dielectric constant of the polymer and ε_0 is the vacuum permittivity, A is the cross sectional surface area and L is the distance between the two plates. R_b varies with the temperature and the particular polymer and geometric parameters used in the experiment.

Since C_e is in series with a parallel combination of R_b and C_b the total impedance can be calculated by adding the impedance of the capacitor C_e to the impedance of the parallel RC combination. To do this it is necessary to know the relationship between resistance, capacitance and their respective impedances.

In a resistor the phase difference between the voltage and the current is zero. Hence the magnitude of the impedance equals the resistance ($|Z| = R$).

With a capacitor the phase difference between applied voltage and the current is -90^o out of phase ie. $\theta = -\pi/2$. Hence $|Z| = 1/\omega C$, as this occurs along the imaginary axis and by convention capacitances are treated as negative values, $|Z| = -j/\omega C$.

In a series circuit impedances are directly additive. However, in a parallel circuit impedances are not directly additive but their reciprocals are. The reciprocal of impedance is termed admittance, Y.

Hence,

$$Y^* = Y^*_1 + Y^*_2 + Y^*_3 + \ldots\ldots \quad (2.2.1.2)$$

$$Y^* = Y' + jY'' = \frac{1}{(Z'-jZ'')} \quad (2.2.1.3)$$

Therefore,

$$Y' = \frac{Z'}{(Z'^2 + Z''^2)} \quad (2.2.1.4)$$

$$Y'' = \frac{Z''}{(Z'^2 + Z''^2)} \quad (2.2.1.5)$$

Thus total admittance is given by,

$$Y_{total} = 1/R + j\omega C \quad (2.2.1.6)$$

Hence total impedance,

$$Z^*total = \frac{1}{(1/R) + j\omega C} \quad (2.2.1.7)$$

$$= R\left[\frac{1}{1+(\omega CR)^2}\right] - jR\left[\frac{(\omega RC)}{1+(\omega RC)^2}\right] \quad (2.2.1.8)$$

Now going back to the original circuit depicted in figure 2.2.1.1, it can be shown that:

$$Z^*_{total} = \left[Rb\ \frac{1}{(1+(\omega RbCb)^2)}\right] - j\left(Rb\left[\frac{\omega RbCb}{1+(\omega RbCb)^2}\right] + \frac{1}{\omega Ce}\right) \quad (2.2.1.9)$$

The complex impedance plot given by equation 2.2.1.9 is shown below in figure 2.2.1.2.

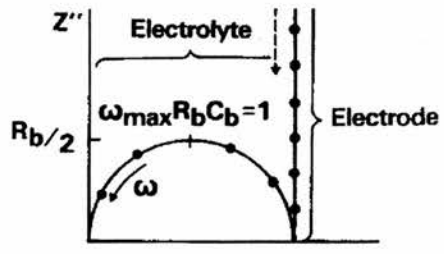

Figure 2.2.1.2 *Simulated complex impedance plot for circuit in fig. 2.2.1.1*

The magnitude of all fundamental electrical properties of the cell can be obtained from the complete impedance data, in particular the dc resistance R_b. From the dc resistance value, R, it is possible to calculate the specific conductivity, σ, of the material being measured using equation 2.13.

$$\sigma = \frac{1}{R}\left(\frac{L}{A}\right) \qquad (2.2.1.10)$$

S (for σ) ; S cm^{-1} (for σ) ; cm^{-1} (for $\frac{L}{A}$)

Where L is the thickness of the electrolyte film, and A is the contact area between the sample and one of the symmetrical electrodes.

The reliability of any conductivity measurement is dependent not only on the polymer under study but on the complete measuring cell – the two measuring electrodes as well as the test material sandwiched between them. The characteristics of the electrodes themselves rarely affect the measurements, but the electrode/electrolyte interfaces often do, for several reasons:

- Processes occurring at the interface

  The processes taking place at the electrodes involving ions can impede the rapid flow of current and affect the measurement. The main processes are;

  1) Diffusion of ions to the surface of the electrode

  2) Adsorption onto the surface

  3) Diffusion across surface to suitable site

  4) Charge transfer.

- Blocking Electrodes

  In the case of 'blocking' electrodes the conducting ions cannot cross the electrode/electrolyte interface. In all electrode systems a double layer capacitance is formed at the interface before any reaction can take place. With blocking electrodes this double layer is formed with no subsequent electrochemical transformation taking place affecting the measurement.

- There may be incomplete electrode contact

  In the typical case of an electrical contact between two solids there is rarely 100% contact since both surfaces will not be perfectly flat. Polishing can reduce the problem of irregularities on the electrode surface, and also reduce the possibility of it being coated with a resistive layer of an impurity. Heating the polymer when in contact with the electrodes can also facilitate greater electrical contact by increasing the likelihood of plastic deformation of the polymer around any imperfections on the electrode surface. Applying pressure to the electrodes has also been used successfully to increase electrode contact.

2.3. Differential Scanning Calorimetry (DSC)

*D*SC is a technique in which the difference in heat flow to a sample and a reference is monitored as a function of temperature or time while the sample and reference are subjected to a controlled temperature program. It has the ability to identify thermal

events in the sample such as melting, sublimation and with sensitive instruments glass transitions.

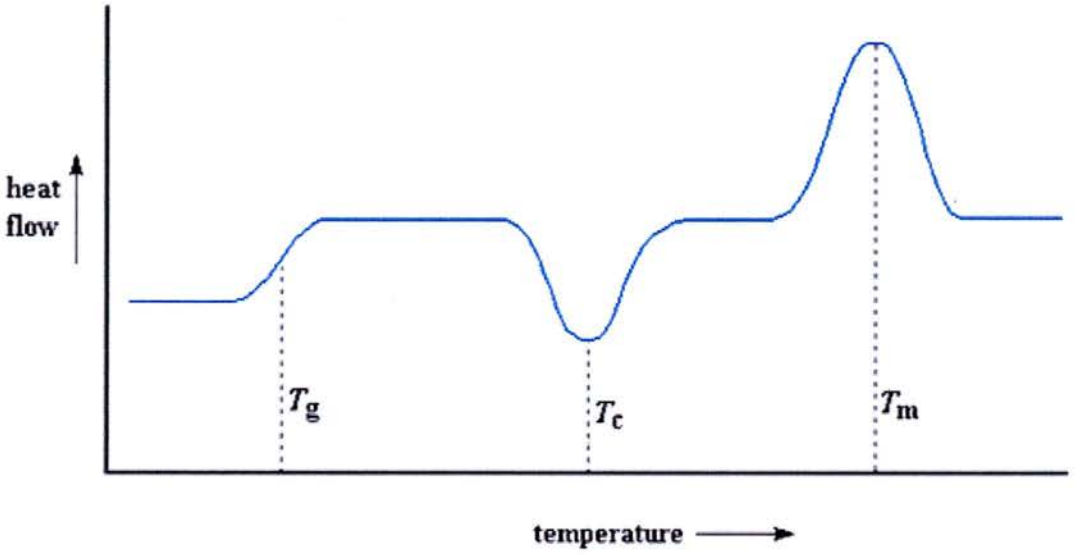

Figure 2.3.1. *Illustration of thermal events witnessed by DSC. T_g, Glass Transition, T_c, Crystallisation, T_m, melting.*

---

[1] Clegg, W., *Crystal Structure Determination*, Oxford Chemistry Primers, 1998

[2] Alberty R.A. and Silbey R.A. *Physical Chemsitry – 2nd Edition*, Wiley Interscience.

[3] Andreev, Y.G., Lightfoot, P. and Bruce, P.G. A general Monte Carlo approach to structure solution from powder-diffraction data: Application to poly(ethylene oxide)$_3$:LiN(SO_2CF_3)$_2$ *J. Appl. Crystallogr.* **30**: 294-305 Part 3 (1997).

[4] Harris K.D.M, *Chem.Mater.*, 1996, **8**, 2554-2576

[5] MacGlashan, G. S., Andreev, Y. G. and Bruce, P. G. *Nature* **398**, 792-794 (1999).

[6] Young, R.A. (Ed.), *The Rietveld Method*, Ch. 8, pg. 147, Oxford University Press

[7] Bruce P.G., *Polymer Electrolyte Reviews - 1*, Ch. 8, Elsevier Applied Science

Chapter 3
Experimental

3.1 Preparation of Polymer Electrolyte Materials

3.1.1 $P(EO)_6LiXF_6$ (X = P, As, Sb) Polymer Electrolyte Preparation.

All polymer electrolyte materials were prepared in a Mbraun argon filled glove box, due to the air/moisture sensitive nature of the final product and the starting materials. Masses of $LiXF_6$ ($LiPF_6$ from Stella SC hemita, 99.99%, used as received, $LiAsF_6$ from ABCR, 99.8%, dried at 40°C under dynamic vacuum for 24 hours and $LiSbF_6$ from Interchim, 99.8%, dried at 40°C under dynamic vacuum for 24 hours) and di-methoxy endcapped poly(ethylene oxide) (dried at close to the polymer's melting point under dynamic vacuum for 3 days) appropriate for the formation of a 6:1 complex (ether oxygen to salt ratio) were weighed out. The salts and polymer were dissolved separately in dry acetonitrile (Aldrich, 99.99%, dried over 4Å molecular sieves) and following complete dissolution mixed together. The acetonitrile was then permitted to evaporate slowly. The resulting white powders were dried overnight under dynamic vacuum at room temperature. IR spectroscopy (FTIR spectrometer, Nicolet 860) confirmed the absence of H_2O and CH_3CN from the powders, as did ^1H NMR using a Bruker 'Varian' 500MHz spectrometer. The material was then analysed by powder x-ray diffraction to check that the phase was comparable with previously obtained patterns.

3.1.2 Preparation of $P(EO)_6LiAsF_6$ Polymer Electrolytes Doped with Lithium Imide.

The procedure detailed above in section 3.1.1 was followed with the exception that an appropriate mol% of $LiAsF_6$ salt was replaced by $LiN(CF_3SO_3)_2$ salt (3M, 99.98%). The dopant lithium imide was dissolved separately in acetonitrile and added to the solution of $LiAsF_6$ prior to addition to the polymer solution.

3.1.3 Preparation of β – $P(EO)_6LiAsF_6$

The synthetic steps carried out in 3.1.1 were repeated in the preparation of β – $P(EO)_6LiAsF_6$. After the initial $P(EO)_6$:$LiAsF_6$ phase was synthesised the complex was heated to 120°C for 40 minutes in a sealed 0.7mm glass capillary then cooled slowly. PXRD was carried out on the resultant complex indicating a new crystalline phase had formed

β – $P(EO)_6LiAsF_6$ prepared for conductivity measurements was prepared by heating the initial $P(EO)_6$:$LiAsF_6$ phase to 115°C for 30 minutes under dynamic vacuum then cooled slowly to room temperature. The product's morphology was then checked using PXRD.

The deuterated sample of β – $P(EO)_6LiAsF_6$ for neutron diffraction was prepared using di-methoxy endcapped deuterated PEO of Mw 1350 (Polymer Source, 98%). After the initial $P(EO)_6$:$LiAsF_6$ complex was prepared by solvent casting the beta

phase was synthesized by heating the complex at 110°C for 30 minutes under dynamic vacuum then cooling slowly to room temperature.

3.1.4 Preparation of Polymer Electrolyte Materials using Monodispersed PEO 1015.

The synthetic steps used in 3.1.1 were also applied here. However the polymer used was obtained by state of the art preparative scale reverse phase HPLC, (Polypure, >97% molecularly pure). The monodisperse nature of this material was confirmed using Matrix Assisted Laser Desorption Ionisation Mass Spectroscopy, MALDI-MS, see figure 7.1.1.

3.1.5 Preparation of Polymer Electrolyte $P(EO)_8$:$NaBPh_4$

Poly(ethylene oxide)$_8$:$NaBPh_4$ was prepared as a film suitable for powder X-ray diffraction by dissolving separately poly(ethylene oxide) of average molar mass 100,000 (Aldrich, >98%) and sodium tetraphenyl borate in acetonitrile at room temperature. Appropriate amounts of polymer and salt were used corresponding to a 8:1 ratio of ether oxygens to salt. The solutions were then mixed together and then cast into Teflon moulds. The solvent was allowed to evaporate until polymer electrolyte film formed.

3.1.6 Preparation of Polymer Electrolyte $P(EO)_4$:$ZnCl_2$

Poly(ethylene oxide)$_4$:$ZnCl_2$ was prepared for powder X-ray diffraction by dissolving separately poly(ethylene oxide) of average molar mass 2,000 (Aldrich, >98%) and zinc chloride in methanol at room temperature. Appropriate amounts of polymer and salt were used corresponding to a 4:1 ratio of ether oxygens to salt. The solutions were then mixed together and then cast into Teflon moulds. The solvent was allowed to evaporate until polymer electrolyte film formed. After dissolution, the solutions were cast into Teflon moulds and the solvent allowed to evaporate until polymer electrolyte films formed.

3.2 Preparation of End Group Modified Polymers.

Endgroups were added to PEO chains terminated with hydroxyl groups using a modified Williamson ether synthesis. See reaction scheme 3.2.1 below. The basis of the method is irreversible reaction of an alkoxide ion and an alkyl halide.

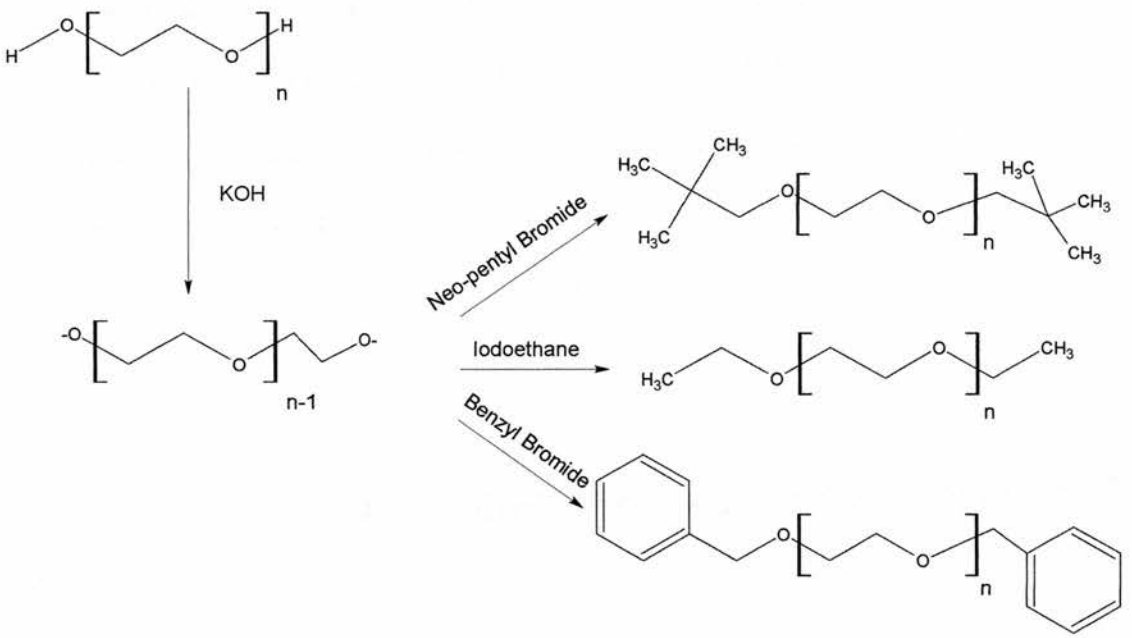

Reaction Scheme 3.2.1

3.2.1 Preparation of Di-ethoxy Endcapped PEO Mw c.1k

64g of KOH (Fischer Scientific, pellets, lab reagent grade) was powdered and added to 80ml of chlorobenzene. The resulting slurry was stirred overnight. To this a solution of 25g of Iodoethane (Aldrich, 99.9%) in 150 ml of chlorobenzene (Acros Organics, 99+%) was made up and cooled to 0°C on in ice bath and purged with N_2. 10g of OH terminated polyethylene glycol Mw = 1000 (Fluka, 98%) was dissolved in 80ml of chlorobenzene and added drop wise from a burette to the iodoethane containing solution over 15 minutes. The PEO solution was added slowly to an 8 fold excess of iodoethane to avoid the β-hydrogen elimination side reaction that could occur. The resulting slurry was then filtered through a glass sinter and the filtrate collected and rotary evaporated at 40°C to yield a crude product. Unreacted di-hydroxy terminated PEO and mono-ethylated PEO present in the mixture were separated by recrystallisation. The crude product was recrystallised twice by dissolution in warm toluene (Riedel de Haën, purum) and precipitated by adding iso-octane (Riedel de Haën, 99%) to yield di-ethoxy terminated PEO (yield = 40%). ^1H NMR assessed the extent of endcapping, no peak associated with the hydroxyl group was present in the spectra, MALDI mass spectroscopy also showed no sign of a peak associated with either di-hydroxy PEO or mono ethylated PEO. The resulting polymer was then dried at 35°C under dynamic vacuum.

3.2.2 Preparation of Di-Benzyl Terminated PEO Mw c.1k

23.3g of KOH (Fischer Scientific, pellets, lab reagent grade) was powdered, added to 48ml of chlorobenzene and stirred overnight. To this mixture 13.7g of OH terminated

polyethylene glycol Mw = 1000 (Fluka, 98%) was added. The mixture was cooled to 0°C on an ice bath and purged for 30 minutes with N_2. 14.0g of Benzyl Bromide (Aldrich 99.9%) was added dropwise to this mixture over a 15 minute period. The resulting product was then filtered through a glass sinter to yield a yellow/brown solution. The volume was reduced by rotary evaporation. The resulting product was then recrystallised by dissolving the crude product in hot toluene and precipitating using iso-octane (Riedel de Haën, 99%). From MALDI-MS peaks associated with unreacted -OH terminated starting product were seen to be present. The product was then purified by phase separation by dissolving in DCM (Bamford Laboratories, 98%) and washing with 5 portions of 8ml 10% sodium carbonate (BDH, 99.5%) solution followed by 5 portions of 5ml of distilled water. The resulting dried product showed no evidence of –OH terminated material by MALDI-MS and ^{1}H NMR. The resulting polymer was then dried at room temperature under dynamic vacuum for 48 hours. (Yield = 20%)

3.2.2 Preparation of Di-Neopentoxy Terminated PEO Mw c.1k

23.3g of KOH (Fischer Scientific, pellets, lab reagent grade) was powdered, added to 48ml of chlorobenzene and stirred overnight. To this mixture 13.7g of OH terminated polyethylene glycol Mw = 1000 (Fluka, 98%) was added. The mixture was cooled to 0°C on an ice bath and purged for 30 minutes with N_2. 14.0g of 1-Bromo 2,2 dimethyl pentane (neo-pentyl bromide) (Aldrich 99.8%) was added dropwise to this mixture over a 15 minute period. The resulting product was then filtered through a glass sinter to yield a yellow solution. The volume was reduced by rotary evaporation at 40°C. From MALDI-MS peaks associated with unreacted -OH terminated starting product

were seen to be present. The product was then purified by phase separation by dissolving it in DCM (Bamford Laboratories, 98%) and washing with 5 portions of 8ml 10% sodium carbonate (BDH, 99.5%) solution followed by 5 portions of 5ml of water. The resulting dried product showed no evidence of –OH terminated material by MALDI-MS and ^{1}H NMR. The resulting polymer was then dried at room temperature under dynamic vacuum for 48 hours (Yield = 15%).

3.3 Preparation of Single Crystals

3.3.1 Preparation of Single Crystals of Glymes and $LiAsF_6$

Crystals of $LiAsF_6$ and triglyme (triethyleneglycol dimethyl ether, Aldrich, 99.8%), tetraglyme (tetraethyleneglycol dimethyl ether, Aldrich, 99%), and hexaethylene glycol (Fluka, 98%) were grown by dissolving appropriate quantities of glyme/glycol and salt to obtain a 6 to 1 ratio of ether oxygens to salt in acetonitrile. The solvent was then allowed to evaporate slowly yielding crystals large enough for analysis by single crystal x-ray diffraction.

3.3.2 Preparation of Single Crystals of PEO_8:$NaBPh_4$

Single crystals of the 8:1 complex formed between 500 molar mass methoxy-end-capped ethylene oxide and sodium tetraphenyl borate were grown by first dissolving appropriate amounts of $NaBPh_4$ (Fluka, $\geq$ 98%) and the oligomer (Aldrich, >98%) in

5 ml of anhydrous methanol (Aldrich, 99.8%), to affect an ether oxygen to salt ratio of 8:1. Once the salt and polymer had completely dissolved, the methanol was removed by slow evaporation, yielding a clear solution from which crystals were seen to precipitate.

3.3.3 Preparation of Single Crystals of PEO_4:$ZnCl_2$

Single crystals of the 4:1 complex formed between 500 molar mass methoxy-end-capped ethylene oxide and $ZnCl_2$ were grown by first dissolving appropriate amounts of $ZnCl_2$ (Fluka, $\geq$ 98%) and the oligomer (Aldrich, >98%) in 5 ml of anhydrous methanol (Aldrich, 99.8%), to obtain an ether oxygen to salt ratio of 4:1. Once the salt and polymer had completely dissolved, the methanol was removed by slow evaporation, yielding a clear solution from which crystals were seen to precipitate.

3.3.4 Preparation of Single Crystals of PEO_3:$LiAsF_6$

Single crystals of the 3:1 complex formed between 1000 molar mass methoxy-end-capped ethylene oxide and $LiAsF_6$ were grown by first dissolving appropriate amounts of $LiAsF_6$ (ABCR, $\geq$ 99.8%) and the polymer (Fluka, >98%) in 5 ml of acetonitrile (Aldrich, 99.8%), to obtain an ether oxygen to salt ratio of 3:1. Once the salt and polymer had completely dissolved, the solvent was removed by slow evaporation, yielding a clear solution from which crystals were seen to precipitate.

3.4 Details of Characterisation Procedures

3.4.1 Powder X-ray Diffraction (PXRD)

Powder X-ray diffraction was carried out using a Stoe STADI/P powder diffractometer with $CuK_{\alpha 1}$ radiation operating in transmission mode and employing a small angle position sensitive detector (PSD). Data were collected with a step width of between 0.02° and 0.5° in 2θ. To avoid contact with air the polymer electrolyte samples were sealed in Lindemann (glass) capillaries or between mylar films, depending on whether the samples were in the form of a powder or a film.

3.4.2 AC Impedance

Conductivity data were obtained using AC impedance measurements carried out with a Solatron 1255 frequency response analyser and 1286 electrochemical interface, both under the control of a PC. A polarising potential of 15 mV was employed and data were collected over the frequency range 10^{-1} to $6x10^{5}$ Hz. The polymer electrolyte disks were sandwiched between 2 stainless steel electrodes in a 2-electrode cell which was itself located within an argon filled stainless steel chamber. The chamber was placed in a thermostatic bath in order to control the temperature of the cells. The temperature program of the thermostatic bath and the collection of data were controlled by in house software. Each measurement at a different temperature was taken after an equilibration period of 1 hour after the bath has reached a constant temperature.

3.4.3 Single Crystal X-ray Diffraction

Single crystal X-ray diffraction data were collected at 125K using Mo K_α on a Bruker SMART diffractometer equipped with a fine-focus sealed tube, a graphite monochromator and a CCD detector. The crystals were covered in oil and then mounted onto the diffractometer to reduce their exposure to air.

3.4.4 Differential Scanning Calorimetry (DSC)

Differential scanning calorimetry was carried out using a Netzch DSC 204 Phoenix with heating and cooling rates of 10°/min. The samples were placed in aluminium pans which were sealed under an argon atmosphere.

3.4.5 Dynamic Mechanical Thermal Analysis (DMTA)

The DMTA measurements were made using a Rheometric Scientific DMTA with MK111 analyser operating in the shear mode. Measurements were recorded at a heating rate of 2°/min and a frequency of 1Hz.

3.4.6 Matrix Assisted Laser Desorption Ionisation – Mass Spectroscopy (MALDI-MS)

Spectra were obtained on a Micromass TofSpec 2E instrument, equipped with a 337nm laser and operated in reflection mode. The sample was dissolved in water before incorporation into the matrix.

3.4.7 Nuclear Magnetic Resonance (NMR)

Solution phase NMR was carried out on a Bruker 'Varian' 500MHz instrument using The sample was dissolved in deuterated chloroform at a concentration of around 10mg/ml. The sample was then filtered to remove any small particles that may affect the NMR measurement and added to a clean NMR tube. The above operation was carried out under argon to avoid exposure to moisture.

3.4.8 Scanning Electron Microscopy (SEM)

SEM was carried out with a Jeol JSM 5600 SEM using a tungsten filament as the electron source with 3.5 nm resolution, with an accelerating voltage of 5kV. The air sensitive polymer electrolyte material was transferred to the microscope under an argon atmosphere in a sealed vial. An Argon filled 'glove bag' was then used to limit the samples exposure to air when placing the sample into the microscope.

Chapter 4

Investigation of the Properties of 6 to 1 complexes of PEO and $LiXF_6$, X = P, As, Sb

The crystalline phases of the polymer electrolytes $P(EO)_6$:$LiXF_6$, X = P, As, Sb have been shown to ionically conduct[1]. In this chapter the physical and electrochemical properties of these materials are explored.

4.1 Comparison of $P(EO)_6$:$LiXF_6$, X = P, As and Sb synthesised using PEO Mw 1000

4.1.1 AC Impedance Studies

Disks of the 3 complexes were subjected to AC impedance measurements and complex impedance plots for each are shown in Fig 4.1.1.2. Since the disks are formed by pressing a powdered polymer it is important to establish whether there are any grain boundary contributions to the total conductivity (density of a typical disk was estimated to be around 97% of the density obtained crystallographically).

In all 3 cases only one well formed semicircle is apparent in the impedance plots, Fig 4.1.1.2. The AC response may be described by an equivalent circuit comprised of a parallel combination of a resistance, representing ion transport through the polymer, and a capacitance, representing the dielectric response of the material. Magnitudes of the permittivities at 30(±0.6) °C were respectively 1.8 $pFcm^{-1}$ ($LiPF_6$), 1.7 $pFcm^{-1}$ ($LiAsF_6$) and 2.0 $pFcm^{-1}$ ($LiSbF_6$) and these are consistent with the bulk electrolyte

response indicating that the associated resistances are those of the bulk (intracrystalline)polymer. Hence the bulk resistance may be obtained from the low frequency intercept of the semicircle on the Z′ axis.[2] The linear region of the impedance at low frequencies is typical of a blocking (no charge transfer) electrode/electrolyte interface. A perfectly smooth interface would give a vertical spike, surface roughness of real interfaces result in an inclined line.

The upper temperature limit was determined by the softening point of the 1000 average molecular weight (Mw) polymer electrolytes and the lower by the ability of the equipment to measure resistive samples. From the plots of log conductivity versus reciprocal temperature shown in figure 4.1.1.1 it can be seen that the level of conductivities for $P(EO)_6$:$LiPF_6$, $P(EO)_6$:$LiAsF_6$ and $P(EO)_6$:$LiSbF_6$ prepared from

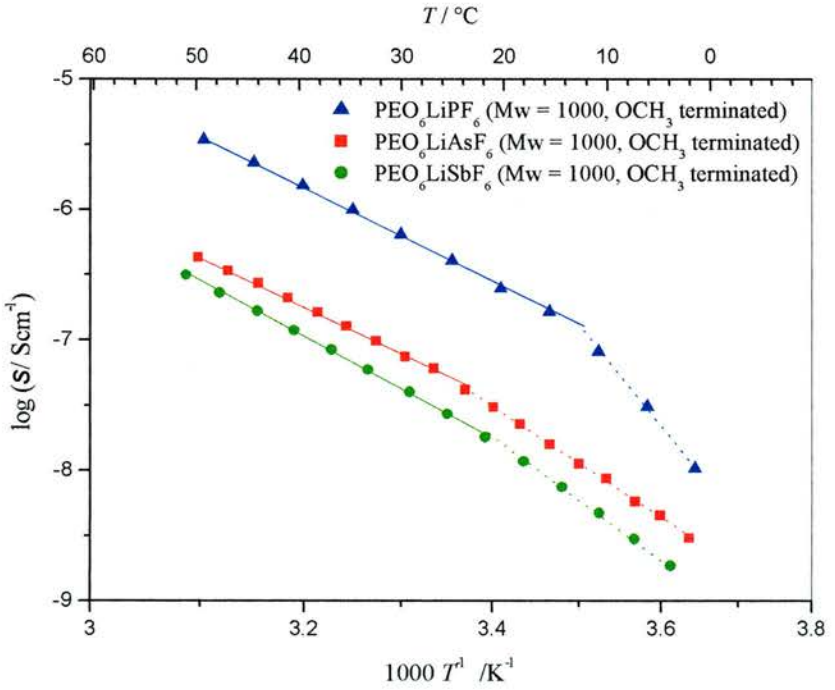

Figure 4.1.1.1. *Plot of log conductivity vs. reciprocal temperature. PEO_6LiPF_6: blue triangles, PEO_6LiAsF_6: red squares, PEO_6LiSbF_6: green circles.*

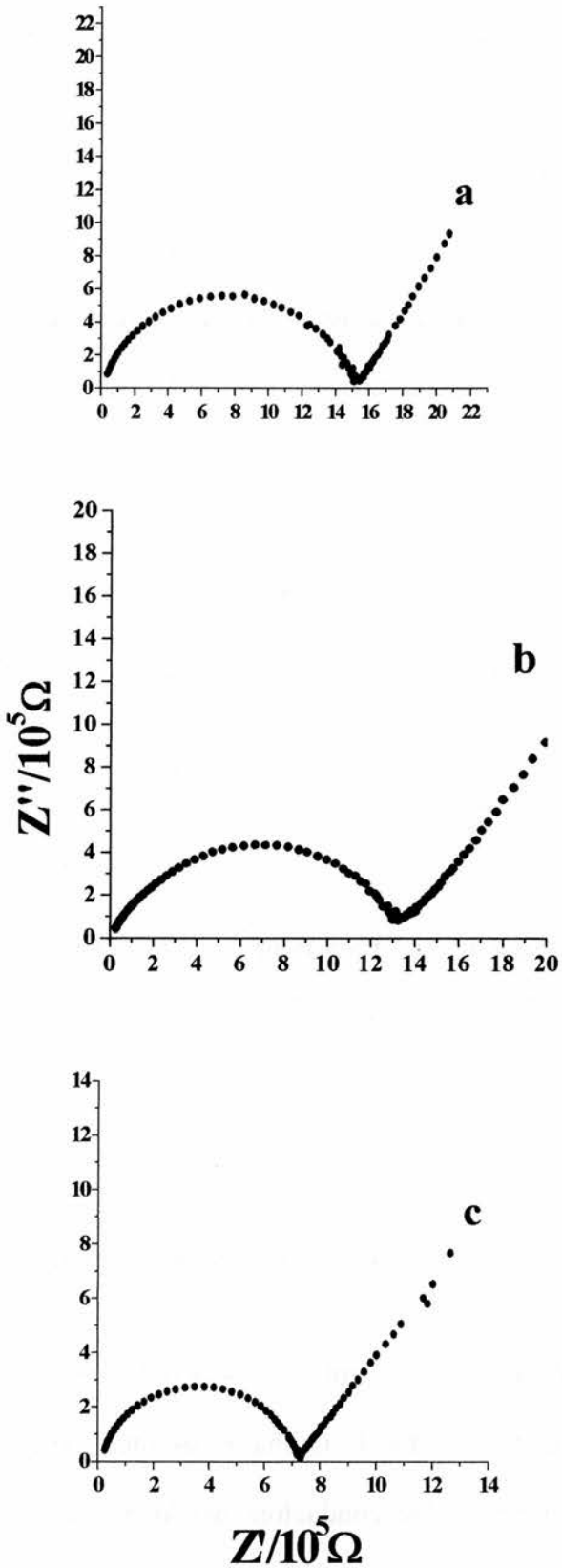

Figure 4.1.1.2. *Complex impedance plot of Imaginary(Z'') vs. Real(Z') components of AC Impedance Response. (a)$P(EO)_6$:$LiPF_6$, (b)$P(EO)_6$:$LiAsF_6$ and (c) $P(EO)_6$:$LiSbF_6$*

PEO Mw 1000 differ despite the materials having very similar structures. The level of conductivity exhibited by these materials decrease with increasing anion size. Since the anion does not co-ordinate the cation in these three materials the likely explanation for this discrepancy in conductivities is the co-ordination environment afforded by the PEO chains that is slightly different in each complex or the difference in packing caused by the different sized anions (see section 4.1.3).

Another feature worthy of note in these conductivity plots is the 'kink' that they all exhibit to some extent. Two straight lines can be drawn for each complex, one that passes through the higher temperature points, and one that passes through the lower. The two different activation energies associated with the different gradients in these lines hint at a different, temperature dependant, mechanism of ion transport.

Anion Type	High Temp. Ea/kJmol^{-1}	Low Temp. Ea/kJmol^{-1}
PF_6	71.9	142.0
AsF_6	69.9	83.5
SbF_6	77.1	87.1

Table 4.1.1.1 – *Activation energies of 6 to 1 complexes with different anions*

These materials are 1D conductors, movement of ions is only possible through the tunnels provided by the geometries of the PEO chains, as such the conductivity is limited. However, 2D or 3D crystalline conductors would no doubt offer higher conductivities.

4.1.2 Phase Analysis of complexes

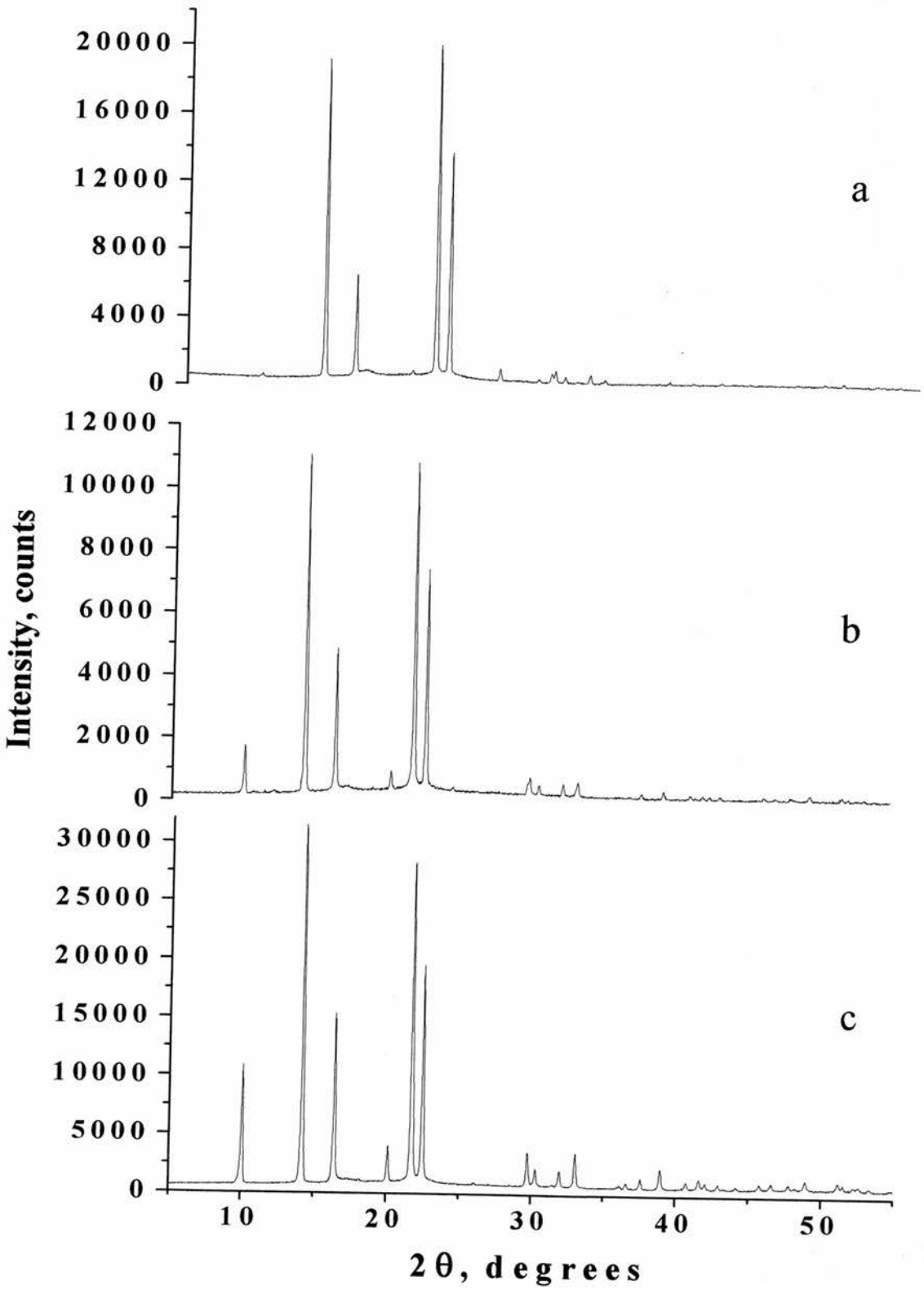

Figure 4.1.2.1 *X-ray powder diffraction patterns (Cu $K_{\alpha 1}$) of PEO_6:$LiPF_6$, (a), PEO_6:$LiAsF_6$ (b) and PEO_6:$LiSbF_6$ (c). All complexes synthesised using methoxy terminated PEO of Mw 1000.*

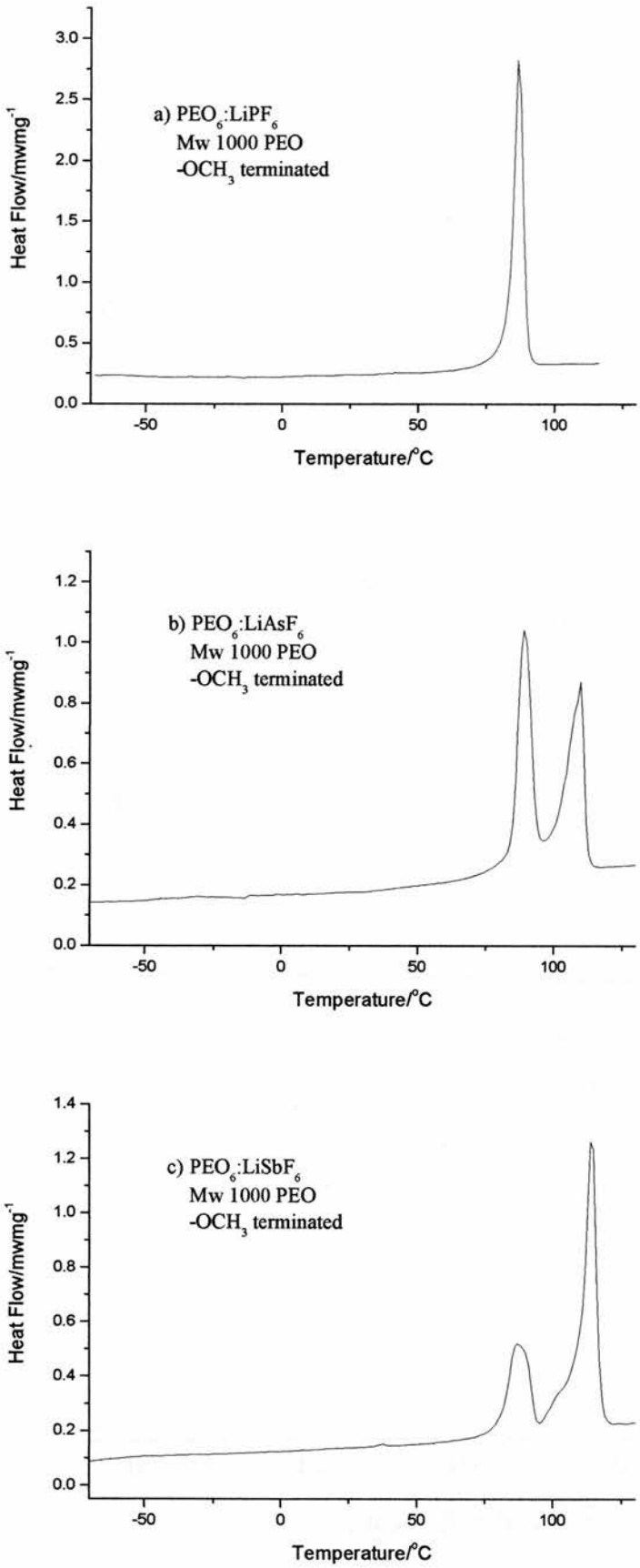

Figure 4.1.2.2. *DSC measurements (10Kmin^{-1}) of PEO_6:$LiXF_6$ X = P, As, Sb synthesised using PEO Mw 1000, methoxy terminated*

The high degree of crystallinity of the 1000 Mw materials can be seen in the X-ray diffraction patterns of these complexes in figure 4.1.2.1. Further evidence for the absence of an amorphous phase has been obtained from DSC and DMTA. NMR spectroscopy carried out by Stoeva et al[1] has also shown no evidence of disordered

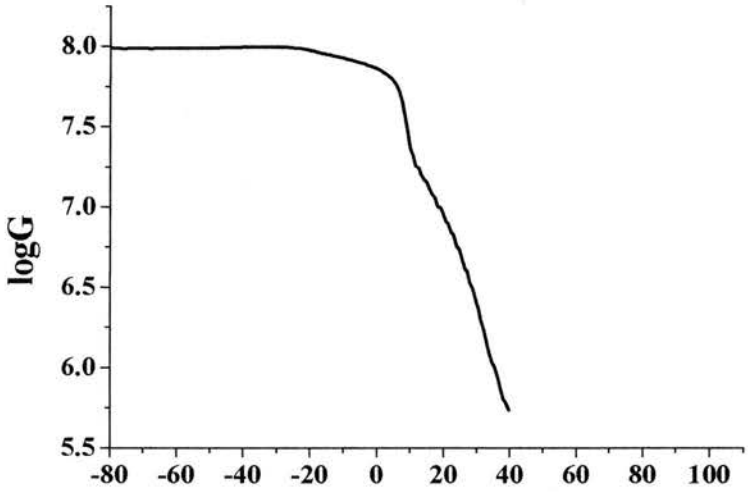

Figure 4.1.2.3 *DMTA (G – Shear modulus, Pa^{-1}) of PEO_6:$LiSbF_6$.*

phase. The Netzch calorimeter used for DSC measurements is an order of magnitude more sensitive than conventional instruments. The results for all three 6:1 complexes, PEO_6:$LiSbF_6$, are shown in Fig 4.1.2.2. There is no evidence of a glass transition temperature over the entire temperature range from -65 to 100° C. For the $P(EO)_6$:$LiPF_6$ complex the endothermic peak is associated with melting of the crystalline complex. The DSC traces of $P(EO)_6$:$LiAsF_6$ and $P(EO)_6$:$LiSbF_6$ show two endothermic peaks, the lower temperature endotherm has been attributed to a phase transfomation from the alpha to the beta phase of these complexes and the higher temperature endotherm is associated with melting of the beta phase polymorph (see chapter 9).

The absence of amorphous phase is reinforced by the DMTA results for PEO_6:$LiSbF_6$ presented in Fig. 4.1.2.3. The measurements had to be carried out in air. PEO absorbs

water aggressively from the atmosphere above 0° C and this is the origin of the large decrease in shear modulus above 10° C.

4.1.3 Comparison of 6 to 1 structures of $P(EO)_6$:$LiPF_6$, $P(EO)_6$:$LiAsF_6$ and $P(EO)_6$:$LiSbF_6$

Although the three complexes have very similar structures, there are however slight differences, as is apparent from the cross sections shown in figure 4.1.3.1. In the case of the $LiPF_6$ complex (a), the tunnels are approximately circular, they become more distorted for the larger AsF_6 anion (b) and in the case of the SbF_6 anion (c) the cross sections are rectangular. $P(EO)_6$:$LiAsF_6$ has the narrowest tunnels, the distance

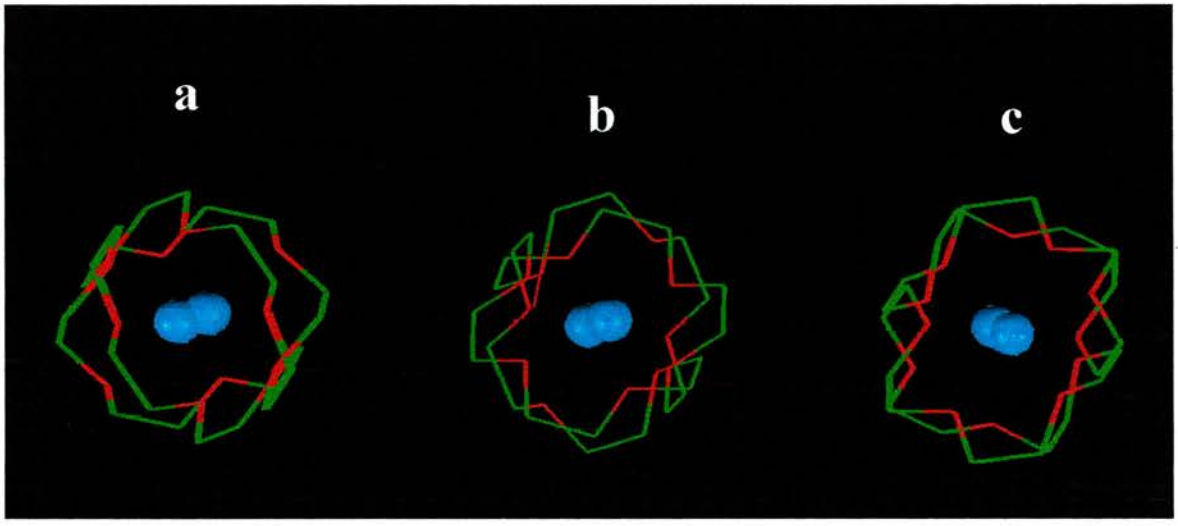

Figure 4.1.3.1. *Cross section of PEO tunnels in (a) - PEO_6:$LiPF_6$, (b) - PEO_6:$LiAsF_6$, (c) - PEO_6:$LiSbF_6$.*

between the ether oxygens opposite each other on the two chains making up the tunnel being 2.8 Å. This value increases to 3Å for the $P(EO)_6$:$LiPF_6$ and 3.3 Å for $P(EO)_6$:$LiSbF_6$.

4.2 Effect of Molecular Weight of PEO on Conductivity

For all three complexes $P(EO)_6$:LiPF6, $P(EO)_6$:$LiAsF_6$ and $P(EO)_6$:$LiSbF_6$ significant differences in the level of ionic conductivity have been obtained by varying the

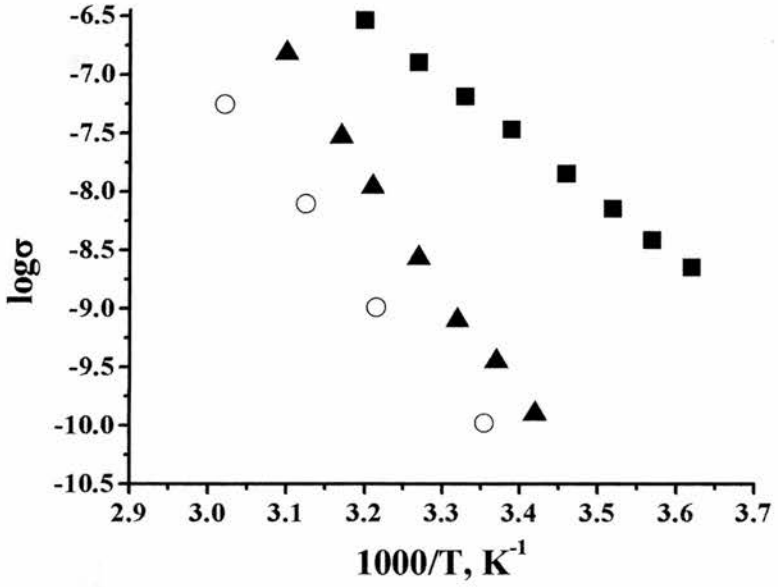

Figure 4.2.1. *Conductivities of $P(EO)_6$:$LiSbF_6$ prepared using methoxy terminated PEO of Mw 1000 (squares), 1500 (triangles) and 2000 (open circles)*

molecular weight of the polymer[3]. In Fig 4.2.1 conductivity data for $P(EO)_6$:$LiSbF_6$ prepared with molecular weights of 1,000, 1,500 and 2,000, illustrates the differences that can arise. Complexes prepared with lower molecular weight PEO exhibit higher levels of conductivity. A clue to the origin of these differences may be obtained by examining the powder diffraction patterns as a function of molecular weight, Fig 4.2.2. For all three complexes the peak positions and relative intensities are the same indicating that the crystal structures are invariant with molecular weight. However, on close examination (Fig 4.2.3) it is evident that the widths of the peaks do vary, increasing with increasing molecular weight.

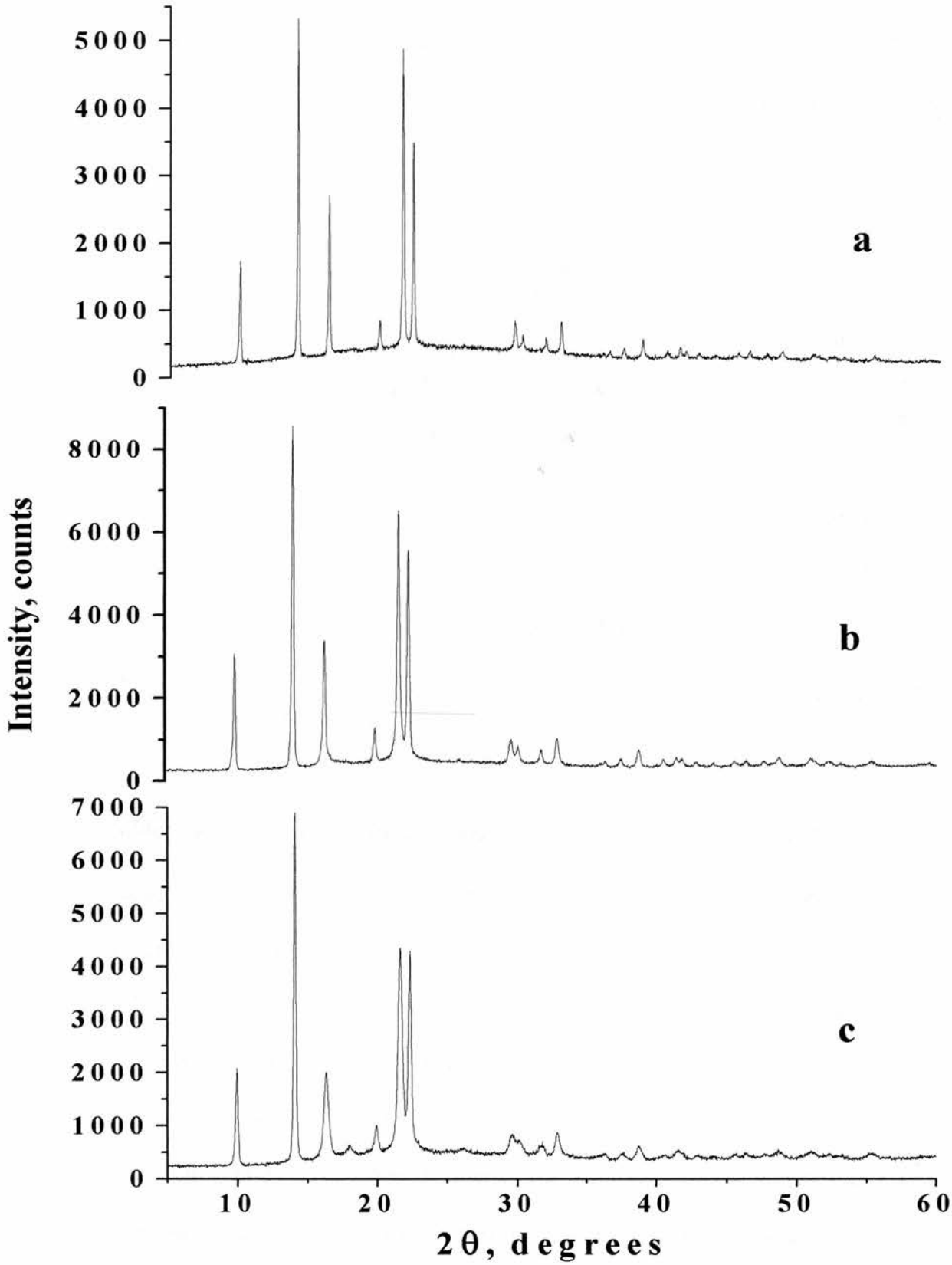

Figure 4.2.2. *X-ray powder diffraction patterns (Cu $K_{\alpha 1}$) of PEO_6:$LiSbF_6$, synthesised with methoxy terminated PEO of Mw 1000 (a), 1500 (b) and 2000 (c).*

The two main factors that determine peak widths in powder diffraction patterns are crystallite size and microstrain. If the former decreases below approximately 3,000 Å the peaks in a powder x-ray diffraction pattern begin to broaden significantly. As the strain within the crystal increases so also do the peak widths in diffraction patterns.

Although there is a clear correlation between the variation of conductivity and the peak widths in the powder diffraction data it is necessary to deconvolute the effects of microstrain from crystallite size to understand, in more detail, the origin of the variation in conductivity with the change in molecular weight.

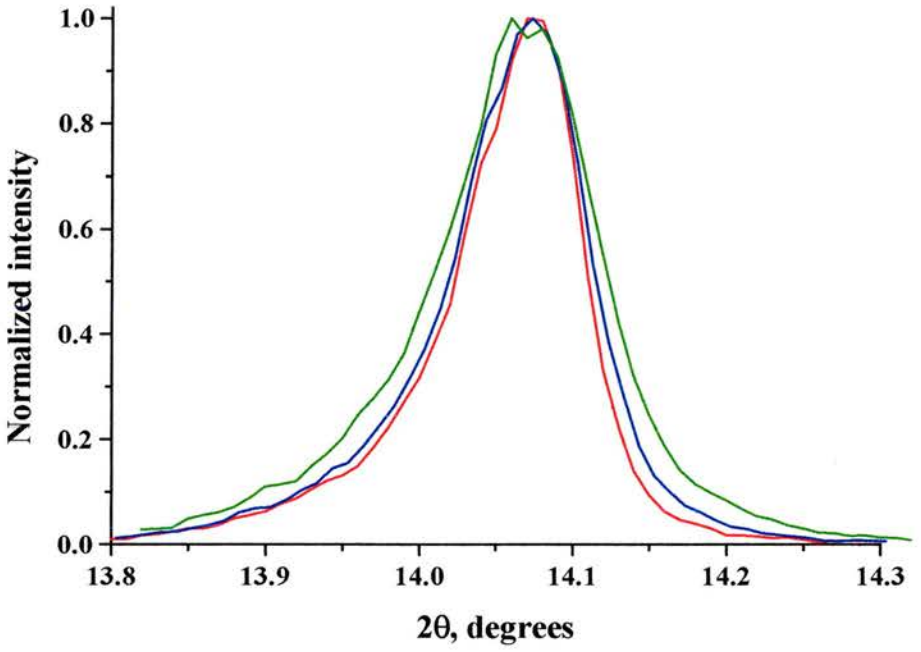

Figure 4.2.3. *021 reflection from PEO_6LiSbF_6 complex prepared from PEO of Mw 1000 (red), 1500 (blue) and 2000 (green)*

The contributions of strain and crystallite size to a Bragg peak appear as Gaussian and Lorentzian components respectively. The most robust single-peak methodology[4] has been employed to decouple these two contributions. The procedure is based on

extraction and analysis of Gaussian, β_G, and Lorentzian, β_L, components of the integral breadth of a single Bragg peak corrected for the instrumental broadening. The volume-weighted crystallite size, $<D>_V$, and weighted average microstrain, $\widetilde{\varepsilon}$, are readily calculated using the values of β_L and β_G, correspondingly (see section 2.1.2

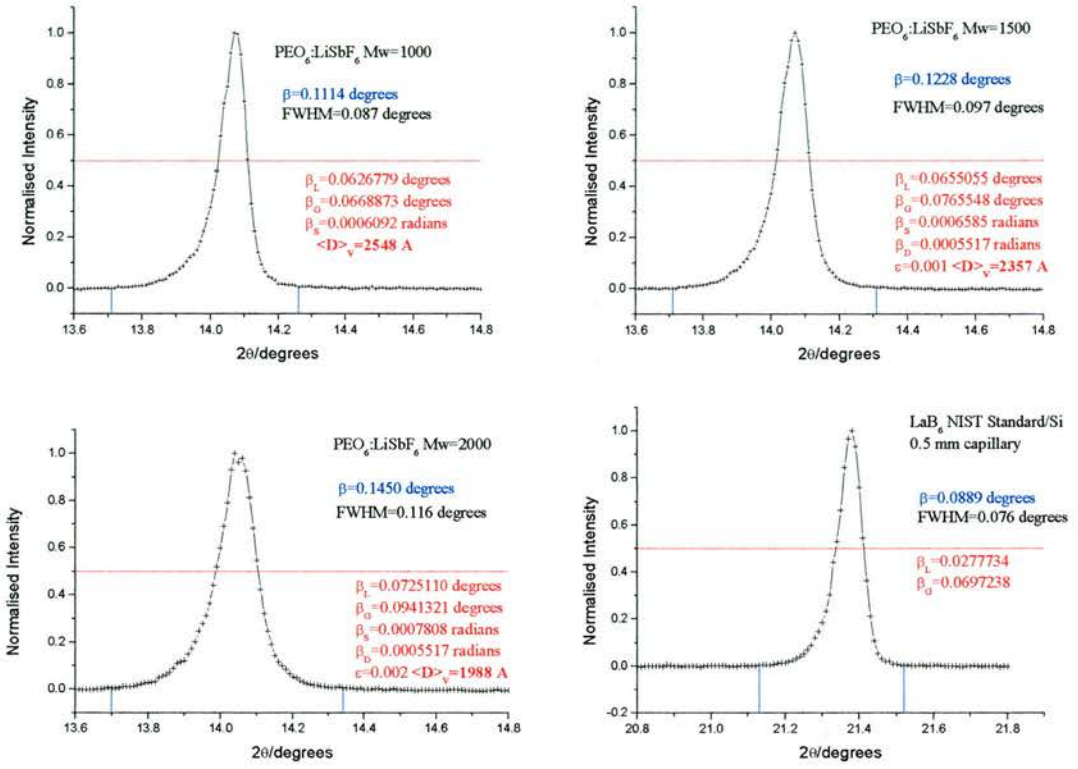

Figure 4.2.4. *021 peak analysis for PEO_6LiSbF_6 made from PEO with Mw 1000 (top left), 1500 (top right), 2000 (bottom left) and LaB_6 standard (bottom right)*

for more details). The size/strain analyses of the polymer electrolyte samples were carried out using a strong non-overlapping 021 reflection.

For these experiments the diffractometer was set up in the high-resolution mode providing full width at half maximum of 0.076° in 2θ for the 100 peak from a NIST line shape standard reference material, LaB_6, (SRM 660a). This peak was used to

correct the β_G and β_L from the polymer electrolyte samples for the instrumental broadening. In order to avoid instrumental smoothing, all reflections were measured with a stationary position sensitive detector. An acquisition time of at least 3 hours ensured the statistical accuracy of better than 1% in the peak intensity.

The results of the size/strain analysis revealed that for the $P(EO)_6$:$LiSbF_6$ complexes the crystallite size decreases with the increasing molecular weight of PEO with no significant microstrain present in any of the samples (less than 0.2%). For the example shown in Fig. 4.2.3 the crystallite size decreases from 2500 Å (Mw = 1000) through 2300 Å (Mw = 1500) to 2000 Å (Mw=2000). There is a clear correlation between molecular weight of PEO used and crystallite size. As the molecular weight of the polymer used is decreased an increase in crystallite size is witnessed. These

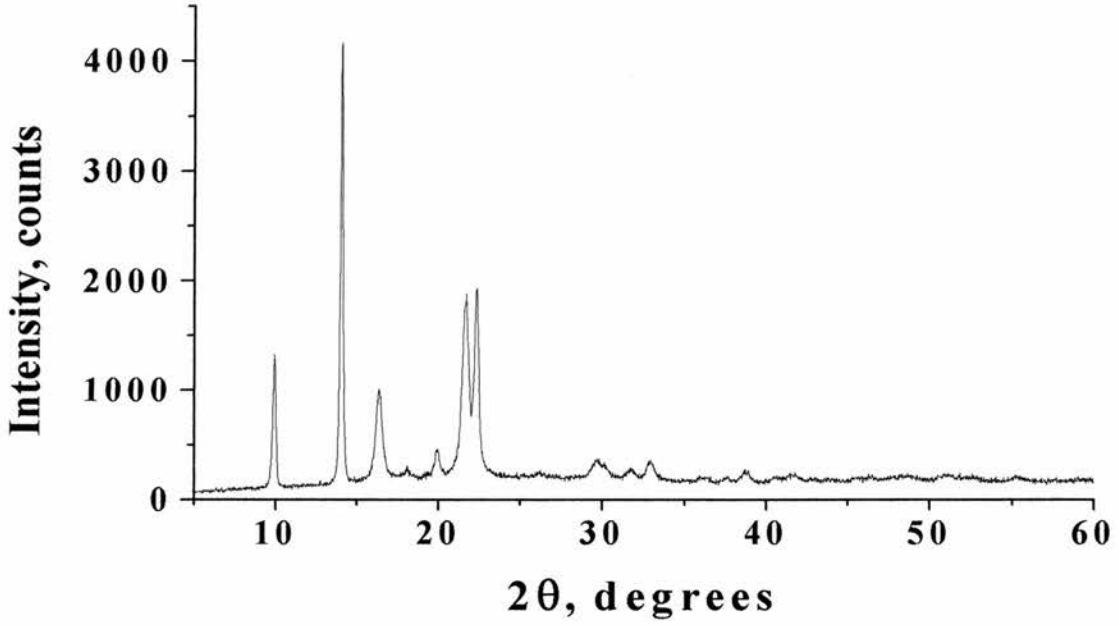

Figure 4.2.4. *X-ray powder diffraction pattern of $P(EO)_6LiSbF_6$ prepared using PEO Mw 2000 by the rapid evaporation of solvent*

materials with larger crystallites exhibit higher conductivities. These results were further reinforced by preparing another PEO_6:$LiSbF_6$ (Mw=2000) sample but in this

case evaporation of the acetonitrile was carried out rapidly. The powder pattern of the resulting material is shown in figure 4.2.4. From this figure it is evident that the peaks are significantly broader than the previously prepared sample using the same polymer and salt but a slower evaporation rate. Analysis of the 201-diffraction peak from the sample prepared by fast evaporation yielded a crystallite size of 1700 Å. This material had extremely high impedance that was immeasurable using our ac impedance equipment. As well as indicating a correlation with crystallite size these results also suggest that a conduction mechanism involving conduction along grain surfaces is unlikely, since such conduction is likely to be enhanced by small grain size and rapid crystallisation.

4.3 Electron Microscopy of $P(EO)_6$:$LiSbF_6$

The crystallite size determined from powder diffraction data is in fact the dimension over which the regular crystalline structure is coherent. Disorder beyond this length is sufficient to destroy further coherence. Crystallite size is not therefore necessarily the same as grain size.

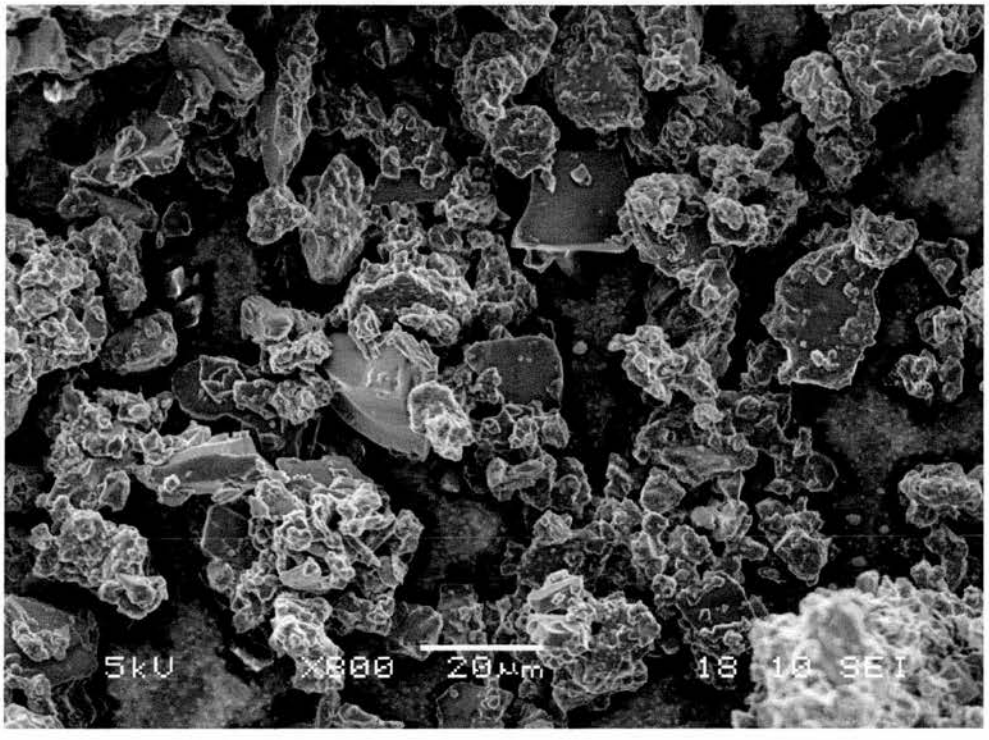

Figure 4.3.1. *SEM image of $P(EO)_6$:$LiSbF_6$*

Indeed it is often the case that these two dimensions are different, the latter being larger. Scanning electron microscopy reveals grain size for the powders in the range 1 to 50 µm (see figures 4.3.1 and 4.3.2).

The picture then emerges of crystalline domains, disordered with respect to each other, within grains of the polymer electrolyte. The boundaries between the domains are likely to impede the ion transport. Furthermore, these materials are 1-D

conductors hence the inevitable misalignment between adjacent domains further hinders the progress of ions.

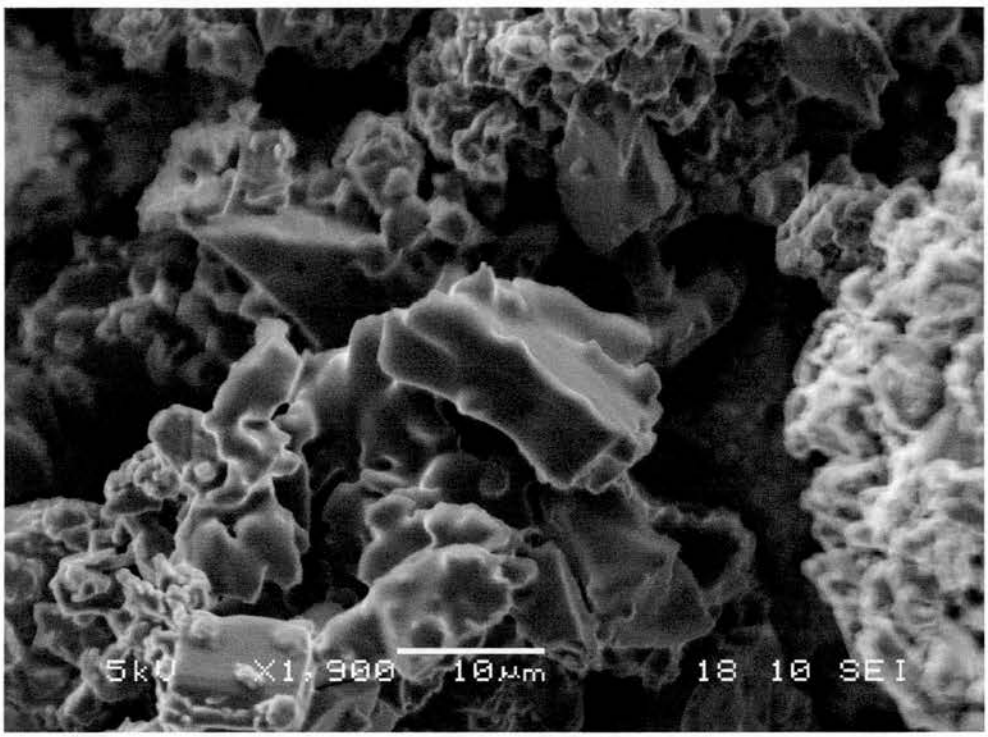

Figure 4.3.2. *SEM image of $P(EO)_6$:$LiSbF_6$*

These factors conspire to make ionic conductivity higher in materials with larger crystallite size. Note that in the pressed powders there appears, from the AC impedance results, little evidence of further resistance to charge flow at the grain boundaries.

4.4 Chapter Conclusion

It can be concluded that ionic conductivity exists in all three crystalline 6:1 polymer electrolyte complexes, that the conductivity is similar in keeping with the crystal structure of each. The crystallite size increases with decreasing molecular weight resulting in higher levels of ionic conductivity.

[1] Gadjourova, Z., Andreev, Y. G., Tunstall, D. P. and Bruce, P. G. *Nature* **412**, 520-523 (2001).

[2] Bruce, P. G. In *Polymer Electrolytes Reviews – 1*; MacCallum, J. R., Vincent, C. A., Eds.; Elsevier Applied Science: London and New York, 1987; p. 237.

[3] Stoeva, Z., University of St. Andrews PhD. Thesis (2001)

[4] Delhez, R.; de Keijser, T. H.; Langford, J. I.; Louër, D.; Mittemeijer, E. J.; Sonneveld, E. J. In *The Rietveld Method*; Young, R. A. Ed.; Oxford University Press: Oxford, 1996; p. 132.

Chapter 5

Enhancing the Conductivity of $P(EO)_6$:$LiAsF_6$ by Doping with Lithium Imide

Crystalline polymer electrolytes have been shown to support ion transport. However the levels of conductivity they exhibit are too low for applications such as SMART windows, electrochromic displays and lithium ion batteries. The 6 to 1 complexes of PEO and $LiXF_6$ are stoichiometric materials. By introducing a species into the structure of these materials that forces the crystal to deviate from stoichiometry, large increases in conductivity can be achieved. This can be done by creating local disorder by doping with a salt that has a larger anion than XF_6^- (isovalent doping). This chapter describes a substantial increases in conductivity afforded by doping $P(EO)_6$:$LiAsF_6$ isovalently to levels where they are of practical use.

5.1 Isovalent Doping of $P(EO)_6$:$LiAsF_6$ with Lithium Imide

Isovalent doping is the incorporation of foreign ions that have a valency or charge the same as the host ion eg. Rb^+ or I^- in AgBr. This process has the ability to increase the conductivity of materials by virtue of elastic displacements or lattice distortions caused by the dopant moiety - which will in general be different in size. The net result of such a strain on the lattice leads to changes in the energetics of point defect creation as well as ion mobility. A noteworthy example of this process is detailed in work by Shahi and Wagner[1, 2], in which the conductivity of crystalline silver bromide is increased by two orders of magnitude by replacing around 25% of the bromide ions with iodide ions.

Lithium imide was chosen as the dopant salt as the TFSI anion, ($N(SO_2CF_3)_2^-$) is significantly different from AsF_6^- in terms of size, shape and charge distribution, but at the same time TFSI is small enough to be integrated into the crystal structures of these materials (see fig 5.1.1.).

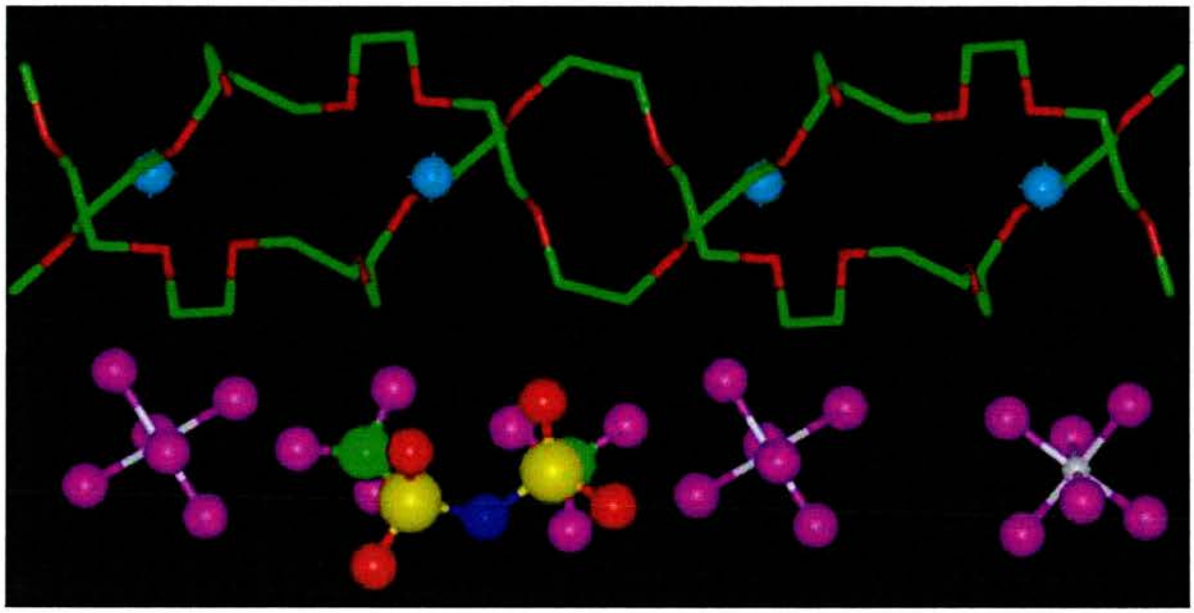

Fig. 5.1.1 *Fragment of the crystal structure of PEO_6:$(LiAsF_6)_{1-x}(LiTFSI)_x$ showing the substitution of the AsF_6^- ion by $TFSI^-$. Light blue, lithium; white, arsenic; purple, fluorine; dark blue, nitrogen; yellow, sulphur; green, carbon; red, oxygen.*

Samples of $P(EO)_6$:$LiAsF_6$ doped to varying degrees with LiTFSI were prepared as in section 3.1.2 . Conductivity isotherms for the varying compositions are shown below in Fig 5.1.2. The isotherm plot can be split into two regions. Region A demonstrates a steep increase in conductivity with respect to the amount of lithium imide added. Starting from the pure 6:1 complex the conductivity rises sharply by 1.5 orders of magnitude with x, up to a maximum composition of around $P(EO)_6$:$(LiAsF6)_{0.95}(LiTFSI)_{0.05}$. Region B shows a different behaviour, a gentle increase in conductivity until pure PEO_6:LiTFSI is reached at x = 1.

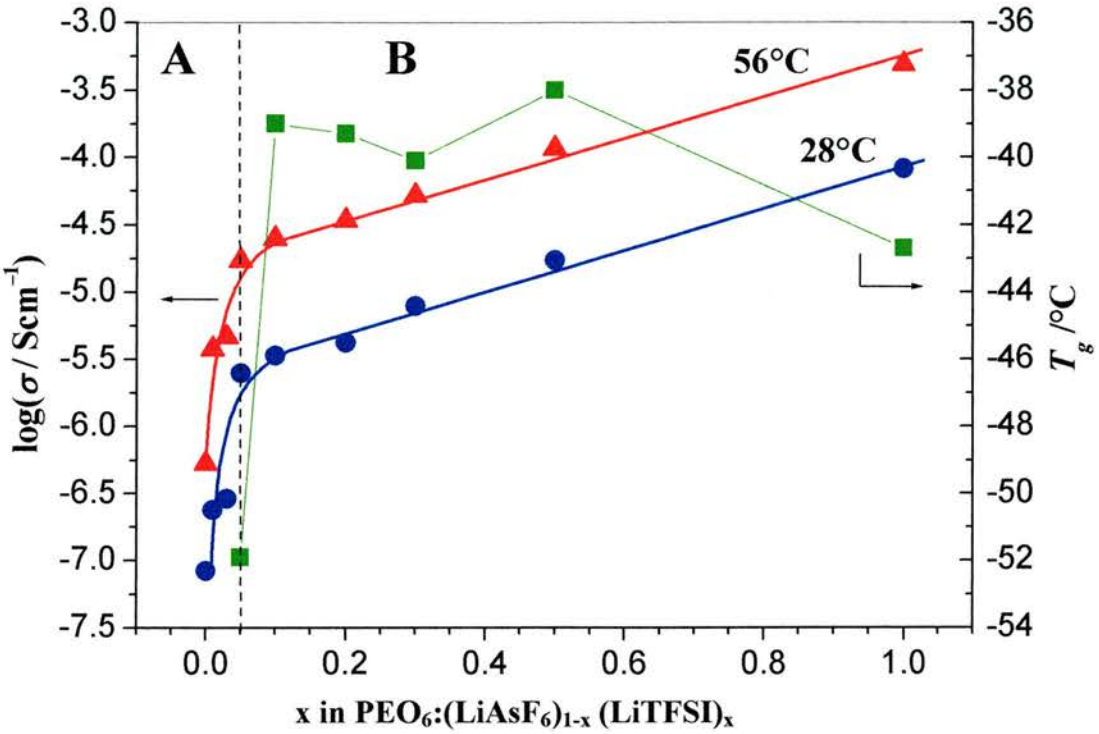

Fig.5.1.2. *PEO_6:$(LiAsF_6)_{1-x}$$(LiTFSI)_x$: Conductivity isotherms as a function of x at 28°C (blue circles) and at 56°C (red triangles). Variation in T_g as a function of x (green squares)*

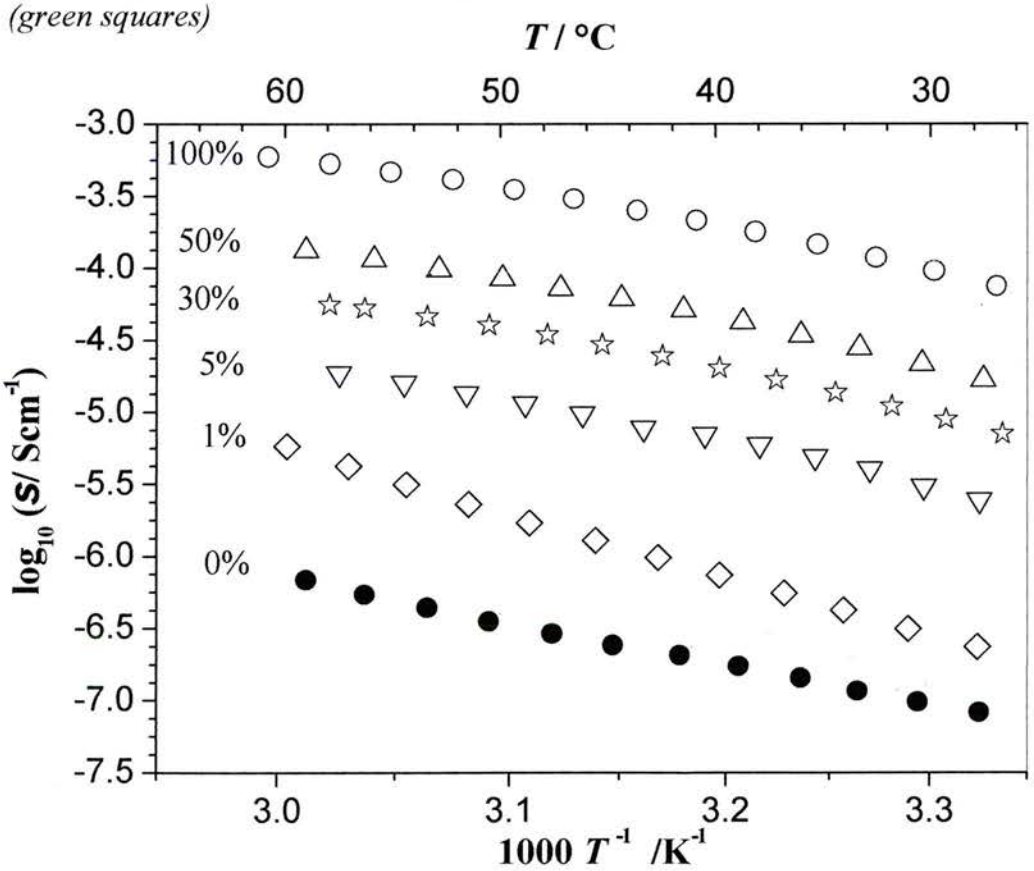

Fig. 5.1.3. *Ionic conductivity as a function of temperature, the numbers are values of x in mol%.*

(Despite it's high conductivity PEO_6:LiTFSI is not a suitable material for a solid separator as it is a liquid at room temperature).

To explain the behaviour exhibited in regions A and B in the isotherm presented in figure 5.1.2, characterisation of the phases present in the PEO_6:$(LiAsF6)_{1-x}(LiTFSI)_x$ system as a function of x is necessary.

Powder x-ray diffraction patterns for several compositions are shown in Fig. 5.1.4. The complex PEO_6:LiTFSI (representing a 100% doping level) is completely amorphous as is evident from the powder diffraction pattern. There is no evidence of any unreacted lithium imide from the powder diffraction data. In the remaining compositions there are no shifts in the peak positions or change in relative peaks intensities of the $P(EO)_6$:$LiAsF_6$, indicating that the level of imide incorporated into the lattice must be below the value necessary for these changes to become apparent in the powder diffraction patterns. It can be concluded that over most of the composition range (region B in Fig. 5.1.2) a two phases mixture is present, consisting of an amorphous component and a crystalline component with the structure of PEO_6:$LiAsF_6$.

Evidence for the amorphous PEO:LiTFSI phase can be seen in the DSC data collected from a range of materials doped with varying levels of imide (see figure 5.1.5). Compositions with $x \geq 0.05$ exhibit a glass transition. The relative level of amorphous material can be estimated by examining the change in the heat capacity before and after the T_g (the step size of the thermal event associated with the glass transition).

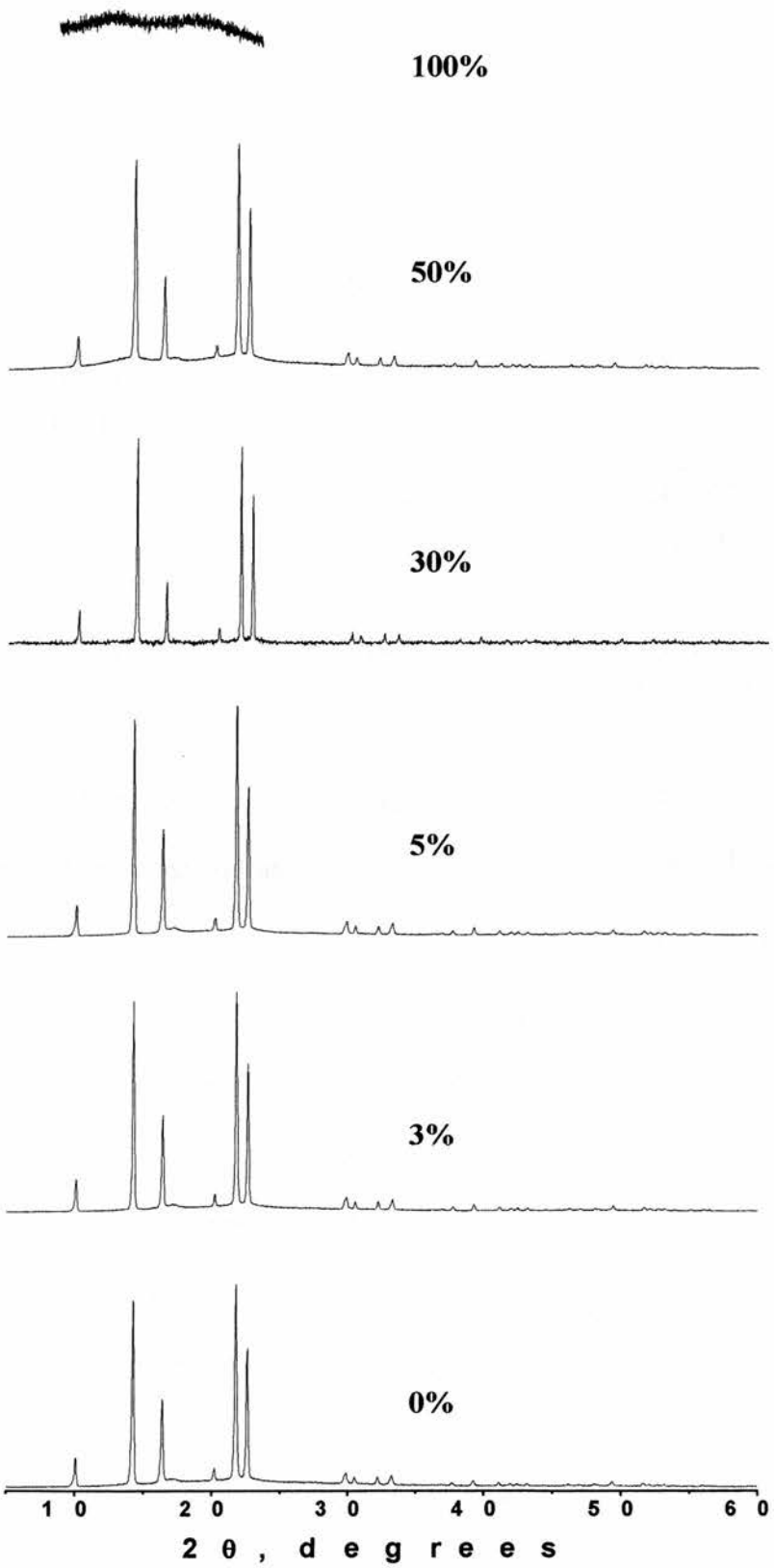

Fig. 5.1.4. *X-ray powder diffraction patterns of PEO_6:$(LiAsF_6)_{1-x}(LiTFSI)_x$, the numbers are values of x in mol%.*

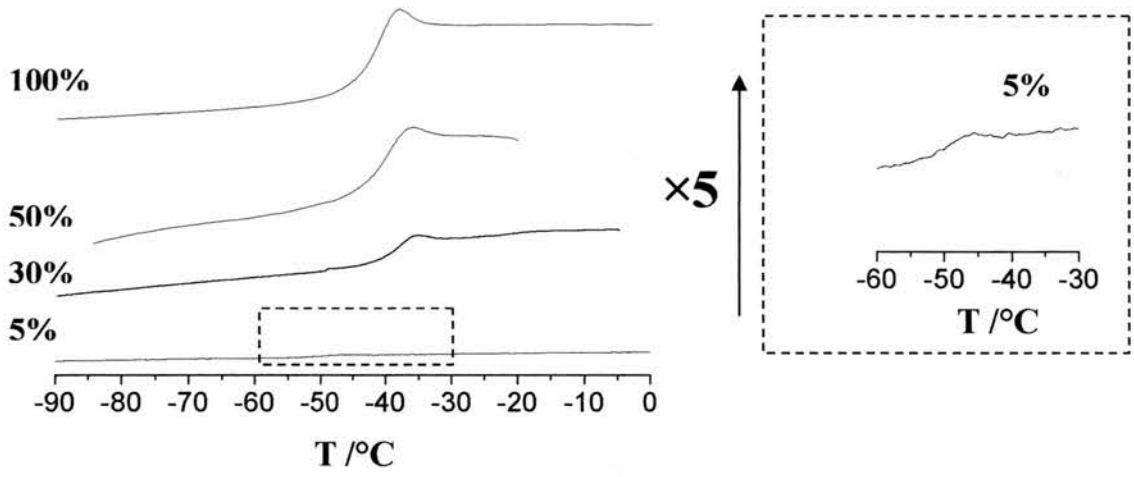

Fig.5.1.5. *DSC of PEO_6:$(LiAsF_6)_{1-x}(LiTFSI)_x$: sections of the traces showing T_g, the numbers are values of x in mol%.*

From Fig. 5.1.7 it can be seen that ΔC_p varies linearly with LiTFSI content, consistent with the hypothesis that a two phase mixture exists and is responsible for the behaviour in region B of the isotherm.

Based on the phase behaviour of this material it is now possible to explain the isotherm exhibited in fig 5.1.2. Starting from the left, there is a rapid increase in conductivity with increasing x (region A). This sharp increase is caused by the isolvalent doping phenomena exhibited by the solid solution (similar to that seen in the $AgBr_{1-x}$ I_x ionic conductor) that is present up to a maximum doping level corresponding to the composition PEO_6:$LiAsF6_{0.95}$ $LiTFSI_{0.05}$. At higher x the lattice can not accommodate further LiTFSI.. Instead a two-phase mixture exists containing the crystalline imide saturated complex, PEO_6:$LiAsF6_{0.95}LiTFSI_{0.05}$, and the amorphous $P(EO)_6$:LiTFSI material, optical microscopy confirms this result (see fig 5.1.6). As the level of imide dopant is increased further the amount of amorphous

material present increases relative to the crystalline phase but with no change in the composition of either the crystalline or amorphous phases. A linear increase in conductivity is consistent with the level of amorphous material being increased. Other mechanisms accounting for the increase in conductivity have been considered and rejected. It has been seen that heterogeneous doping, which occurs above the percolation limit when a poorly conducting crystalline phase is added to a more

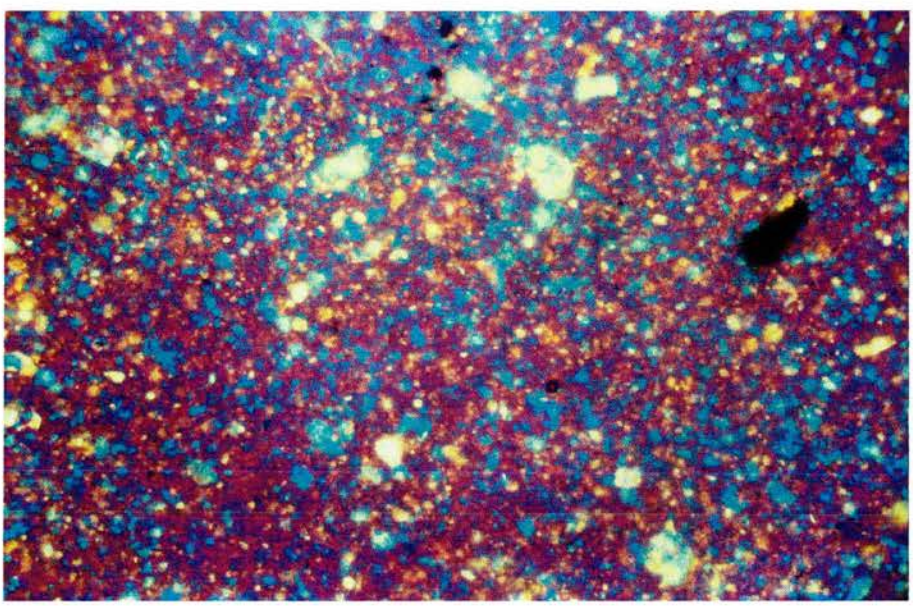

Figure 5.1.6. *Optical microscopy of PEO_6:$LiAsF6_{0.5}LiTFSI_{0.5}$. Red regions indicate amorphous material. Incandescent areas represent crystalline material.*

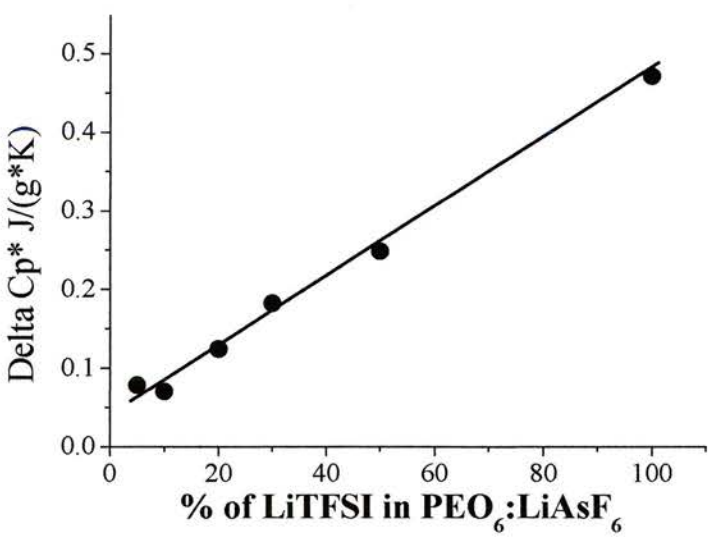

Fig 5.1.7. *Change in heat capacity associated with T_g as a function of x.*

highly conducting liquid or amorphous phase, can increase the conductivity of the material by generating a higher concentration of charge carriers at the interface between the two phases, due to space charge effects[3,4,5]. If the present system consisted of a random distribution of similarly sized particle this effect would be expected to be exhibited in the region of x = 0.2 to 0.3[6]. No such behaviour is apparent in Fig. 5.1.2.

Confirmation that conduction in region A occurs by a hopping mechanism and is different from region B is obtained by least-squares fitting to the temperature-dependant conductivities in figure 5.1.3. The 0%, 1% and 3% materials exhibit linear $\log\sigma$ versus reciprocal temperature plots, and are well described by an Arrhenius expression. Activation energies of 55, 83 and 70 kJ mol^{-1} for the 0, 1 and 3 % doped materials were obtained by the fitting procedure. An Arrhenius expression may also be used to describe the 5% doped material, although the use of the Vogel-Tamman-Fulcher (VTF) expression ($\sigma = \sigma_o T^{-1/2} \exp(-B/(T-To))$) gives a slightly better fit. However taking account of the fact that the VTF expression involves a 50% increase in the number of variables used to fit the conductivity data compared with the Arrhenius expression, the improvement of the fit is marginal. The onset of such a marginal curvature at 5% is exactly what is expected for a composition on the border between regions A and region B, and hence is further confirmation of the doping mechanism. With increasing LiTFSI content in region B the $\log\sigma$ versus reciprocal temperature plots become more curved, and can only be described by the VTF equation.

In conclusion, it has been shown that the conductivity of $P(EO)_6$:$LiAsF_6$ can be raised by 1.5 orders of magnitude by the incorporation of lithium imide in the lattice up to a maximum content of around 5%, corresponding to a room temperature conductivity of 10^{-5} S cm^{-1}. After the complex has been saturated with dopant, the lithium imide salt then, instead of incorporating within the lattice, forms an amorphous complex with PEO, producing a conductive amorphous phase which further increases the conductivity of the material. Isovalent doping has been shown to be a successful technique in raising the conductivities of these ordered polymer electrolytes.

---

[1] Shahi K. and Wagner Jr. J.B., *Appl. Phys. Lett.* **37**, 757 (1980)

[2] Shahi K. and Wagner Jr. J.B., *Solid State Ionics* **12**, 511-516 (1984)

[3] Liang, C.C. *J. Electrochem. Soc.* **120**, 1289-1292 (1973)

[4] Wagner, J.B. Jr. Composite Solid Ion Conductors. In *High Conductivity Solid Ionic Conductors – Recent Trends and Applications* : T. Takahashi Ed., pp 146-165. World Scientific Publishing Co. Pte. Ltd, Singapore

[5] Maier, J. *Prog. Solid St. Chem.* **23**, 171-263 (1995)

[6] Consiglio, R., Baker, D. R., Paul, G. and Stanley, H.E. *Physica A* **319**, 49-55 (2003)

Chapter 6

Effects Of Modifying PEO Chain Ends of $P(EO)_6LiXF_6$ X = P, As

In order to ensure that the PEO chain ends are chemically similar to the main chain, especially when employing relatively short chains, the ends are capped with methoxy groups ($-OCH_3$).

In this chapter the effect that changing the end group has on the thermal, structural and electrochemical properties of complexes between 1000 M_w PEO are investigated. End groups evaluated include ethoxy ($-OC_2H_5$), neopentoxy ($-OCH_2C(CH_3)_3$) and benzyl ($-OCH_2C_6H_5$). They were chosen to vary the length, size and geometry of the end groups.

In particular, we wished to probe the influence that the end groups would have on the structure of these complexes and their ion transport. Concerning the latter property, there is evidence that chain ends may play a role was presented in chapter 4, where it was shown that shorter chains (with more ends) exhibited higher levels of conductivity (see section 4.2). This may be due to the creation of more defects or higher polymer dynamics at the chain ends. By varying the end groups we hope to explore these issues further. By functionalising the end groups of these chains a greater number of defects throughout the crystal would be present causing deviation from stoichiometry. Creating defects has been shown to be effective in increasing the conductivity of these materials (see chapter 5).

By analogy with plastic crystalline conductors[1] it can be seen that molecules that exhibit some degree of rotational or conformational freedom exhibit high levels of ionic conductivity. By adding end groups to the PEO chains that are essentially non-co-ordinating to lithium, such as ($-C_2H_5$), ($-CH_2Ph$), ($-CH_2C(CH_3)_3$) these moieties have license to exhibit rotational or conformational disorder (see fig. 6.1)

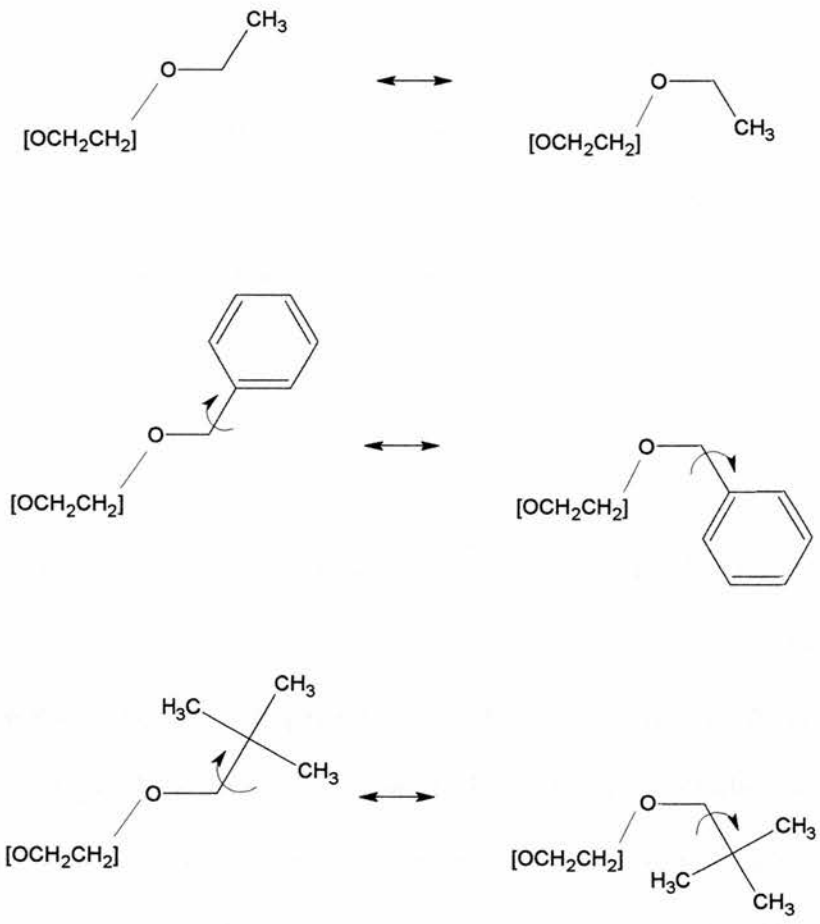

Figure 6.1. *Illustration of conformational and rotational freedom of selected end groups.*

Another effect that was anticipated was the structure directing effect of the end-groups of the PEO chains. The functionality at the chain terminus has been found to affect the crystal structures of these materials.

The conductivities of the phases that are produced by modifying the termini of the polymer are significantly higher than the conductivity of comparable phases prepared using PEO terminated by the standard $-OCH_3$ end groups.

6.1 Properties of 6:1 Complexes Synthesised using Ethoxy ($-OC_2H_5$) Endcapped PEO of Mw 1000

6.1.1 $P(EO)_6$:$LiPF_6$ Synthesised using Ethoxy Terminated PEO of Mw 1000

Samples of the 6:1 complex were prepared using di-ethoxy PEO Mw 1000 and $LiPF_6$ in the standard manner (see section 3.1.1.). Ethoxy groups were chosen as they offer only a slight change in the functionality of the end groups. The PXRD pattern of the complex prepared from solvent casting is shown below in fig. 6.1.1.1. The pattern exhibited a number of peaks not present in the 6:1 complex prepared using PEO with methoxy end groups (extra peaks denoted by an asterisk). These peaks are attributed to the presence of a different crystalline phase of the polymer electrolyte, which is referred to as γ – $P(EO)_6$:$LiPF_6$. (See section 6.1.2 for further details on the gamma phase).

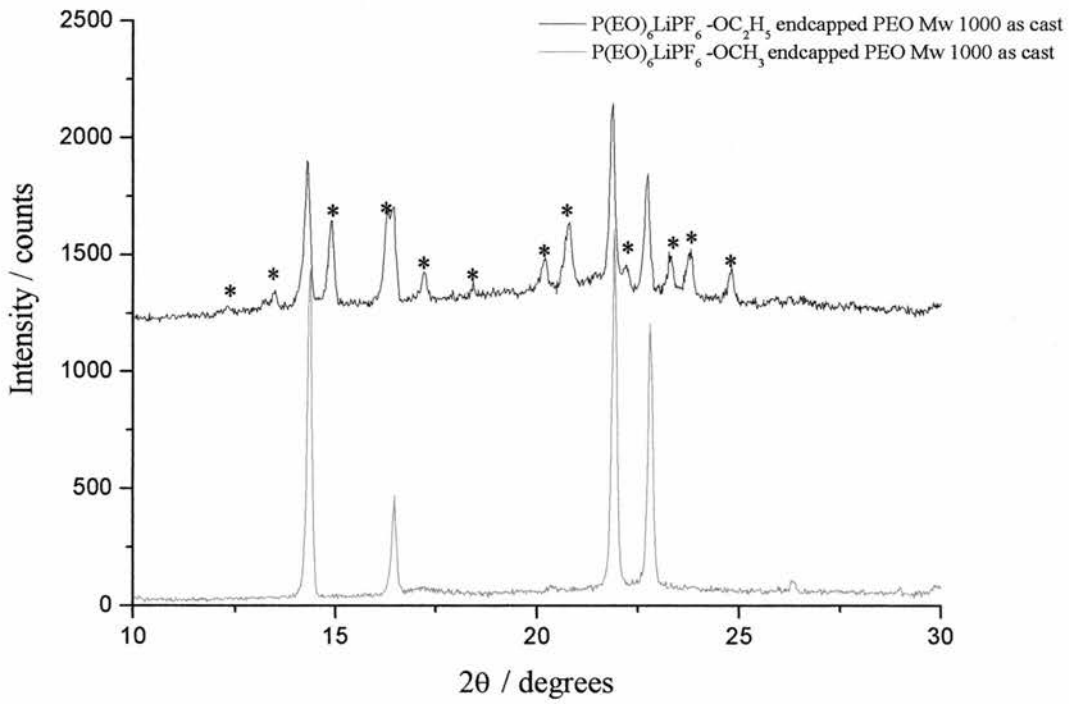

Figure 6.1.1.1 *Comparison of PXRD patterns of $P(EO)_6$:$LiPF_6$ 'as cast' PEO Mw 1000 $-OC_2H_5$ endcapped (top, black) and $-OCH_3$ end capped (bottom, red).*

The sample was then heated to above its melting point and cooled slowly. The resulting melt-cooled product was found to be pure alpha phase by powder x-ray diffraction (alpha phase refers to the 'normal' phase described in chapter 4) . All the peaks associated with the gamma phase had disappeared (see fig. 6.1.1.2). The PXRD pattern of the melt-cooled sample of the complex made with the ethoxy terminated PEO was similar to the PXRD pattern of the methoxy endcapped $P(EO)_6$:$LiPF_6$ complex, indicating that it had a comparable structure.(see fig. 6.1.1.2).

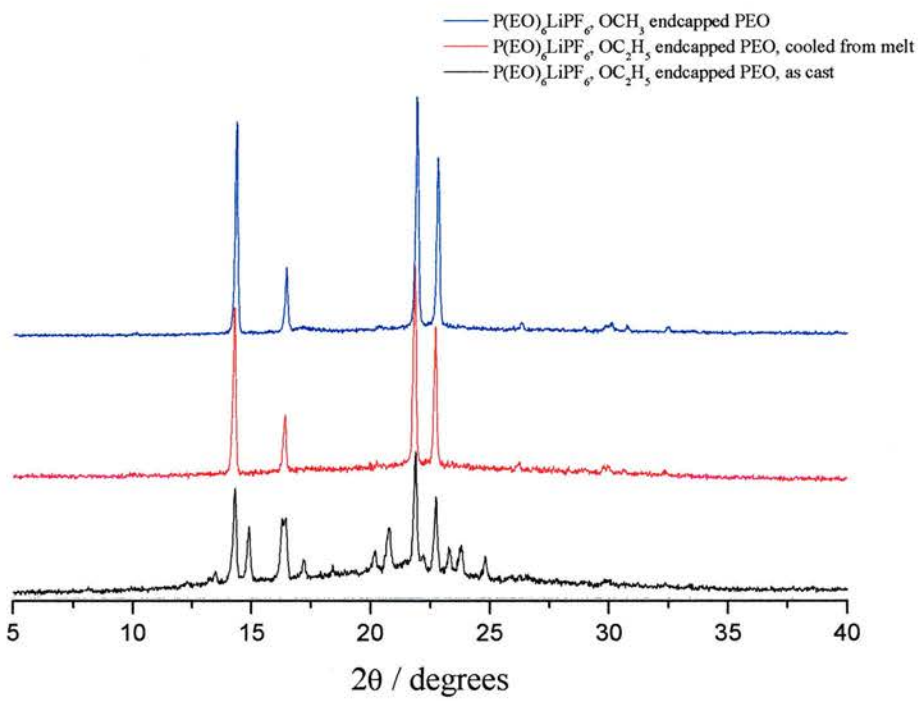

Figure 6.1.1.2 *PXRD patterns of PEO_6:$LiPF_6$ synthesised using PEO endcapped with methoxy groups (top, blue), ethoxy cooled from melt (middle red), and ethoxy as cast (bottom, black).*

Although the PXRD data for the methoxy endcapped alpha phase material and the ethoxy endcapped alpha phase material cooled from melt are broadly similar, there were significant shifts in peak positions in the PXRD (see fig 6.1.1.3). From these peak shifts it can be seen that the material prepared with the ethoxy terminated

polymer has different unit cell dimensions. Careful Le Bail fitting to the powder diffraction pattern yielded the unit cell parameters of the complex.

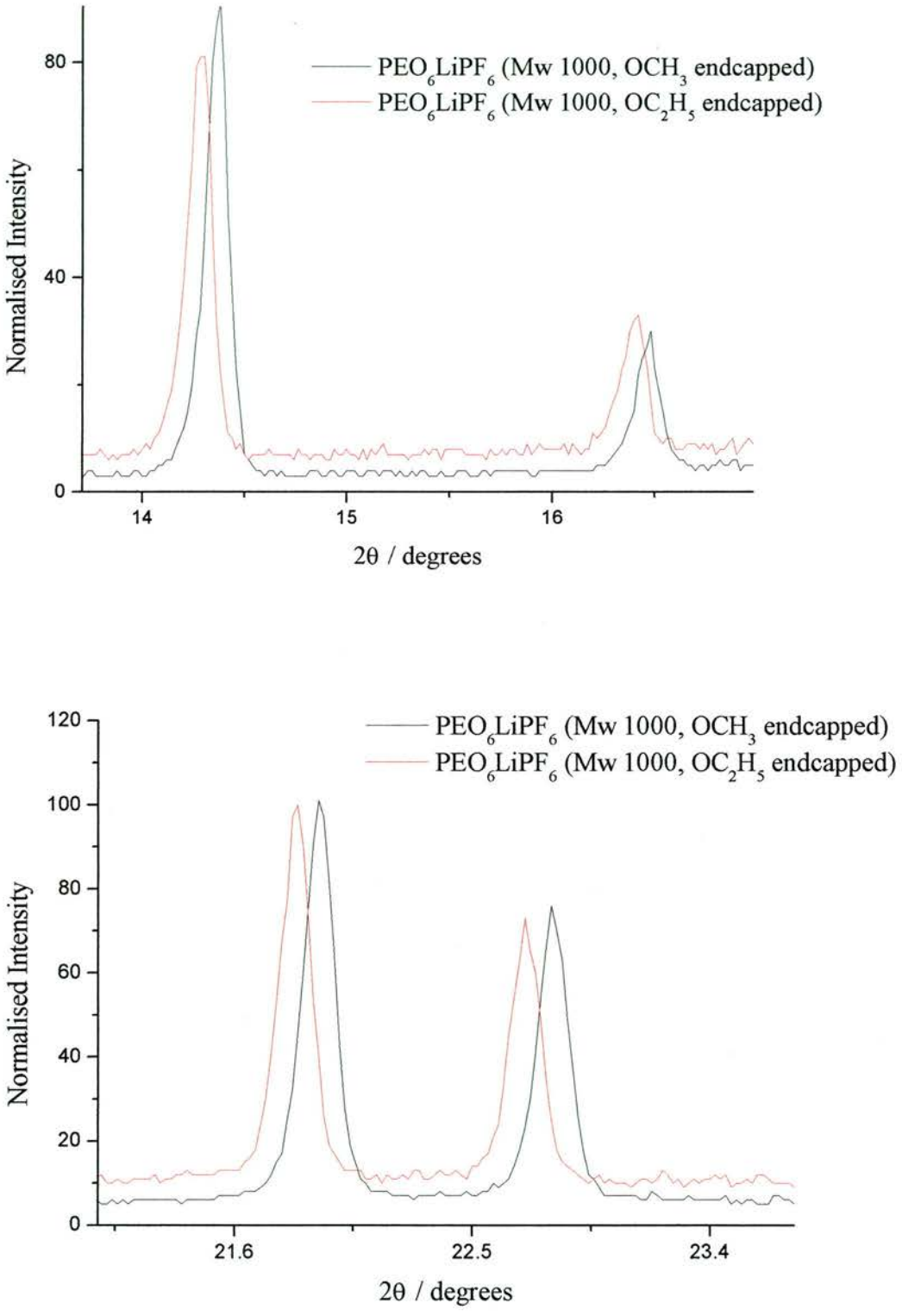

Figure 6.1.1.3. *PXRD data for $P(EO)_6$:$LiPF_6$ synthesised using methoxy end capped PEO (black) and ethoxy end capped PEO (red). The data shows a shift in peak position to lower angles for the ethoxy end capped complex*

prepared with the ethoxy terminated PEO and are displayed in table 6.1.1.1 along with the unit cell parameters of the methoxy terminated complex for comparison.

Unit Cell Parameter	$P(EO)_6LiPF_6$, 1k, $-OC_2H_5$ terminated	$P(EO)_6LiPF_6$, 1k, $-OCH_3$ terminated	Difference Ethoxy-Methoxy
a	11.778(4) Å	11.924(4) Å	-0.146(6) Å
b	17.492(2) Å	17.335(6) Å	0.157(6) Å
c	9.381(3) Å	9.202(3) Å	0.179(4) Å
β	111.33(5)°	108.85(3)°	2.48(6)°
Volume	1799(1) $Å^3$	1800(1) $Å^3$	1(1)$Å^3$

Table 6.1.1.1 *Unit cell parameters of $P(EO)_6$:$LiAsF_6$ prepared from ethoxy and methoxy end capped PEO.*

The c-lattice parameter exhibits the largest change in size, a contraction of around 2.0%. The 'c' direction is perpendicular to the axis of the PEO tunnels which lie in the 'a' direction. This indicates that the distance between the co-ordination tunnels is increasing in size, possibly as a result of the structure accommodating the protruding $-C_2H_5$ chain ends. There is also a contraction along the 'a' direction of around 1.2%. The contraction in this direction

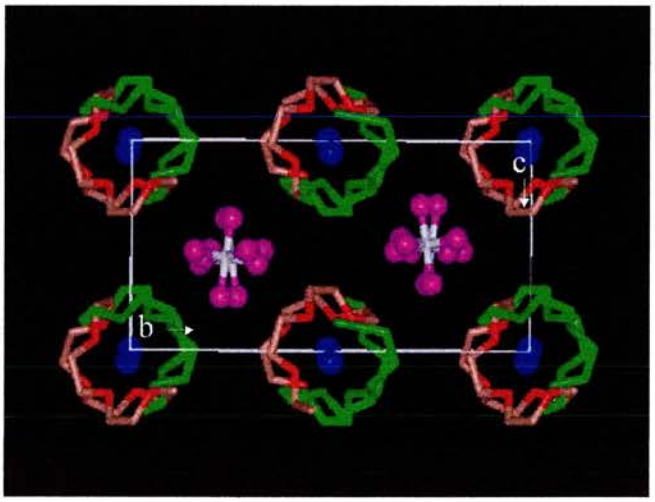

Figure 6.1.1.4. *Structure of a 6 to 1 complex with unit cell parameters annotated*

suggests the terminal C_2H_5 units are sticking out from the tunnels, rather than lying along their axis. The 'b' direction also increases by around 1.0% indicating a protrusion of the chain ends. This makes sense as there are no oxygens in the C_2H_5 fragment necessary to co-ordinate to lithium, thus the chain ends are more likely to move away from the sterically crowded environment of the co-ordination tunnels.

Thermal analysis by DSC indicates that the melting temperature of the complex with ethoxy end capped PEO is lower than its methoxy endcapped analogue by around 19K (see figure 6.1.1.5). This suggests that more disorder in the crystalline phase due to more defects and/or conformational disorder of the chain ends.

There was no evidence of an amorphous phase present from the DSC data over the range of –100 to 100°C.

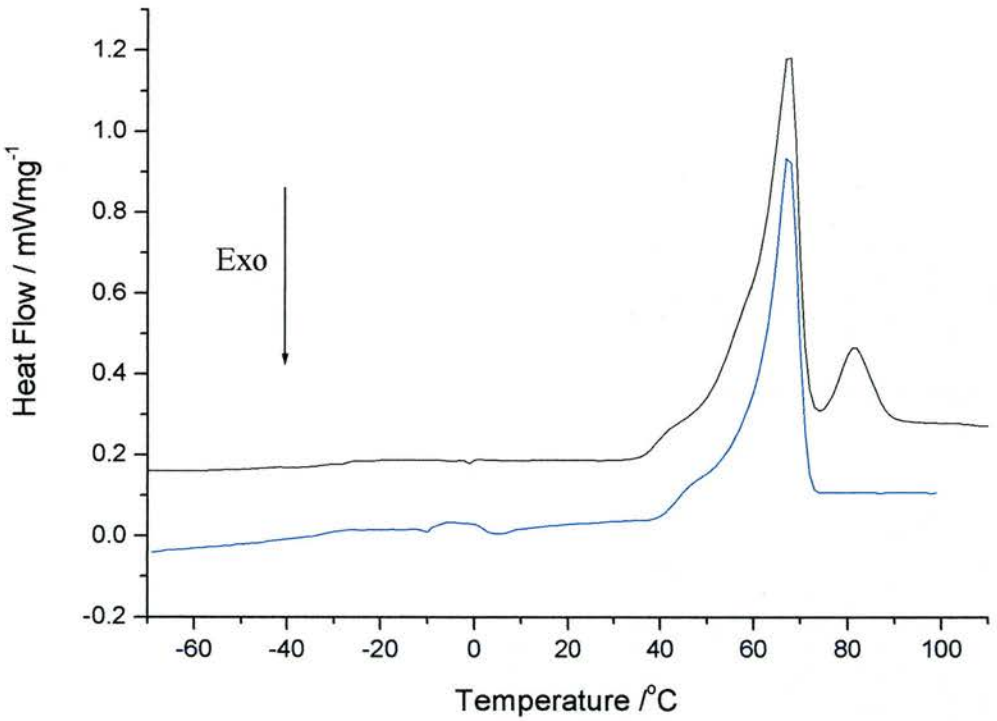

Figure 6.1.1.5. *DSC traces of $P(EO)_6$:$LiPF_6$ prepared from ethoxy terminated PEO. As prepared (black). Recrystallised fom melt (blue).*

The slight change in functionality going from methoxy to ethoxy has the result of increasing the conductivity of the material 10 fold (see figure 6.1.1.6). Interestingly the 'as cast' sample that exhibited the extra peaks in its powder x-ray diffraction pattern from the gamma phase had a slightly lower conductivity indicating that the 2nd phase is likely to be an insulator (see section 6.1.2).

The reason for the increase in conductivity could be the result of a higher concentration of lattice defects caused by the presence of the 'extra' CH_2 moiety within the structure. Also the change in lattice parameters could be having an effect on the conductivity of this material.

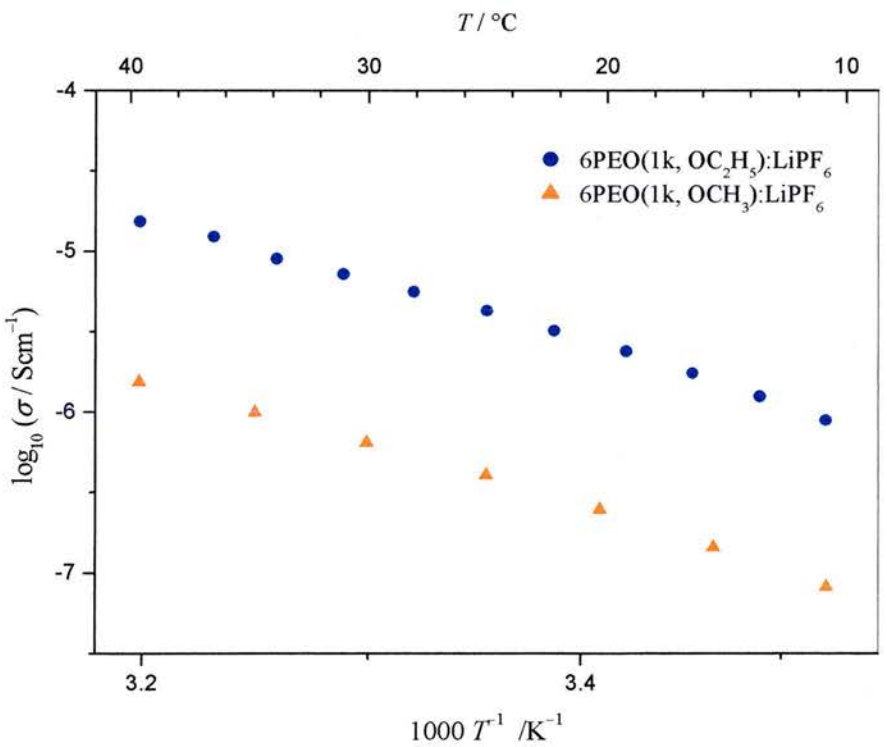

Figure 6.1.1.6. *Plot of log σ vs reciprocal temperature for pure α-phase $P(EO)_6$:$LiPF_6$ prepared from methoxy terminated PEO (orange triangles) and α-phase ethoxy terminated PEO (blue circles)*

Close examination of the conductivity data shows a slight step in conductivity of the complex prepared with ethoxy terminated PEO highlighted in figure 6.1.1.7, compared to the methoxy endcapped material.

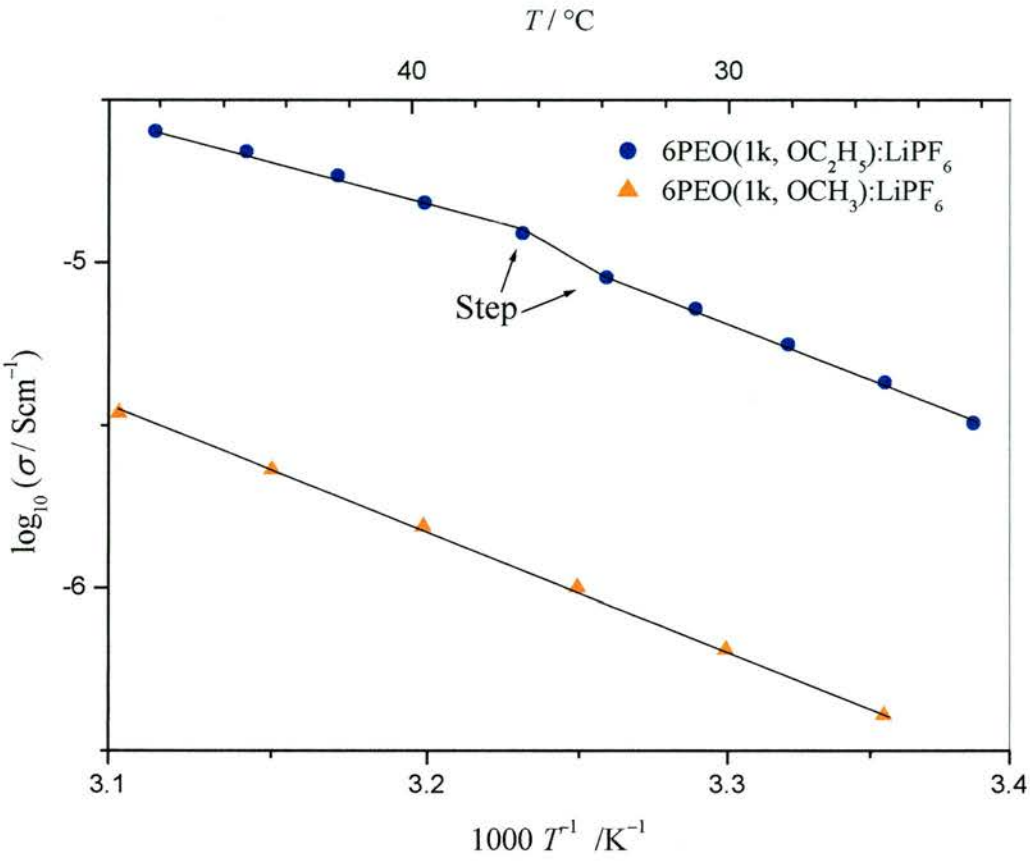

Figure 6.1.1.7. *Plot of log σ vs reciprocal temperature for pure α-phase $P(EO)_6$:$LiPF_6$ prepared from methoxy terminated PEO (orange triangles) and pure α-phase ethoxy terminated PEO (blue circles)*

This step correlates with a shoulder on the low temperature side of the melting endotherm which starts at ~ 36°C and continues for around 15 degrees before the onset of melting (see fig 6.1.1.5), such phenomena (a step in conductivity and the presence of an endotherm at the same temperature) are similar to effects observed with plastic crystalline conductors[2].

Plastic crystals are mesophases formed by molecules that can exhibit orientational disorder while retaining long-range translational order. A pre-melting endotherm is witnessed (referred to as the plastic transition (Tpc)). This endotherm is caused by the onset of conformational disorder within the lattice (analogous to the movement of C_2H_5 end groups in our case) and coincides with an increase in conductivities when these materials are doped with lithium salts[1]. It is interesting that the increase in conductivity is relatively modest. This may suggest that the static disorder that exists below the onset of dynamic or conformational disorder has a more profound influence on conductivity than does the conformational disorder.

6.1.2 $P(EO)_6$:$LiAsF_6$ Synthesised using Ethoxy Terminated PEO of Mw 1000

Samples of $P(EO)_6LiAsF_6$ were prepared in the standard manner using ethoxy terminated PEO of Mw 1000 (see section 3.1.1). The powder x-ray diffraction pattern is similar to that for the as cast $P(EO)_6$:$LiPF_6$, with peaks corresponding to the α – phase accompanied by by additional peaks from the γ – phase (see figure 6.1.2.1.).

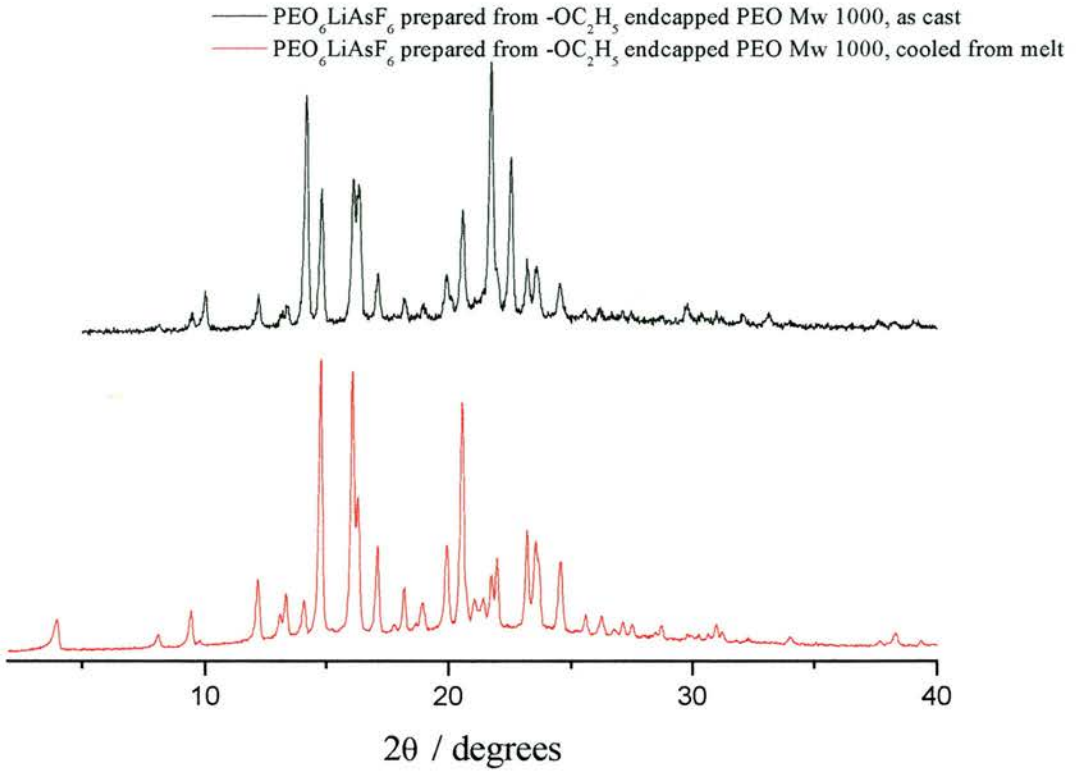

Figure 6.1.2.1 PXRD pattern of $P(EO)_6$:$LiAsF_6$ prepared from ethoxy terminated PEO of Mw 1000 'as cast' (black) and cooled from melt (red).

However, whereas melting and cooling the phosphate complex removed the γ – phase, this action when applied to the arsenate complex served to produce a pure phase γ–$P(EO)_6$:$LiAsF_6$, (fig. 6.1.2.2). DSC analysis shows two endothermic features on the first heating. These events have been assigned to a phase change from alpha to gamma and then subsequent melting of the gamma phase (figure 6.1.2.3). This reduces to only one peak on the second heating cycle, indicating that on the timescale

of DSC (10 $Kmin^{-1}$) the phase transformation from alpha to gamma $P(EO)_6$:$LiAsF_6$ (-OC_2H_5 endcapped PEO) is irreversible. Subsequently, PXRD carried out on the same gamma phase 3 months after initial conversion, showed no evidence of reversibility. A possible unit cell for the γ-$P(EO)_6$:$LiAsF_6$ sample was obtained from the powder diffraction pattern using the TREOR90 program[3] and the first 18 reflections. This cell has a volume compatible with known unit cell volumes of polymer electrolyte complexes.

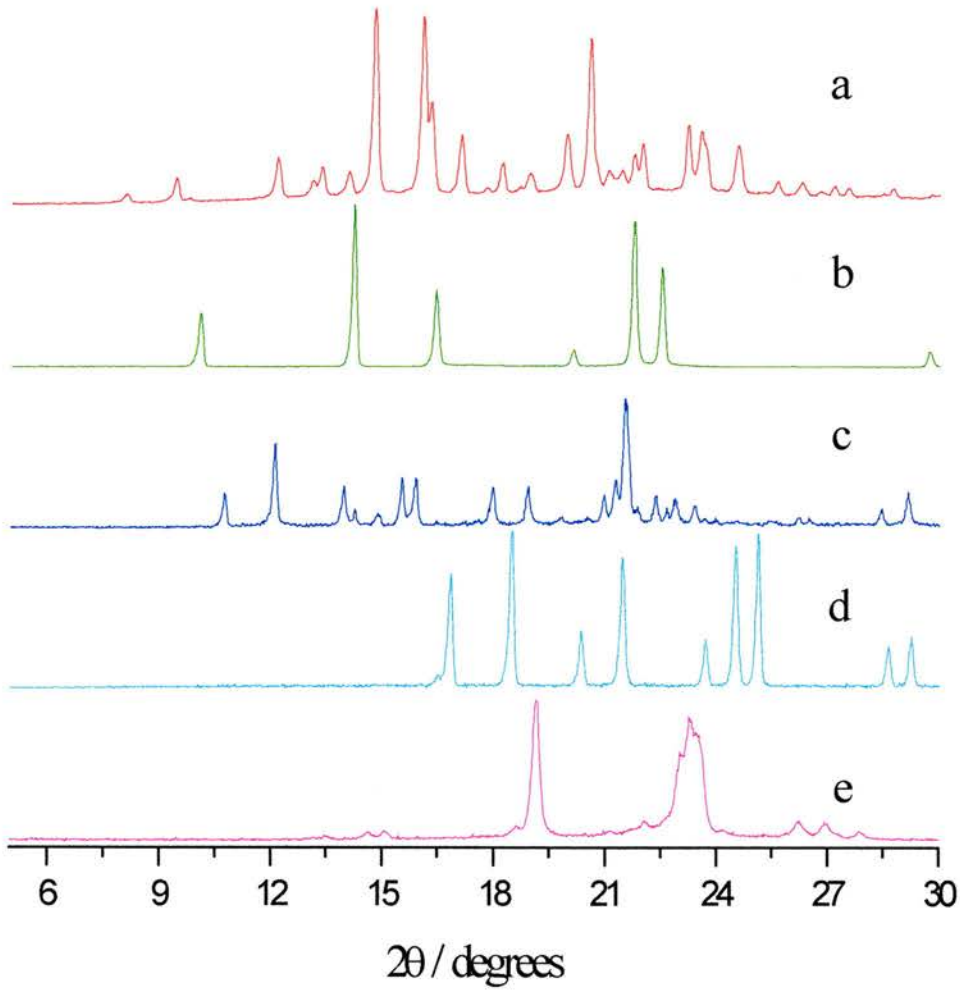

Figure 6.2.1.2 PXRD patterns of (a) γ-$P(EO)_6$:$LiAsF_6$ (-OC_2H_5 end capped PEO), (b) α-$P(EO)_6$:$LiAsF_6$ (-OCH_3 terminated PEO), (c) $P(EO)_3$:$LiAsF_6$, (d) $LiAsF_6$, (e) PEO

It has dimensions a = 22.7375 , b = 9.7336, c = 9.4070, β = 106.929°. However despite spirited efforts to elucidate the structure *ab-intio* from the powder diffraction data, no solution has yet been reached.

The new γ-phase obtained from the melt-cooled complex has a much lower conductivity than the as cast material which consists of a mixture of α/γ phase (see figure 6.1.2.4)

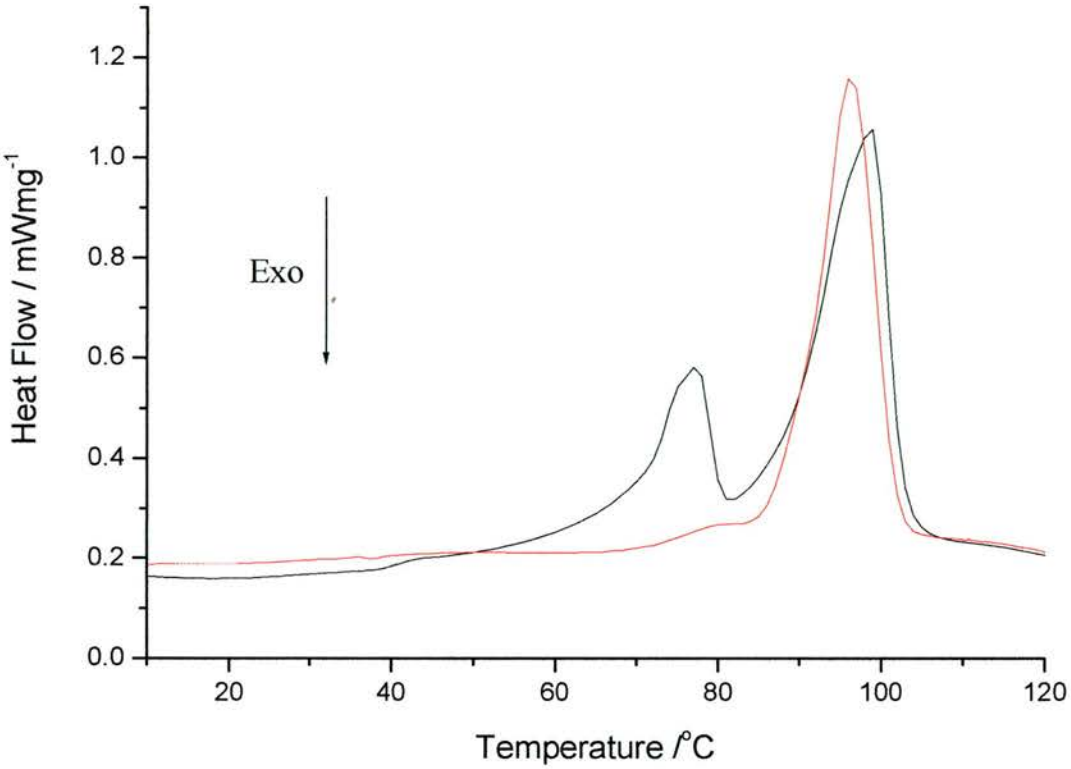

Figure 6.2.1.3. *DSC trace of $P(EO)_6$:$LiAsF_6$ prepared from ethoxy terminated PEO of Mw 1000. As prepared (black), cooled from melt (red).*

The conductivity of the ethoxy terminated gamma phase also has a significantly lower conductivity than the pure alpha phase of $P(EO)_6$:$LiAsF_6$, synthesised from methoxy terminated PEO (see fig. 6.1.2.4).

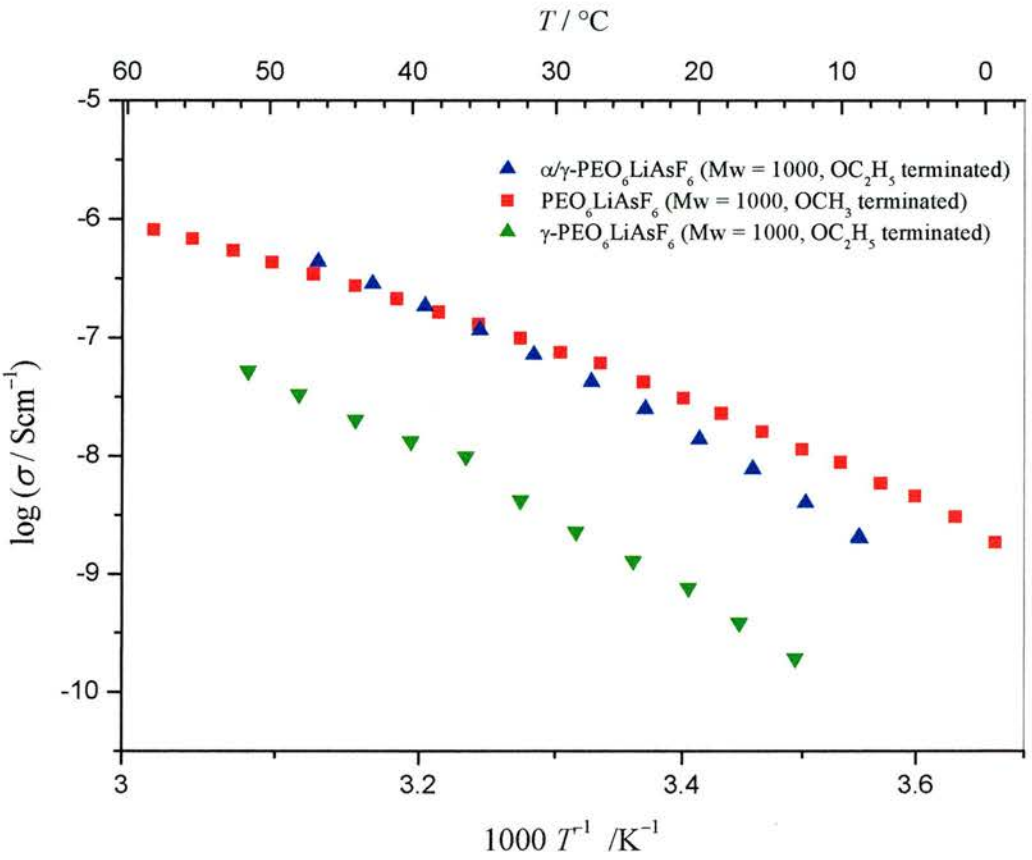

Figure 6.1.2.4. *Plots of log σ vs reciprocal temperature for α-P(EO)$_6$:LiAsF$_6$ -OCH$_3$ terminated PEO (red squares), α/γ P(EO)$_6$:LiAsF$_6$ phase mixture –OC$_2$H$_5$ teminated PEO (blue triangles), γ-P(EO)$_6$:LiAsF$_6$ –OC$_2$H$_5$ terminated PEO (green triangles)*

Interestingly, the levels of conductivity exhibited by the alpha/gamma phase mixture of P(EO)$_6$:LiAsF$_6$ prepared from ethoxy terminated PEO, are comparable to that of the pure alpha phase P(EO)$_6$:LiAsF$_6$ prepared with methoxy terminated PEO. This indicates that although there in a high proportion of low conductivity gamma phase in the sample, the alpha phase of ethoxy terminated P(EO)$_6$:LiAsF$_6$ that is present must, by inference, be of higher conductivity than the methoxy terminated α-P(EO)$_6$:LiAsF$_6$ to compensate.

From the work carried out on the 6:1 complexes of both LiPF$_6$ and LiAsF$_6$ prepared with ethoxy endcapped PEO, it can be seen that the slight change in functionality of

the PEO chain ends, has a structure directing effect. This is shown by the crystallisation of γ-$P(EO)_6$:$LiXF_6$, X = P, As, a phase never witnessed when preparing these complexes with methoxy terminated PEO (preliminary results with propxy end capped PEO also exhibit a structure directing effect towards the gamma phase). The conductivity increases below the 'plastic transition' can be explained as a consequence of introducing defects into the crystal lattice and at higher temperatures above the 'plastic transition' a relative increase in conductivity is caused by conformational disorder of the chain's terminal groups.

6.2 Properties of 6:1 Complexes Synthesised using Benzyl (-OCH_2Ph) Endcapped PEO of Mw 1000

6.2.1 $P(EO)_6$:$LiPF_6$ Synthesised using Benzyl Terminated PEO of Mw 1000

Samples of the 6:1 complex of $LiPF_6$ and di-benzyl PEO Mw 1000 were prepared in the standard manner (see section 3.1.1). The materials produced were soft solids, self supporting and highly viscous. Benzyl groups were chosen as they offer a large departure from the methoxy endcapped PEO both in terms of sterics and functionality. The benzyl groups also offer the possibility of creating both rotational and conformational disorder within the complexes.

The benzyl end groups have a profound effect on the complexes. The materials contain both amorphous and crystalline phases. In this respect they differ from the 'completely' crystalline complexes made from methoxy and ethoxy endcapped PEO. There is evidence of crystalline material from their PXRD patterns (see fig. 6.2.1.1) and also from the melting peaks in the DSC data for these samples (see fig. 6.2.1.2). The presence of a glass transition in the DSC data indicates the presence of amorphous material (see figure 6.2.1.2). The DSC data are clearly complex and different to that of the methoxy terminated complexes.

From their similar PXRD patterns, it can be seen that the complexes prepared from benzyl terminated PEO are structurally comparable to that of the complexes prepared from methoxy and ethoxy terminated PEO (figure 6.2.1.1). However the complex departs from the high degree of order seen with the complexes prepared from methoxy and ethoxy endcapped PEO. There is some hkl dependent peak broadening

in the PXRD pattern, the peak at 16.5 degrees is especially broad. This corresponds to the 210 reflection and indicates disorder in the ab plane, parallel to 'c'.

Despite the amorphous/crystalline phase mixture these materials have high levels of ionic conductivity around $3x10^{-5}$ S cm^{-1} at room temperature (see figure 6.2.1.3). It has previously been shown by detailed IR spectroscopy carried out by Bruce, Frech et al[4] that the structures of crystalline material can, to a large extent, be retained when a phase change from crystalline to amorphous occurs, with just a loss of register between chains. A recent study using solid state NMR has also confirmed this phenomenon[5]. It is possible that the structural aspects of the crystalline material that lend themselves to ionic conductivity ie. dissociation of cation and anion and also the presence of a conduction pathway through the matrix prevail despite the crystalline-amorphous transformation.

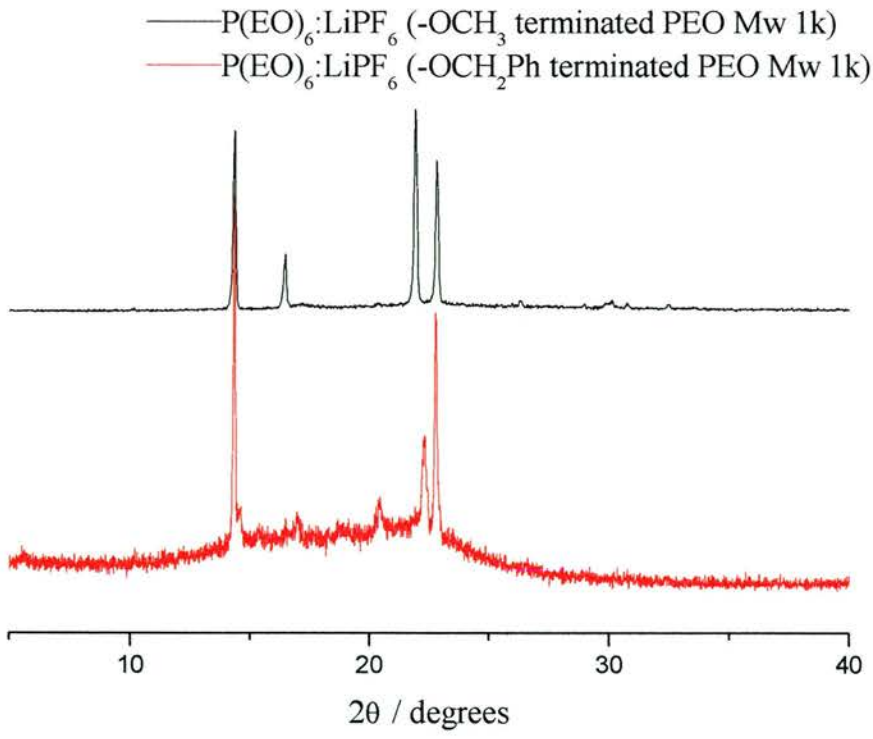

Figure 6.2.1.1. *PXRD patterns of $P(EO)_6LiPF_6$ prepared using benzyl terminated PEO (red) and methoxy terminated PEO (black)*

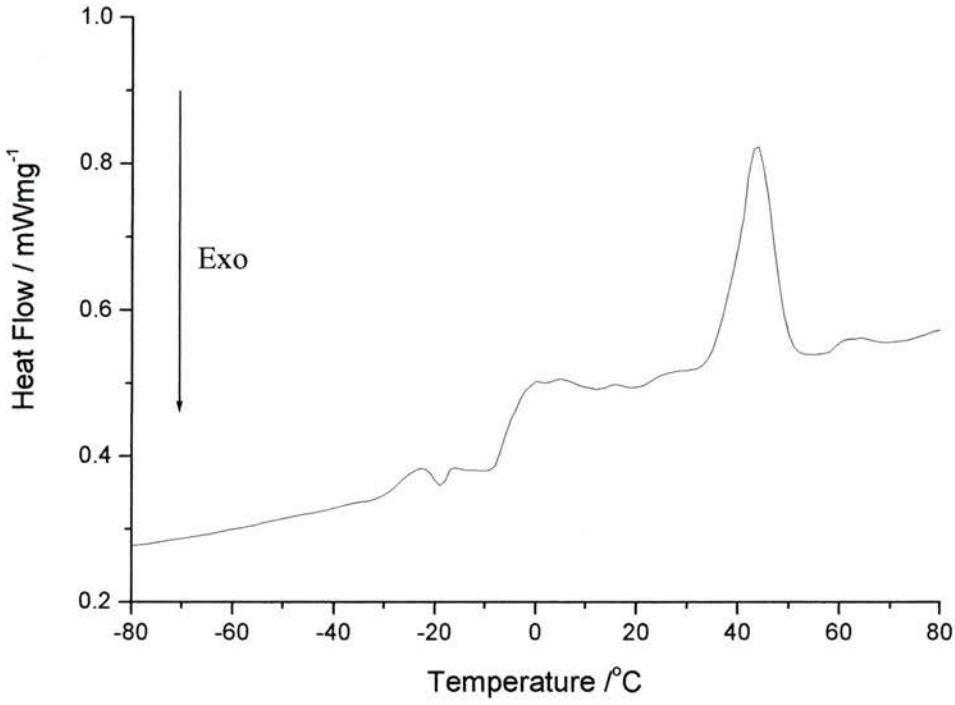

Figure 6.2.1.2. *DSC trace of $P(EO)_6$:$LiPF_6$ prepared from benzyl terminated PEO*

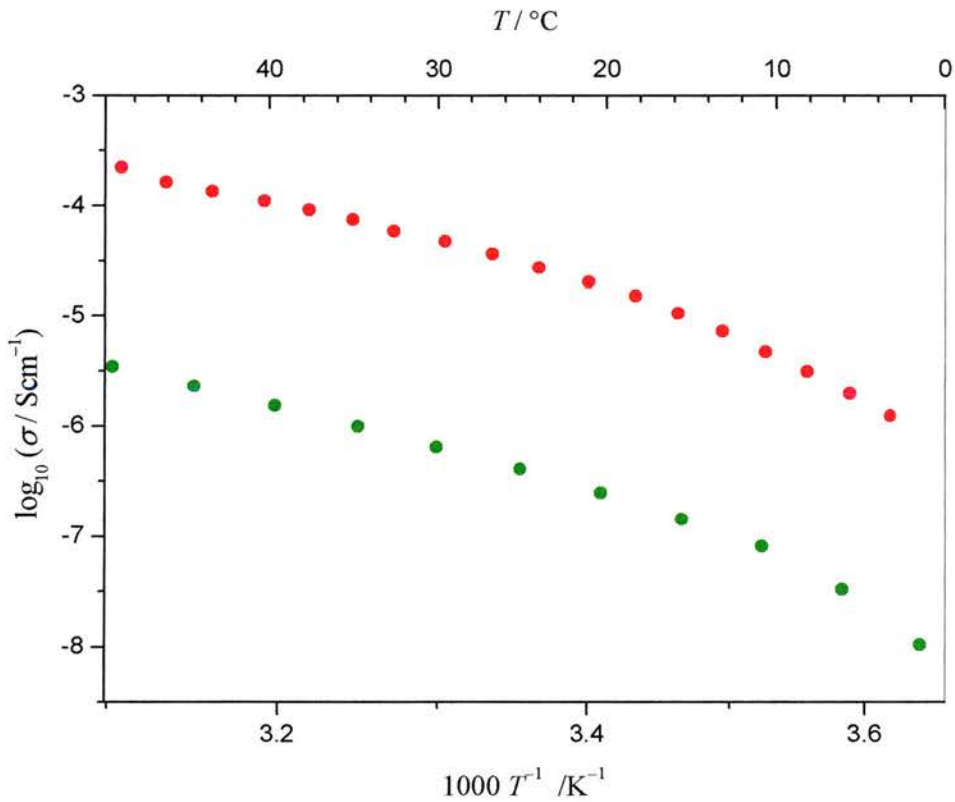

Figure 6.2.1.3. *Plot of log conductivity vs reciprocal temperature for $P(EO)_6$:$LiPF_6$ prepared from benzyl terminated PEO* (red) *and prepared from methoxy terminated PEO (green)*

The effect that the benzyl groups have on the ion transport mechanism is hard to deconvolute. Are these increases in conductivities a result of the benzyl group's presence in a crystalline phase or are they due to a highly conducting amorphous material caused by their presence? Further work to better understand this material should include varying the length of PEO chains, hence varying the % of endgroups. Probing the dynamics of these systems using MAS-NMR seems to be the next obvious action to provide more information about the nature of conductivity in these materials.

6.2.1 $P(EO)_6$:$LiAsF_6$ Synthesised using Benzyl Terminated PEO of Mw 1000

The arsenate analogue of this complex shares many similar properties with the phosphate complex. Similar to the phosphate, the complex possesses both crystalline and amorphous material, as is evident from the glass transition seen in the DSC data witnessed at around –15°C. However from the DSC data (more precisely the magnitude of the change of heat capacities before and after the glass transitions per unit mass of sample), the arsenate complexes seem to have comparatively less amorphous material (there is also some anecdotal evidence for this ie. peak to background ratios on the PXRD data are higher for the arsenate complex and also the arsenate material is more a powder rather than a viscous film).

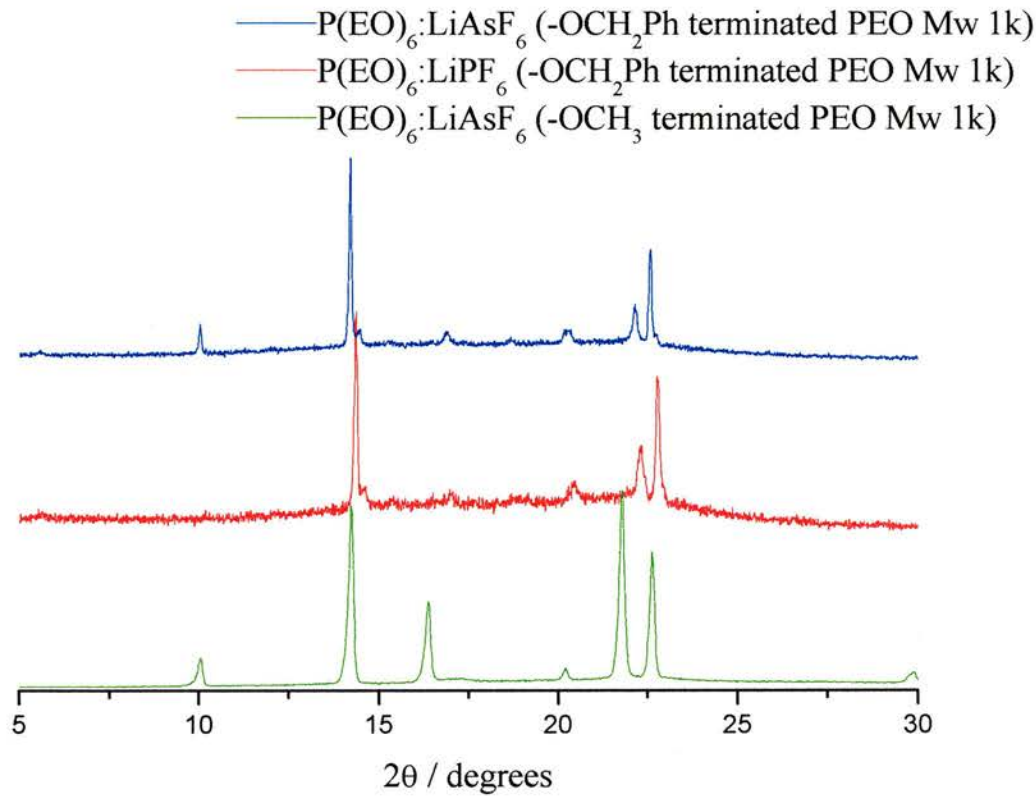

Figure 6.2.1.1. *PXRD patterns of $P(EO)_6$:$LiAsF_6$ prepared using benzyl terminated PEO of Mw 1000 (blue), $P(EO)_6$:$LiPF_6$ prepared using benzyl terminated PEO of Mw 1000 (red), $P(EO)_6LiAsF_6$ prepared using methoxy terminated PEO of Mw 1000 (green.)*

The PXRD patterns of $P(EO)_6$:$LiAsF_6$ are similar to that of the phosphate containing complex prepared from benzyl terminated PEO and also to the PXRD pattern of the $P(EO)_6$:$LiAsF_6$ complex prepared using methoxy terminated PEO (see figure 6.2.1.1). Again as with the phosphate, there is some peak broadening of the 021 reflection, indicating disorder in the ab plane.

The levels of conductivity of the arsenate complexes yield are substantially lower than their phosphate counterparts (see fig. 6.2.1.2). Around 10^{-6} S cm^{-1} at room temperature.

Although the levels of conductivity are significantly lower than the phosphate analogue the effect of endcapping the chains with benzyl groups is a 5 fold increase in conductivity at room temperature.

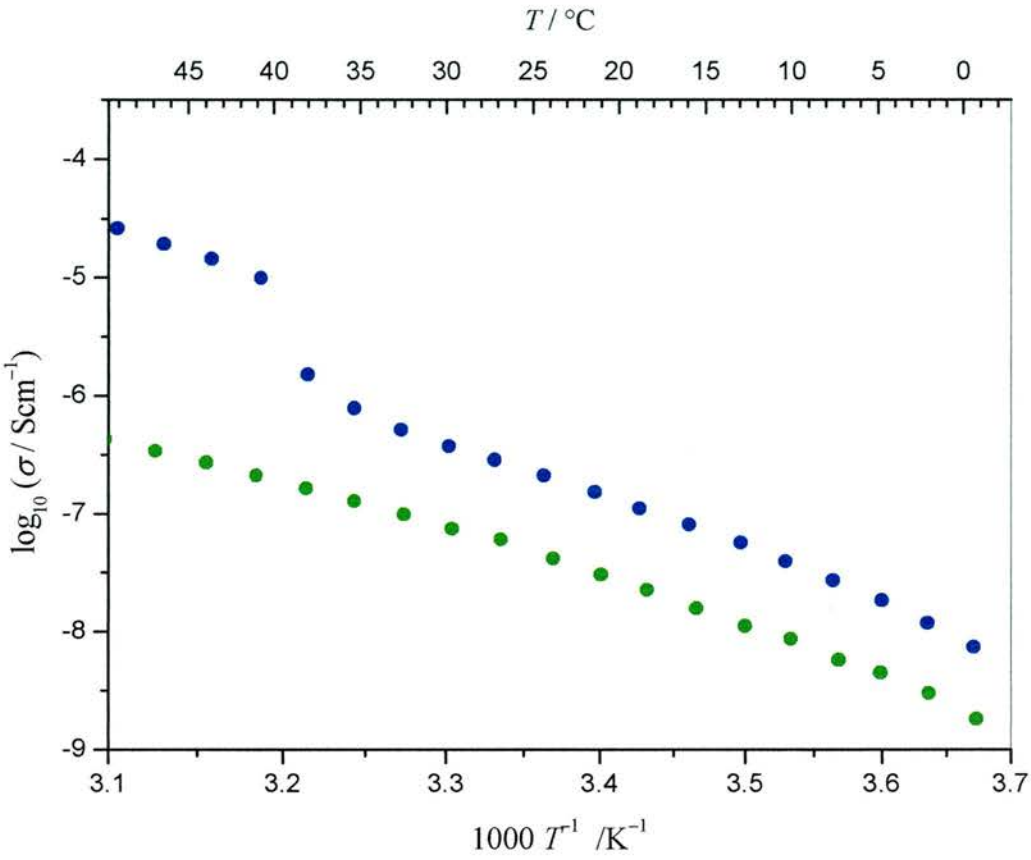

Figure 6.2.1.2. *Plot of log conductivity of $P(EO)_6$:$LiAsF_6$ prepared from PEO Mw 1k terminated with benzyl groups (blue) and prepared from PEO Mw 1k terminated with methoxy groups*

However, more interestingly, trends in the conductivity of $P(EO)_6$:$LiAsF_6$ prepared with benzyl end capped PEO may be correlated with the DSC data for this material (see figure 6.2.1.3). The large increase in conductivity (one order of magnitude) that occurs at around 38°C correlates with an endothermic event on the DSC trace (see figure 6.2.1.3). It is hypothesised that this thermal event is due to the benzyl end groups becoming conformationally disordered, (analogous to a plastic transition), and this disorder is, in turn, causing the large increase in ion mobility in the material. The

higher temperature endotherm in the DSC is due to the melting of the conformationally disordered crystalline phase.

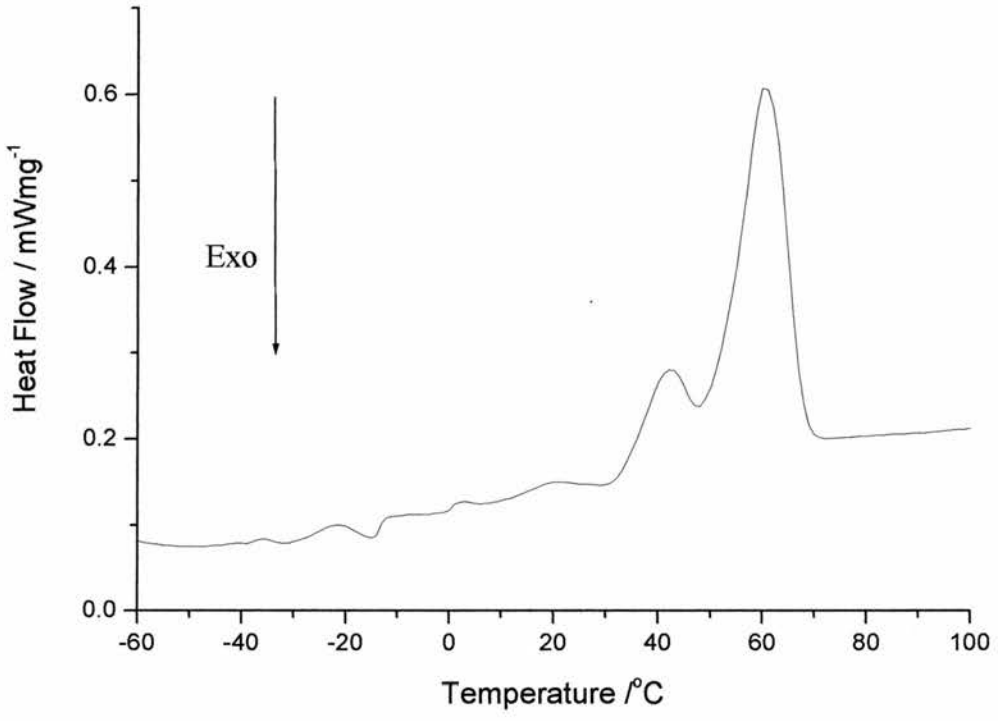

Figure 6.2.1.3. *DSC trace of PEO_6:$LiAsF_6$ prepared from benzyl endcapped PEO of Mw 1k.*

Essentially, below the 'pseudo plastic transition' the conductivity varies linearly with temperature and above the transition it varies binomially as a function of temperature. A characteristic conductivity profile of plastic crystal ionic conduction[1,6].

There is no evidence of this material producing any crystalline phases other than the one characterised by the PXRD pattern in figure 6.2.1.1.

In essence, the conductivities observed in the complexes of $P(EO)_6$:$LiP(As)F_6$ prepared using PEO end capped with benzyl groups can be attributed to two distinct effects. As the complexes are semi-crystalline, either the presence of a highly conducting amorphous phase, or more likely, as the correlation between DSC

endotherms and change in conductivity profile suggests, crystalline phase conduction enhanced by static defect creation below the onset of conformational/rotational disorder, and further enhanced by this dynamic disorder of the benzyl groups above the onset.

6.3 Properties of 6:1 Complexes Synthesised using Neo-pentoxy (-$OCH_2C(CH_3)_3$) Endcapped PEO of Mw 1000

6.3.1 $P(EO)_6$:LiPF6 Synthesised using Neopentoxy Terminated PEO of Mw 1000

Samples of $LiPF_6$ and di-neopentoxy terminated PEO of Mw 1k were prepared in the standard manner (see section 3.1.1.). The materials produced were soft solids, self supporting and highly viscous. Neopentoxy end groups were chosen as they offered a large difference in terms of sterics compared to methoxy end groups, while at the same retaining their aliphatic nature.

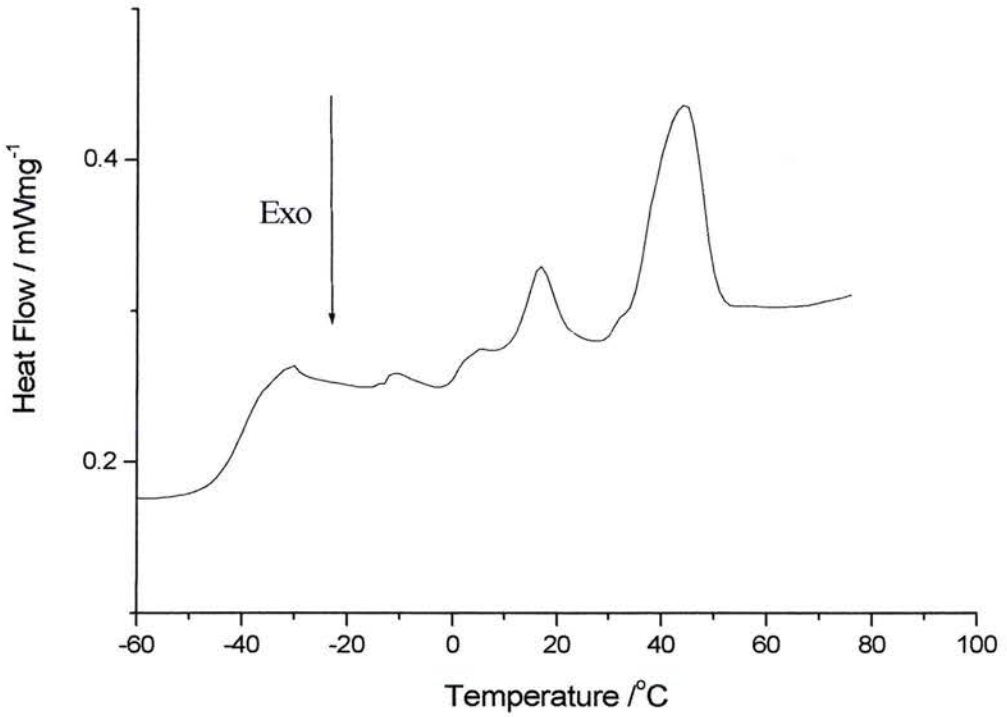

Figure 6.3.1.1. *DSC of P(EO)6:LiPF6 prepared using PEO Mw 1000 with neopentoxy end groups*

As with the complexes prepared with benzyl terminated PEO, these materials are semi-crystalline and contain both crystalline and amorphous phases, as is shown by DSC evidence (see figure 6.3.1.1). The onset of a glass transition is seen at around -45°C, indicating amorphous material. Endothermic peaks with maxima at around 16°C and 46°C indicate the presence of crystalline material.

The existence of a crystalline phase is also apparent from the PXRD pattern of this material. (see fig. 6.3.1.2). We see a pattern very similar to the benzyl endcapped material, with the same prominent peaks present in the methoxy phase. It seems that the crystal lattice of this material can also accommodate the presence of the bulky neopentyl group at the chain ends.

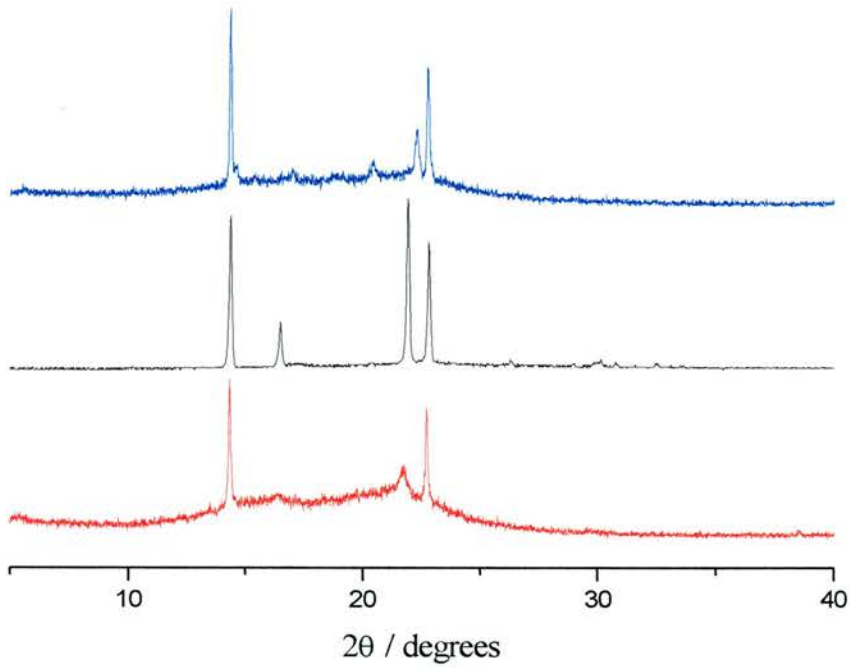

Figure 6.3.1.2. *PXRD patterns of $P(EO)_6$:$LiPF_6$ prepared from benzyl terminated PEO Mw 1000 (blue), methoxy terminated PEO Mw 1000 (black) and neopentoxy terminated PEO Mw 100 (red).*

There is peak broadening in the PXRD pattern of the neopentoxy endcaped complex, occurring with the peaks at 16.5 and 21.7 degrees corresponding to 210 and 140 relections. This indicates disorder in the ab plane parallel to 'c'.

Similar to $P(EO)_6$:$LiPF_6$ prepared using PEO Mw 1000 terminated in benzyl groups these materials exhibit high levels of conductivity (see figure 6.3.1.3). However due to the complicated mixture of amorphous and crystalline phases these materials exhibit, it is hard to prove conclusively whether conduction is taking place in the disordered amorphous phase or ordered crystalline phase.

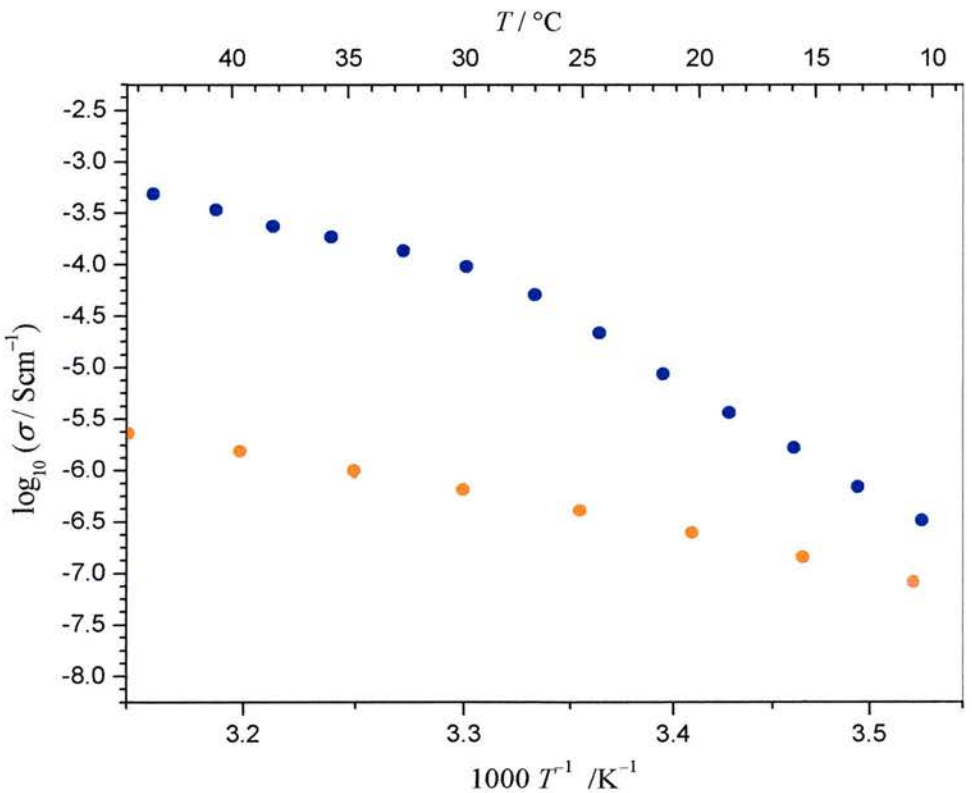

Figure 6.3.1.3. *Plot of log conductivity vs reciprocal temperature for $P(EO)_6$:$LiPF_6$ prepared from OCH_3 terminated PEO (orange circles)and $P(EO)_6$:$LiPF_6$ prepared from neopentoxy terminated PEO (blue circles)*

Of the numerous endotherms witnessed in the DSC data of this material, the only one that correlates with a change in the conductivity profile of the material is the melting peak which has its onset at 30°C. At this point on the plot of log conductivity vs reciprocal temperature there is a noticeable change in the slope of the collected data. This suggests that the melting of the crystalline component of the material decreases the activation energy associated with ion movement. If conduction occured in the amorphous phase that co-exists with the crystalline phase below 30°C then a step change in magnitude but a similar activation energy would have been expected on melting of the crystalline phase. The change of slope suggests that the conductivity below 30°C is due to the crystalline phase.

6.3.2 $P(EO)_6$:LiAsF6 Synthesised using Neopentoxy Terminated PEO of Mw 1000

Samples of $LiAsF_6$ and di-neopentoxy terminated PEO of Mw 1k were prepared in the standard manner (see section 3.1.1.). The materials produced were soft solids, self supporting and highly viscous. These materials are semi-crystalline and contain both crystalline and amorphous phases as is shown by DSC (see figure 6.3.2.1). The onset of a glass transition is seen at around -30°C, indicating amorphous material. Endothermic peaks at around 18°C and 50°C and 57°C indicate the presence of crystalline material.

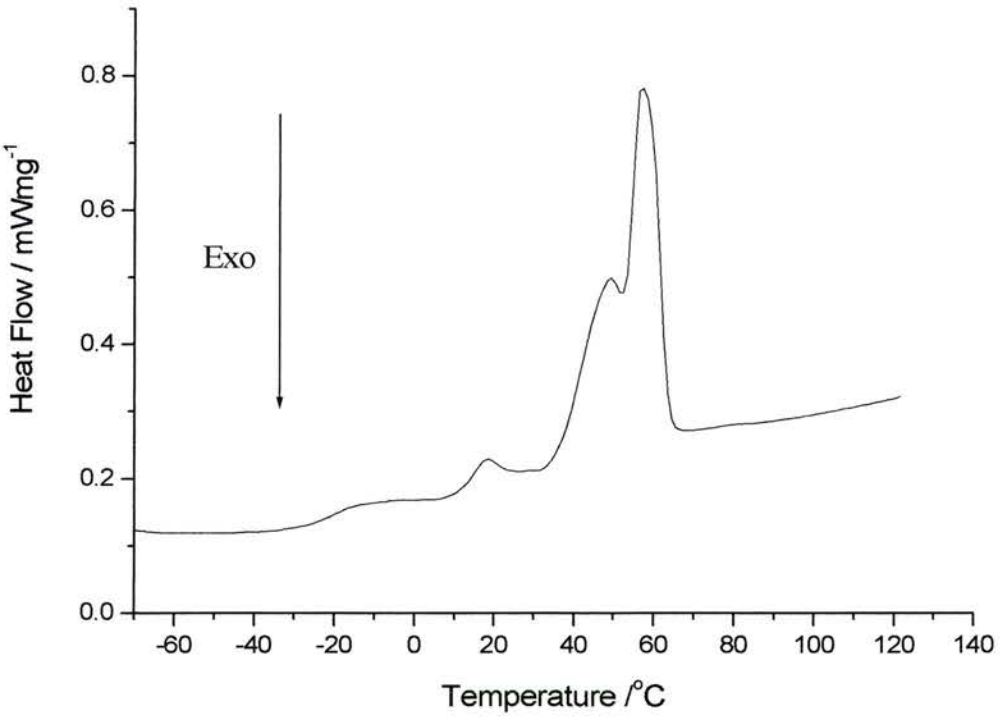

Figure 6.3.2.1. *DSC of $P(EO)_6$:$LiAsF_6$ prepared from neopentoxy terminated PEO of Mw 1000*

The PXRD patterns of $P(EO)_6$:$LiAsF_6$ prepared from neopentoxy terminated PEO indicate the presence of a crystalline phase, with similar features to the one obtained when the complex is prepared from methoxy and benzyl terminated PEO (see figure 6.3.2.2). As is the case with the phosphate analogue the ordered crystalline structure seems to be able to accommodate the bulky neopentyl endgroups within the lattice. Again there is some hkl dependant peak broadening indicating disorder in the ab plane. There was no evidence of any different crystalline phases or polymorphism in the samples prepared using this PEO.

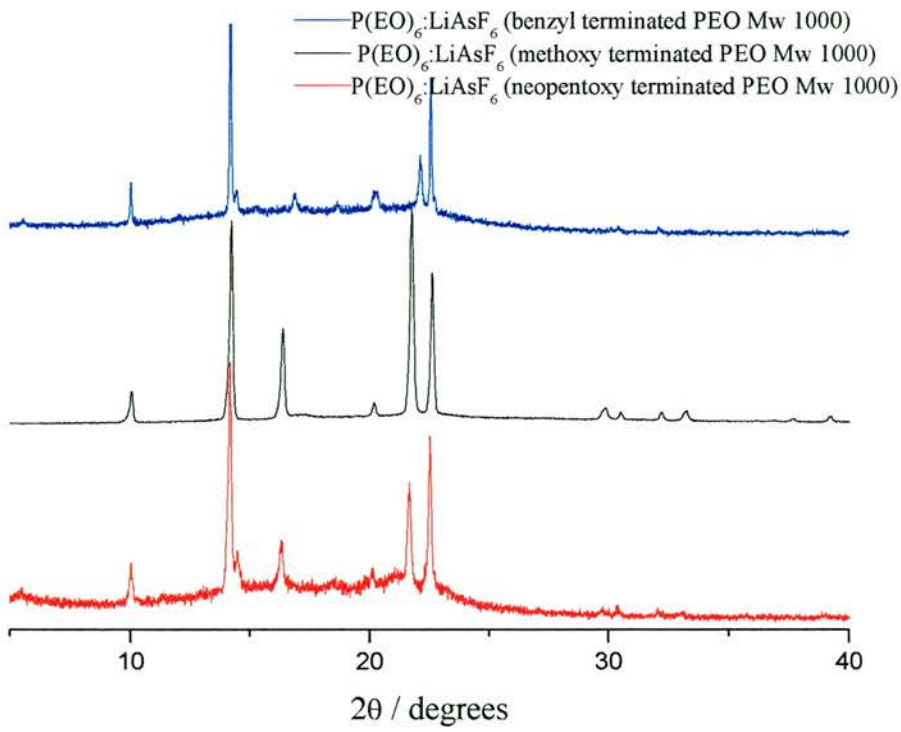

Figure 6.3.2.2. PXRD pattern *of $P(EO)_6$:$LiAsF_6$ prepared from PEO of Mw 1000 neopentoxy terminated (red), methoxy terminated(black) and benzyl terminated (blue).*

Again, as can be seen with the phosphate analogue of this complex, the effect of changing the endgroups from methoxy to neopentoxy is an increase in the level of

conductivity (see figure 6.3.2.3). The complex prepared from neopentoxy PEO exhibits a conductivity of around 10^{-5} at 30°C, an increase in conductivity of almost 2 orders of magnitude.

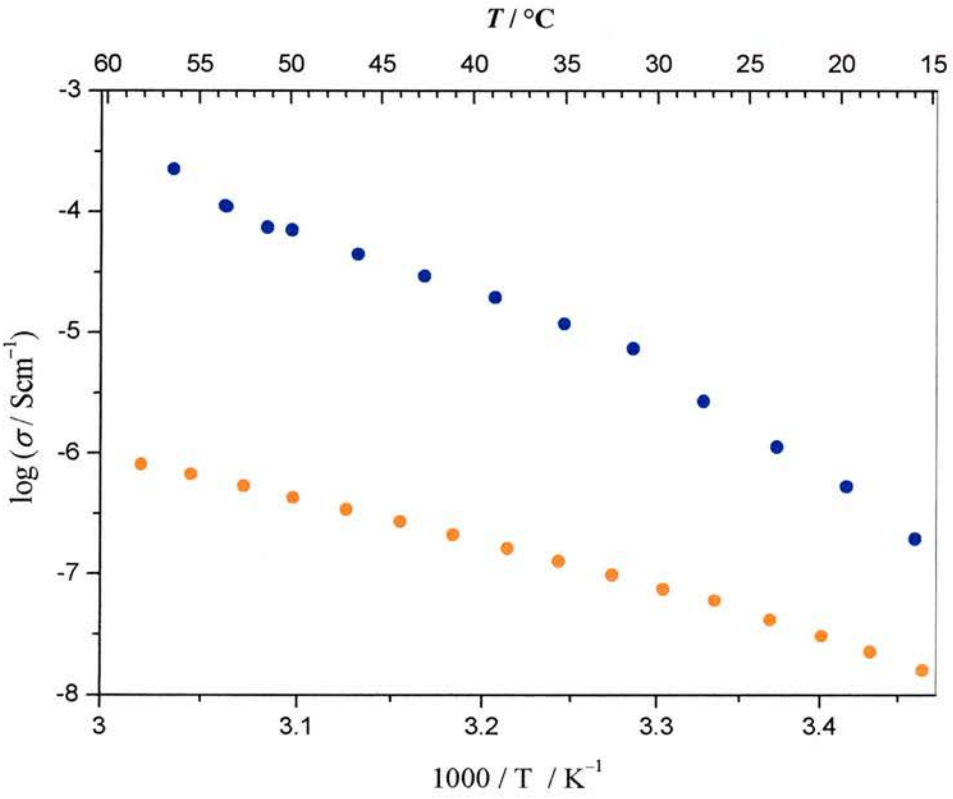

Figure 6.3.2.2. *Plot of log conductivity vs reciprocal temperature for $P(EO)_6$:$LiAsF_6$ prepared from neopentoxy terminated PEO of Mw 1000(blue circles)and methoxy endcapped PEO of Mw 1000(orange circles)*

Again, because of the mixture of crystalline and amorphous phase present within the sample, it is hard to definitively identify the mechanism by which the conductivity is being enhanced. From the profile of the plot of log conductivity vs. reciprocal temperature, changes in activation energies can be seen that roughly correlate with endothermic events seen in the DSC data. There is a definite change in slope of the conductivity profile between 31 and 35 degrees. At this temperature in the DSC data there is an onset of an endothermic event.

This points to the conductivity arising mainly in the crystalline phase. If the conductivity in this material were occurring in the crystalline phase, this endothermic event could be the result of conformational disordering of the bulky neo-pentoxy chain ends, lowering the activation energy associated with ion movement. On the other hand, it could be associated with the melting of a conductivity inhibiting crystalline phase.

More work is needed to quantify the effects seen with this system. Possibly MAS-NMR will be able to probe the dynamics of the functionally different chain ends as a function of temperature to better understand the dynamics they exhibit. Also, diluting the effect of chain ends by increasing the length of the PEO chains would provide materials capable of determining the method by which these modified materials allow increased levels of conductivity.

---

[1] Alarco, P.J., Abu-Lebdeh, Y., Abouimrane, A., Armand, M., *Nature Materials*, **3**, 476-480 (2004) MacFarlane, D.R., Huang J., Forsyth, M., *Nature*, **402** (1999)

[2] Pas, S.J., Pringle, J.M., Forsyth, M., MacFarlane, D.R., *Phys. Chem. Chem. Phys.*, **6**(13), 3721 - 3725

[3] Werner, P.-E., Eriksson, L. and Westdahl, M., TREOR, a semi-exhaustive trial-and-error powder indexing program for all symmetries. *J. Appl. Crystallogr.* **18** (1985) 367-370

[4] Frech, R., Chintapalli, S., Bruce P.G. & Vincent C.A., *J. Chem. Soc. Chem. Commun.* 157-158 (1997)

[5] Spevacek, J., Brus, J., Dybal, J., *Solid State Ionics*, **176**. 163-167 (2005)

[6] Abu-Lebdeh Y., Alarco P.J. and Armand, M., *Angewandte Chemie – International Edition*, **42** (47), 4499 (2003)

Chapter 7

6 to 1 Complexes of PEO and $LiXF_6$ (X = P, As) Prepared Using Monodispersed PEO of Mass 1015 Daltons.

One of the features that distinguishes polymers from lower molecular weight molecules is their polydispersity. Such polydispersity does however make an understanding of the physical properties of polymers, especially those dependant on the chain length, more difficult to study in terms of understanding structure/property relationships. As a result we have prepared and investigated monodispersed ethylene oxide and its 6:1 complexes with $LiXF_6$ (X = P, As).

Some recent studies suggest monodispersity promotes order within polymeric material. Seungja *et al* give an example of monodispersity inducing order into polymers[1]. They prepare a film of a monodispersed polymer that exhibits smectic ordering. They show by small angle x-ray diffraction that their 'rod-like' macromolecules are organised into layers. Also, Le Fevere De Ten Hove *et al* use monodispersed polyethylene regions within their materials to affect a structure controlled crystal thickness[2].

The result of the distribution of chain lengths in the complexes of $P(EO)_6$:$LiXF_6$ is that chain ends are randomly distributed throughout the lattice, essentially acting as point defects (instead of the intra chain case where there are two adjacent CH_2 groups, there would be two CH_3 groups next to each other at the chain termini). To probe the effect that this dispersion of chain lengths has on the properties of these polymer

electrolytes, a monodispersed di-methoxy endcapped PEO consisting of 22 repeat units was custom synthesised using state-of-the-art prep scale reverse phase HPLC.

The structure of the 6 to 1 complexes of PEO and $LiXF_6$, X= P, As, Sb consists of two non-helical chains that interconnect to form a tunnel in which the lithium ions reside[3] (see fig 1.3). When there is a distribution of chain lengths as there is in the polydispersed case, chain ends must be randomly distributed throughout the length of the tunnels[4]. However with chains of equal length, chain ends occur regularly and the possibility then arises that they become aligned or staggered relative to each other (see fig 7.1).

In this chapter the effects that dispersion has on these materials is investigated by comparison between polymer electrolytes prepared using polydispersed and monodispersed PEO of equivalent weight average molecular mass.

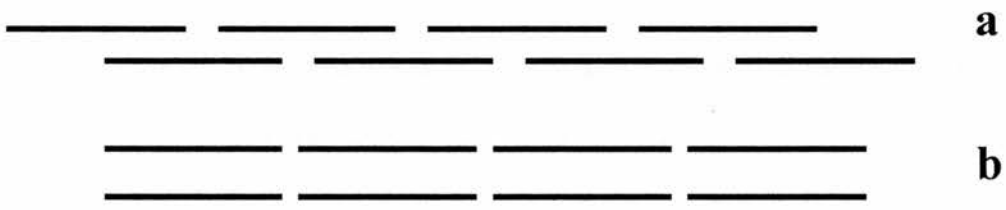

Figure 7.1 *Illustration of possible chain end modulation within the structures of $P(EO)_6$:$LiXF_6$, X = P, As, Sb. a) Staggered arrangement of chain ends, b) Aligned arrangement of chain ends*

7.1 $P(EO)_6$:$LiPF_6$ synthesised using monodispersed PEO of mass 1015 Daltons.

The monodispersed nature of this unique material was confirmed by MALDI-MS. Only one major peak was present (see figure 7.1.1.), corresponding to a polymer with 22 repeat units (1015 Daltons). The peaks to the immediate left hand side of the main peak are due to the presence of different naturally occurring isotopes of carbon, hydrogen and oxygen incorporated in the chain. The small peaks at 44 Daltons either side of the main peak are associated with a small amount of polymer with 21 and 23 repeat units. The polymer was assayed as being >97% molecularly pure by reverse phase HPLC.

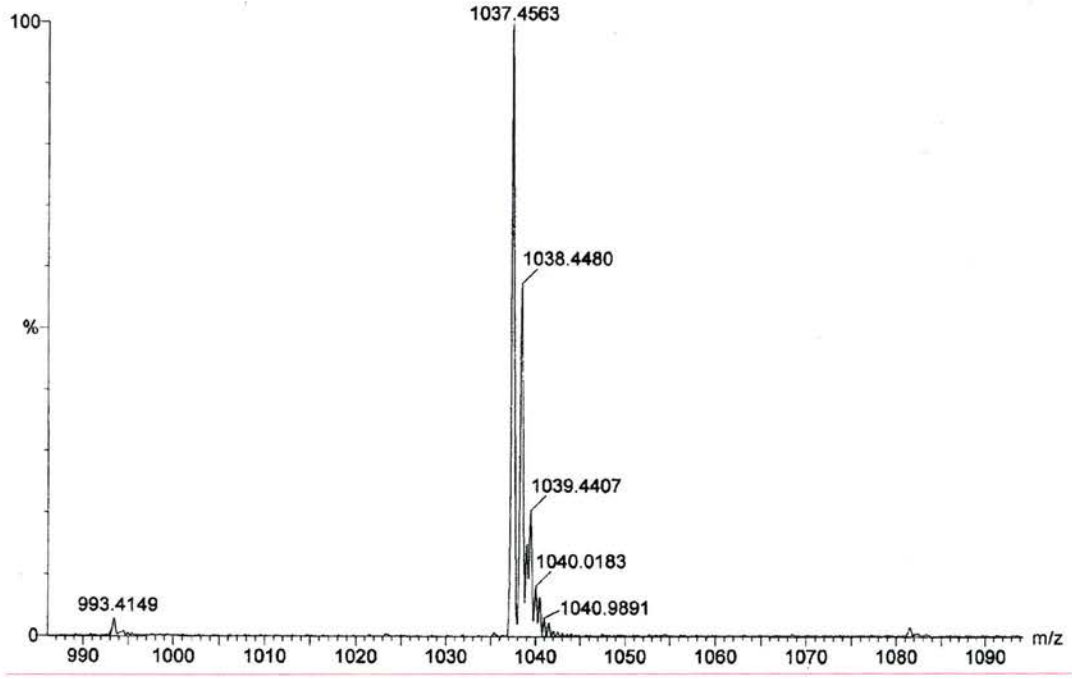

Figure 7.1.1. *MALDI-MS of monodispersed PEO*

Complexes of $P(EO)_6$:$LiPF_6$ were prepared in the standard manner using monodispersed PEO (see section 3.1.1). As expected, the complexes prepared exhibited similar PXRD patterns to the material prepared from the polydisperse

polymer. However there are subtle but important differences in the data (see figures 7.1.2 to 7.1.5). The peak widths are different; the complex prepared with monodispersed PEO has broader peaks indicating crystallite sizes are smaller for these monodispersed complexes (figure 7.1.5). Also peak positions vary when comparison with the pattern obtained of the complex prepared from the polydisperse is made (most evident in figures 7.1.3 and 7.1.4.), Some peaks shift to higher and some to lower 2θ values compared with the polydispersed material.

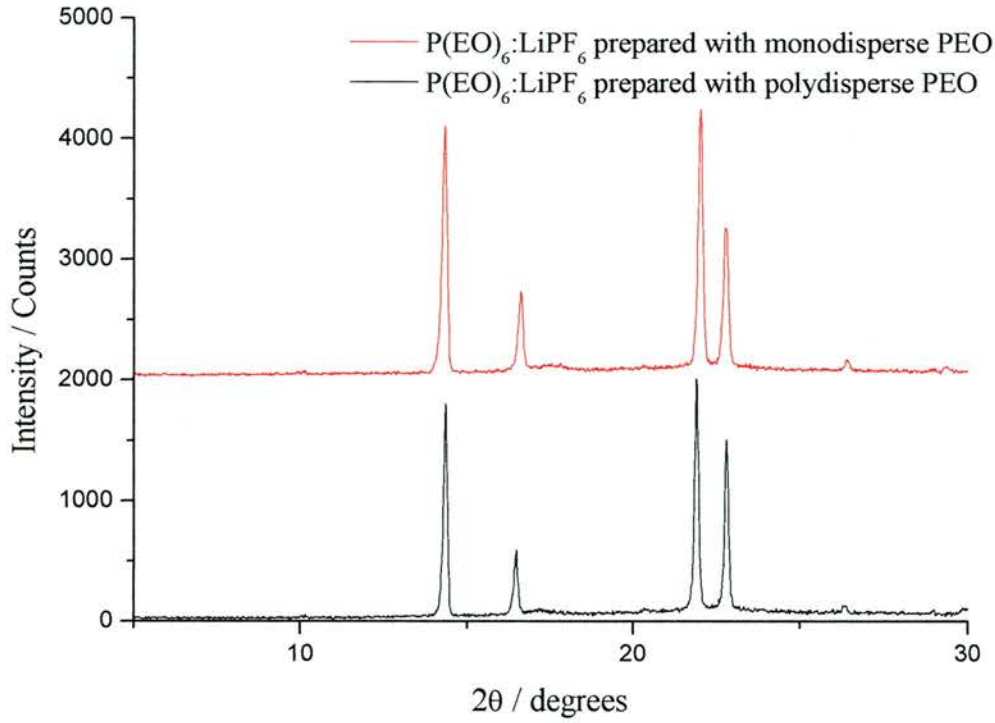

Figure 7.1.2. *PXRD patterns of $P(EO)_6$:$LiPF_6$ prepared from monodispersed PEO (red) and polydisperse PEO 1000 (black).*

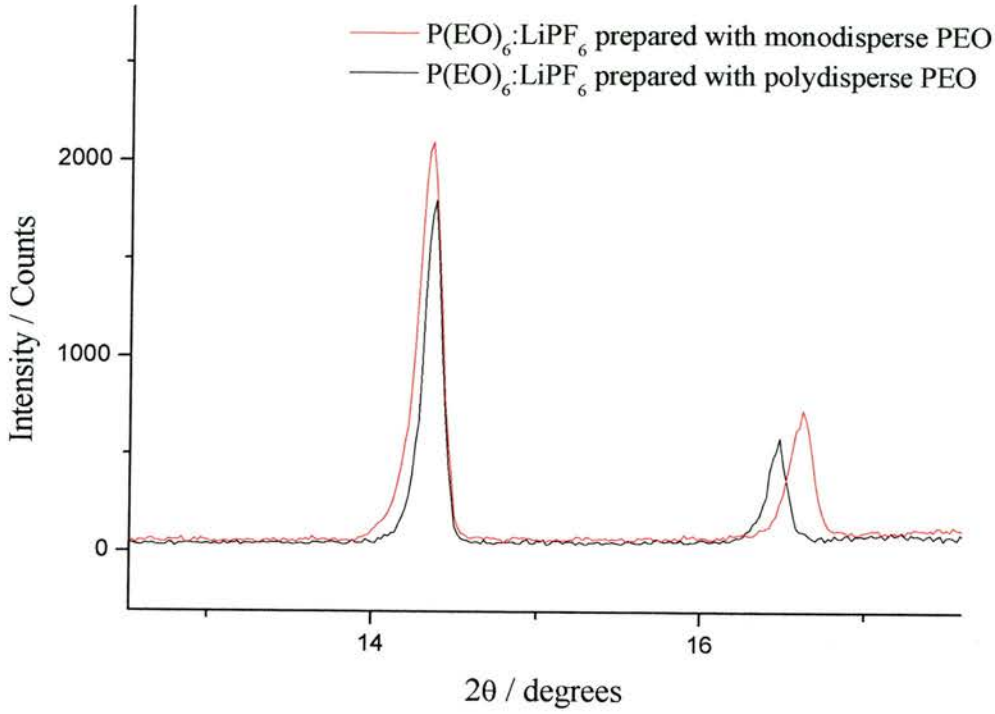

Figure 7.1.3. *Comparison of peak positions in the PXRD patterns of $P(EO)_6$:$LiPF_6$ prepared from monodispersed PEO (red) and polydisperse PEO 1000 (black).*

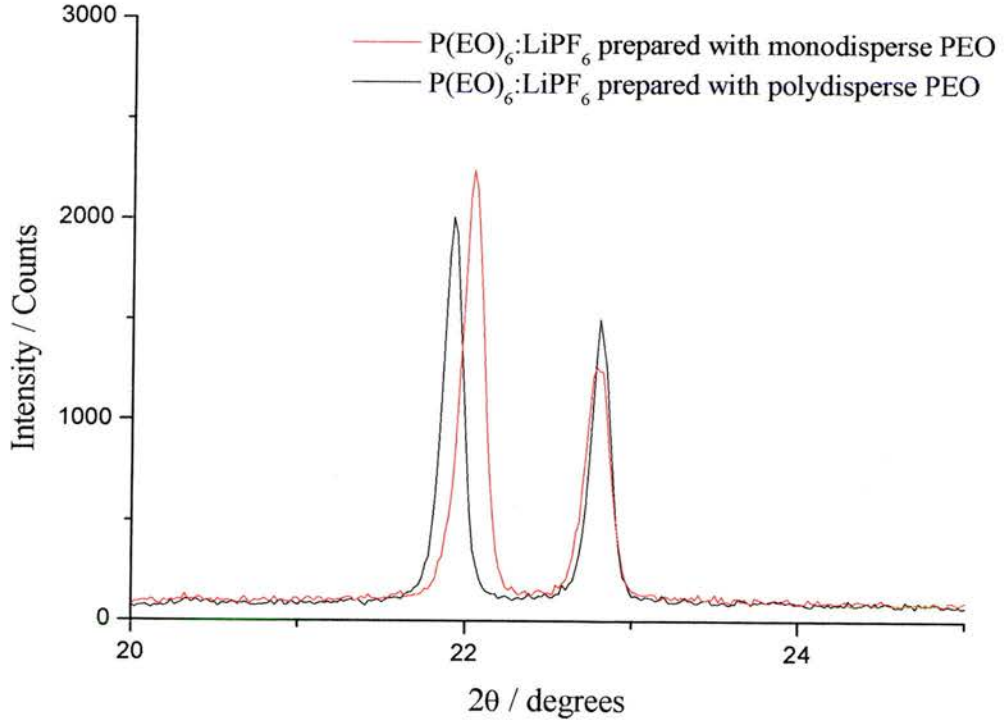

Figure 7.1.4. *Comparison of peak positions in the PXRD patterns of $P(EO)_6$:$LiPF_6$ prepared from monodispersed PEO (red) and polydisperse PEO 1000 (black).*

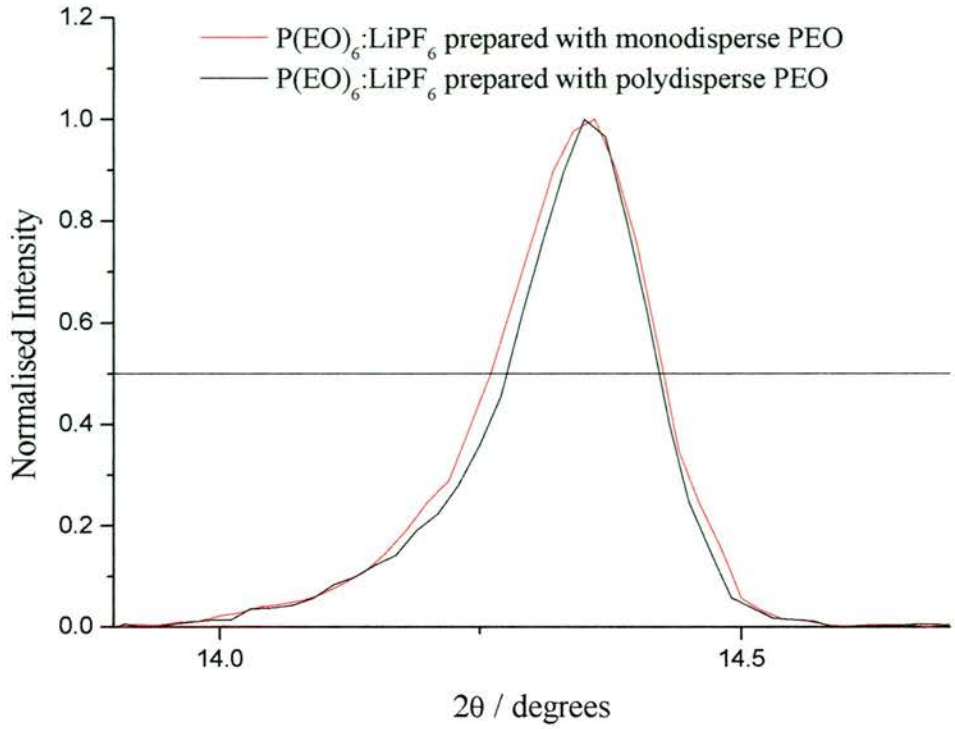

Figure 7.1.5. *Comparison of peak width of the 021 non-overlapping reflection in the PXRD patterns of $P(EO)_6$:$LiPF_6$ prepared from monodispersed PEO (red) and polydisperse PEO 1000 (black).*

There are also differences in the relative intensities of the peaks in the patterns. This indicates that the structures of these materials, although intimately related are subtly different. Careful Le Bail refinement using the powder diffraction pattern obtained for the monodispersed material showed differences in unit cell parameters for the complexes prepared with polydispersed and monodispersed PEO. The unit cells for the monodispersed and polydispersed complexes prepared are shown in table 7.1.1. The biggest change in unit cell parameter occurs along the 'a' direction, which is the direction in which the tunnels of PEO chains project. The 'a' parameter shrinks by around 1% in the complex prepared with monodispersed PEO. This change suggests that the regular nature of chain end occurrence, seen in the monodispersed complex, allows more intimate packing of the PEO chains along the 'a' direction, possibly as a result of the chains being aligned in the structure. At the moment there is no direct

evidence as to whether the chains are adopting a staggered or aligned arrangement within the PEO tunnels. It is hoped that low temperature TEM may be able to clarify the situation. There is also a slight expansion in the 'b' parameter of the unit cell of around 0.5%.

Unit Cell Parameter	**$P(EO)_6LiPF_6$, 1k, Polydisperse PEO**	**$P(EO)_6LiPF_6$, 1k, Monodispersed PEO**	**Difference Poly-Mono**
a	11.924(4) Å	11.801(4) Å	0.122(6) Å
b	17.335(6) Å	17.419(2) Å	-0.084(6) Å
c	9.202(3) Å	9.198(4) Å	0.004(5) Å
β	108.85(3)°	108.72(3)°	0.13(4)°
Volume	1800(1)Å^3	1790(1) Å^3	9(2) Å^3

Table 7.1.1. *Unit cell dimensions of $P(EO)_6$:$LiPF_6$ complex prepared from polydisperse and monodispersed PEO*

The DSC data collected for the monodispersed material is also significantly different from that seem for the polydisperse analogue. A dual endothermic feature is witnessed on heating the monodispersed complex whereas the complex prepared from the polydisperse material shows just one endothermic peak (see figure 7.1.6).

This phenomenon was probed further by the use of variable temperature PXRD. From the PXRD pattern collected at 70 degrees, an extra phase is observed. This phase only seems to exist at high temperature, cooling to room temperature from the melt

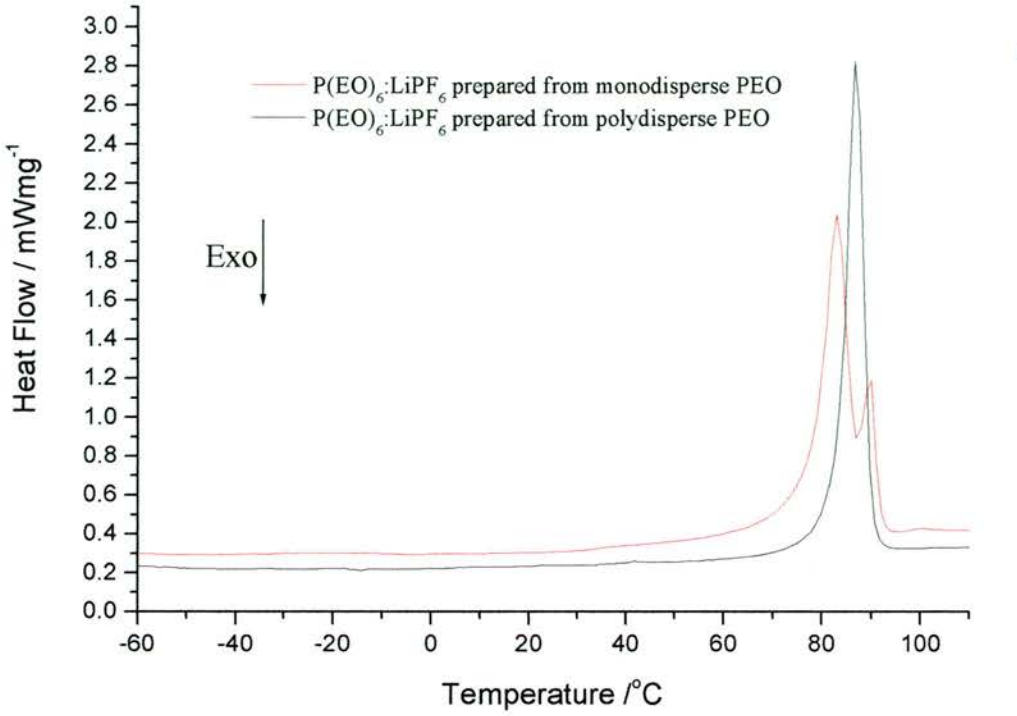

Figure 7.1.6. *DSC data showing a dual endothermic feature for $P(EO)_6$:$LiPF_6$ prepared from monodispersed PEO (red) and data showing one endothermic event for $P(EO)_6$:$LiPF_6$ prepared from polydisperse PEO (black)*

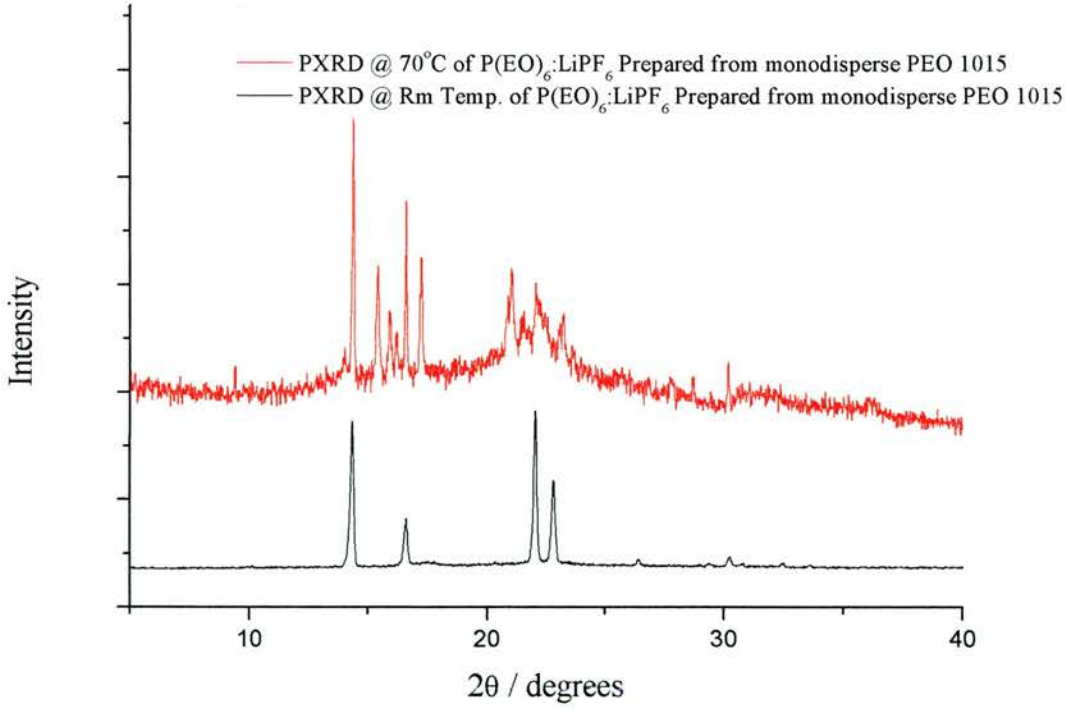

Figure 7.1.7. *PXRD patterns o f $P(EO)_6$:$LiPF_6$ prepared from monodispersed PEO at 70°C (red) showing peaks of an unidentified crystalline phase and room temperature (black) showing only the original material (black)*

produced only the pattern associated with the original phase, indicating that the change in phase is reversible. This high temperature phase is unique to $P(EO)_6$:$LiPF_6$ prepared from monodispersed PEO. Further work may be able to isolate a phase pure powder pattern suitable for structure solution.

Despite the chemical similarities between the mono and polydispersed PEO and the structural similarity of the complexes they make with $LiPF_6$ there is a significant difference in conductivities (see figure 7.1.8). The decrease in the levels of conductivity that the monodispersed material exhibits is around one order of magnitude. The complex prepared from monodispersed PEO has a slightly smaller crystallite size (as indicated from the peak widths in the PXRD patterns). From previous studies (see section 4.2) it has been seen that complexes with larger crystals exhibit higher conductivities and this rationale seems to hold true in this situation. However, the small change in crystallite size is unlikely to account for such a large change in conductivity. The monodispersed electrolyte material also exhibits noticeable changes in the unit cell parameters, it is possible that this shrinkage in the 'a' direction and smaller expansion of the 'b' direction is also having an effect on the conductivity.

In these two samples there are roughly the same number of chain ends, however the manner in which they are distributed in the conduction tunnels is somewhat different.

Conductivity is the product of the concentration of mobile species, their charge, and their mobility. Charge and mobility are independent of the dispersity of the PEO used (as can be seen from the very similar activation energies these materials exhibit)

which leaves concentration of mobile species as the only variable. The regularity of the chain end occurrence in the conduction tunnels may reduce the number of mobile lithium ions. The 6:1 complexes are stoichiometric materials. Every lithium site is occupied by a lithium ion except for thermally created defects or defects due to disorder that was 'built-in' to the crystallite during their growth.

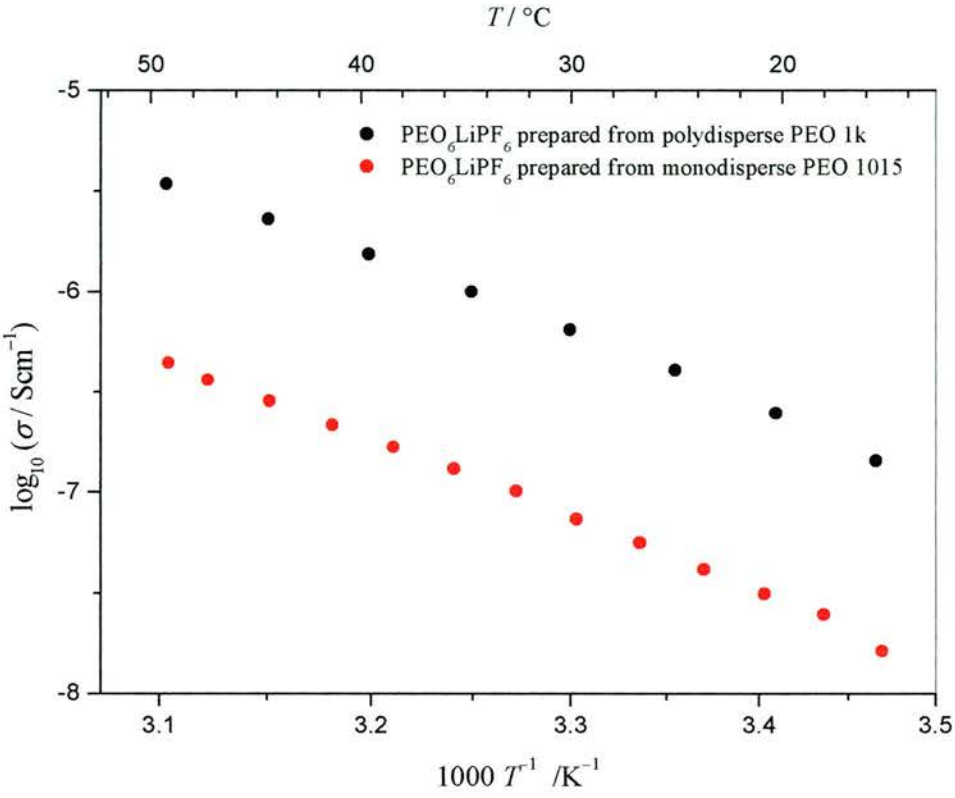

Figure 7.1.8. *Plot of log of conductivity vs reciprocal temperature for $P(EO)_6$:$LiPF_6$ prepared from polydisperse PEO (black) and monodispersed PEO (red)*

If we were to assume that chains are aligned in the structure of $P(EO)_6$:$LiPF_6$ prepared from monodispersed PEO, then three conduction tunnels would co-ordinate exactly 23 lithium ions. This motif would then be repeated infinitely throughout the crystal structure. This represents a very ordered arrangement of atoms. Any disruption that

the chain ends cause can be compensated for in the three tunnel fragment by a co-operative rearrangement. The PXRD data indicates a contraction of the unit cell along the 'a' direction, which is the dimension into which the chains project. However if the chain ends were randomly dispersed throughout the conduction tunnels no repeating motif can develop and these defects cannot be compensated for, (see figure 7.1.9) thus a larger 'a' unit cell parameter is predicted.

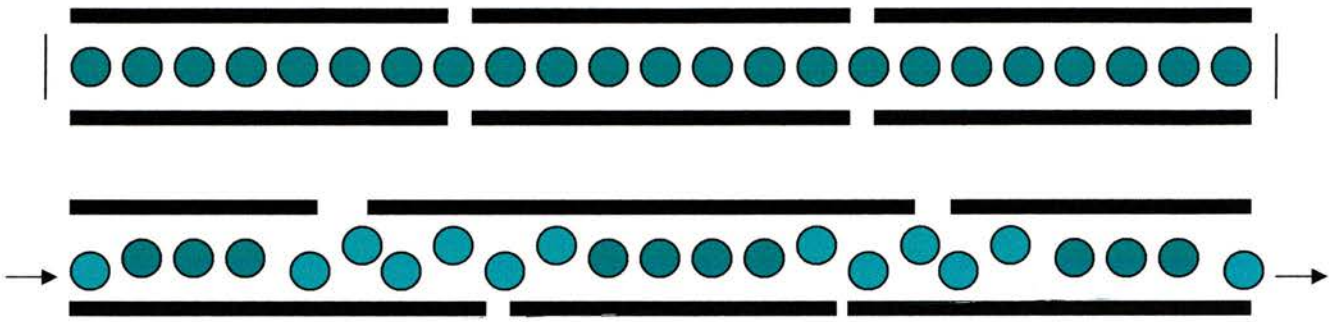

Figure 7.1.9. *Illustration of the effect of regularly repeating chain ends (top) and randomly occurring chain ends (bottom)\on the lattice. Li ions, green, polymer chain, black*

The presence of these random chain end defects in the polydisperse complex disrupts the potential surrounding the lithium ions, allowing a greater concentration of charge carriers and hence a higher conductivity. Polydispersity may lead to more defects thus increasing the conductivity.

Further evidence of the deleterious effect that the contraction of the unit cell in the 'a' direction has on conductivity can be seen in work published by Golodnitsky et al[5,6,7] Their studies show that stretching of polymer electrolytes material in the direction the PEO tunnels project increases the conductivity of the samples. By inference this suggest that contraction of the material in the direction would inhibit the conductivity.

7.2 $P(EO)_6$:$LiAsF_6$ synthesised using monodispersed PEO of mass 1015 Daltons.

As with the phosphate analogue, the 6:1 crystalline complex based on monodispersed PEO with $LiAsF_6$ exhibits a very similar PXRD pattern to that of the complex with $LiAsF_6$ prepared with the polydisperse PEO, and hence they have structures that are related (see figure 7.2.1). Again similar to the situation witnessed with the phosphate analogue, there are differences in the PXRD patterns of the complex prepared with monodispersed and polydisperse PEO.

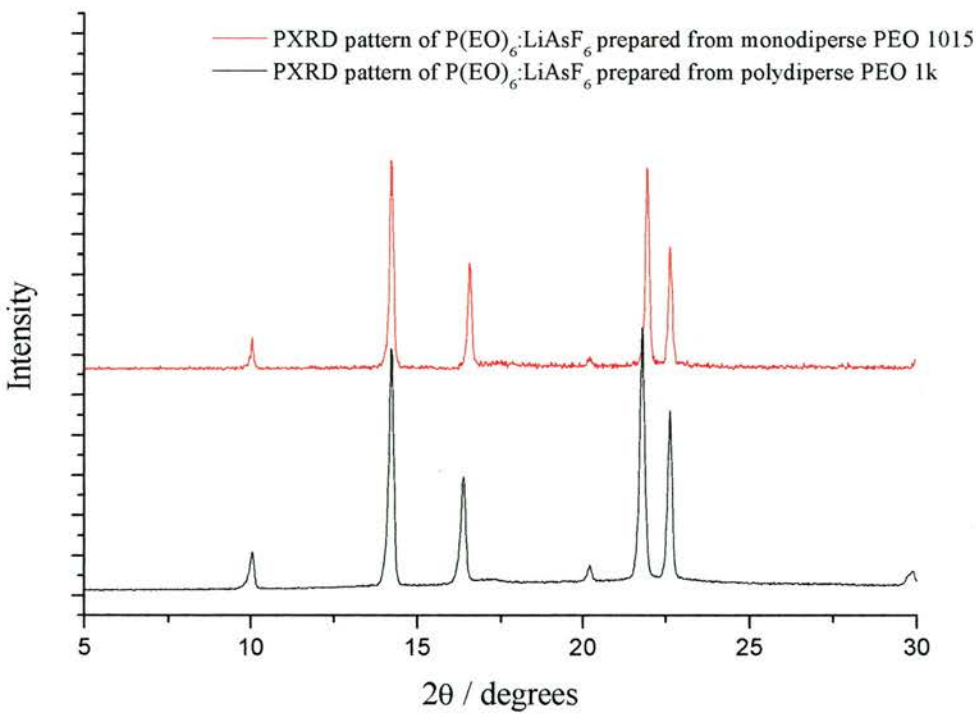

Figure 7.2.1. *PXRD patterns of $P(EO)_6$:$LiAsF_6$ prepared from monodispersed PEO1015 and polydisperse PEO 1k.*

Peak widths from PXRD are slightly narrower for the monodispersed complex compared with the polydisperse complex (see figure 7.2.4), indicating that crystallite size for these materials is larger when they are prepared from polymer chains of the same length. This is in contrast to the effect monodispersity has on the phosphate

complexes. The differences in peak positions are also similar to the shift witnessed with the monodispersed phosphate analogue (see figure 7.2.2 and figure 7.2.3). These differences in peak positions relate to a contraction of the unit cell dimensions compared with the complex synthesised using the polydispersed material (see table 7.2.1). Careful Le Bail refinement of the PXRD pattern of $P(EO)_6$:$LiAsF_6$ yielded the unit cell parameters of this material. In the complex of $P(EO)_6$:$LiAsF_6$ prepared using monodispersed PEO, the largest change in the cell dimensions belongs to the 'a' parameter, a contraction of almost 1.3%. As is the case with the phosphate analogue, these changes are most probably the result of more intimate packing of the monodispersed poly(ethylene) oxide chains due to the regular nature of their chain length. No expansion of the 'b' parameter is seen with the monodispersed arsenate complex.

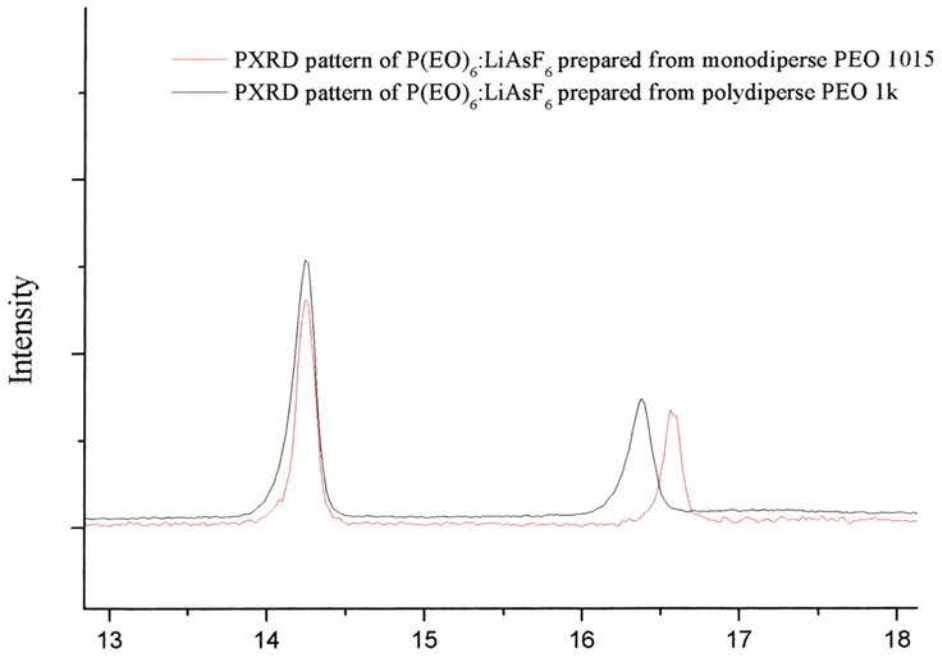

Figure 7.2.2. *PXRD patterns of $P(EO)_6$:$LiAsF_6$ prepared from monodispersed PEO1015(red) and polydisperse PEO 1k (black) highlighting the differences in peak positions of the two complexes*

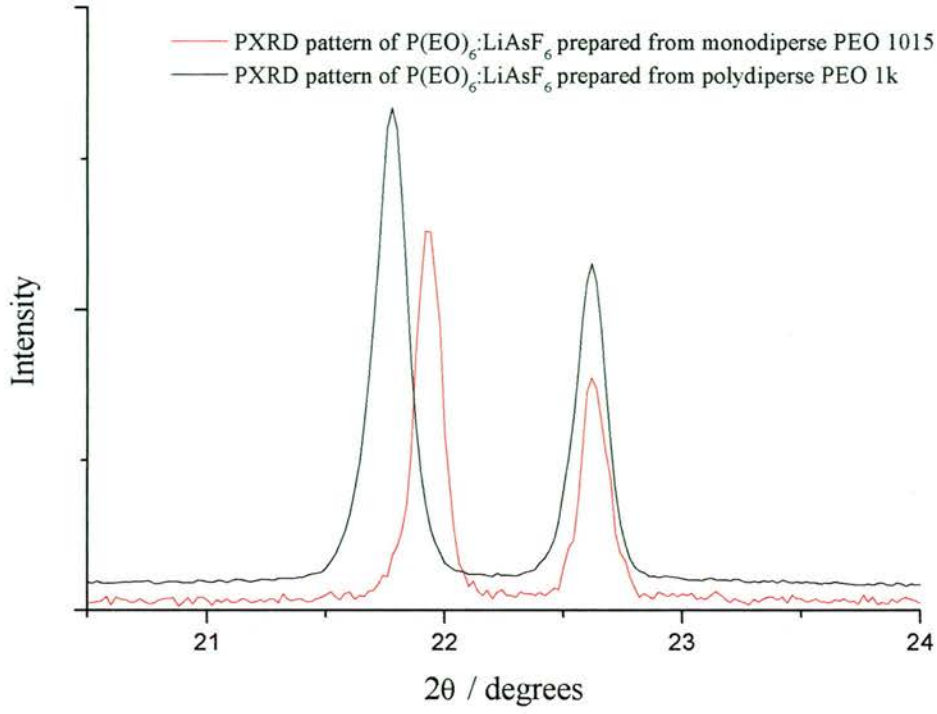

Figure 7.2.3. *PXRD patterns of $P(EO)_6$:$LiAsF_6$ prepared from monodispersed PEO1015 (red) and polydisperse PEO 1k (black) highlighting the differences in peak positions of the two complexes*

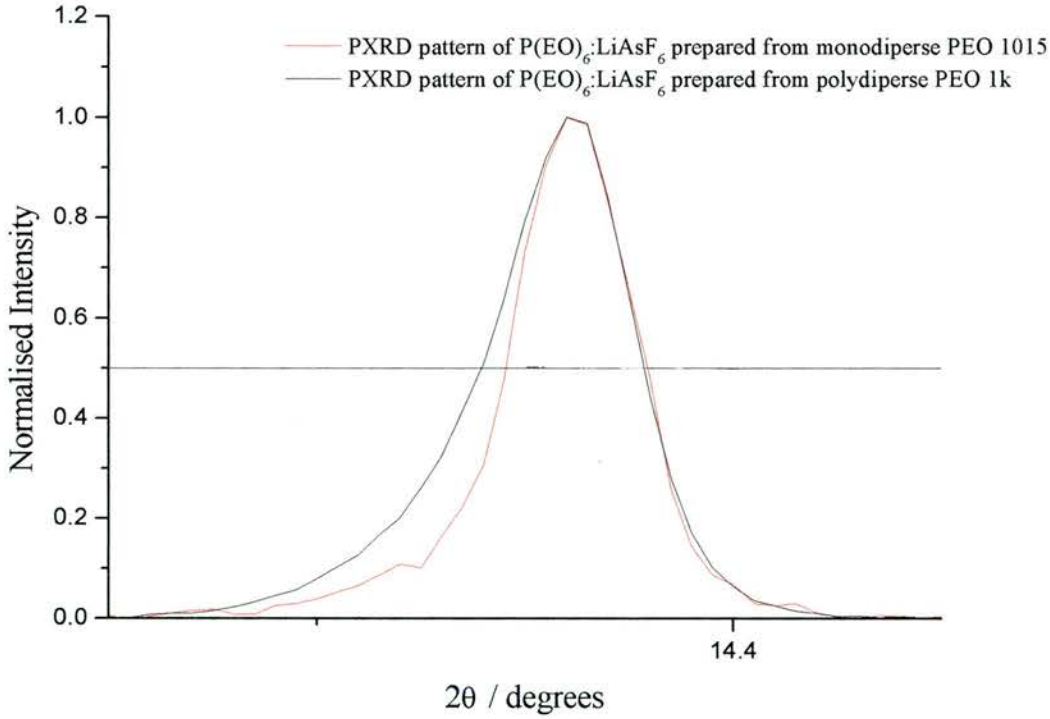

Figure 7.2.4. *Comparison of peak width of the 021 non-overlapping reflection in the PXRD patterns of $P(EO)_6$:$LiAsF_6$ prepared from monodispersed PEO (red) and polydisperse PEO 1000 (black).*

Unit Cell Parameter	$P(EO)_6LiAsF_6$, 1k, Polydisperse PEO	$P(EO)_6LiAsF_6$, 1k, Monodispersed PEO	Difference Poly-Mono
a	11.982(2) Å	11.827(3) Å	0.155(4) Å
b	17.488(4) Å	17.474(5) Å	0.014(6) Å
c	9.268(1) Å	9.263(1) Å	0.005(1) Å
β	108.24(1)°	108.60(2)°	-0.36(2)°
Volume	1844.4(6) $Å^3$	1814.3(7) $Å^3$	30.0(9)$Å^3$

Table 7.2.1. *Comparison of unit cells parameters of $P(EO)_6$:$LiAsF_6$ prepared from monodispersed PEO 1015 and polydisperse PEO 1k*

The DSC data for $P(EO)_6$:$LiAsF_6$ prepared from monodispersed polymer is also noticeably different (see figure 7.2.5) from the polydispersed material. The phase transition temperature from α to β - $P(EO)_6$:$LiAsF_6$ (see chapter 10) is lower by around 7K. This suggests that monodispersed chains can rearrange more readily to form the beta complex than polydisperse chains, ie. formation of the beta phase is more energetically favourable, possibly as a result of entropic considerations. The temperature at which the beta phase melts is higher by around 6K, Indicating that the beta phase is more stable when prepared with monodispersed PEO.

The relative level of conductivity the complexes of $P(EO)_6$:$LiAsF_6$ prepared from monodispersed PEO 1015 compared with their polydisperse counterpart is very similar (see figure 7.2.6). The complex prepared from monodispersed PEO exhibits a slightly higher level of conductivity. This is in contrast to the situation seen in the

previous section with $P(EO)_6$:$LiPF_6$ where the effect of preparing the complex with monodispersed PEO reduces the conductivity of the material. From PXRD data it can be seen that the monodispersed complex has narrower peaks than the polydisperse, indicating that the crystallite size is larger for the complex prepared from monodispersed polymer (see figure 7.2.4). Again as with the phosphate salt we only see a significant decrease in the 'a' unit cell parameter. The 'a' unit cell parameter contracts by 1.3% Despite the crystallite size being larger with the monodispersed $P(EO)_6$:$LiAsF_6$ complex, the increase in conductivity is only marginal. Possibly, contraction of the unit cell in the 'a' direction inhibits conductivity, as is also suggested in the case of $P(EO)_6$:$LiPF_6$. Another reason for the relatively different levels of conductivity exhibited by the monodispersed arsenate and phosphate complexes is the 'b' unit cell parameter. An expansion of this parameter is seen with the monodispersed phosphate complex but it remains unchanged in the arsenate monodispersed complex.

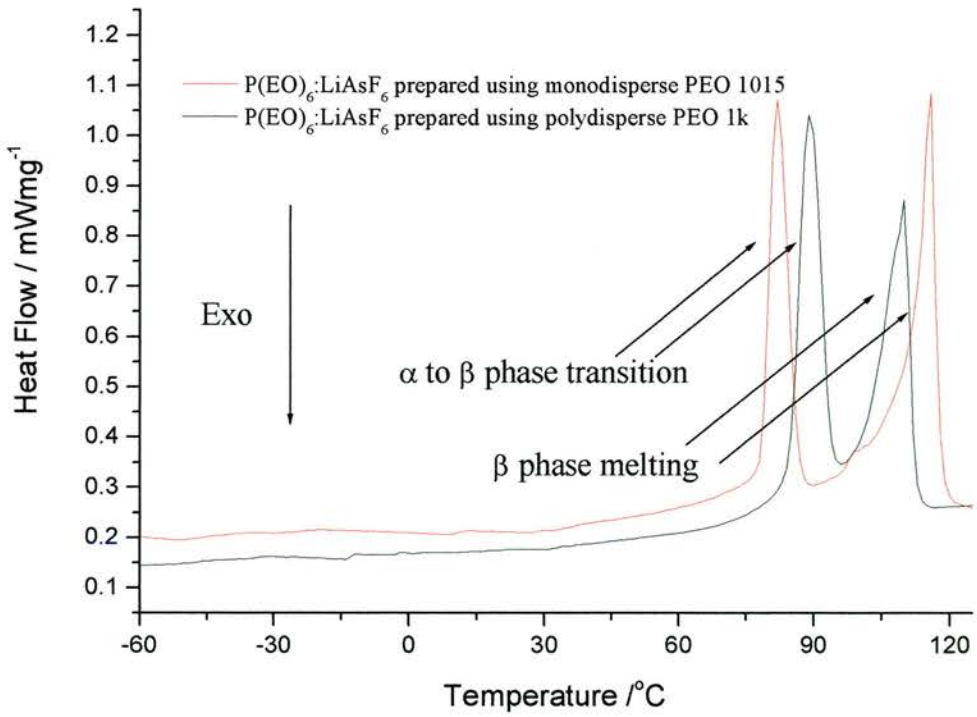

Figure 7.2.5. *DSC data of $P(EO)_6$:$LiAsF_6$ prepared from monodispersed PEO 1015 (red) and polydisperse PEO 1k (black).*

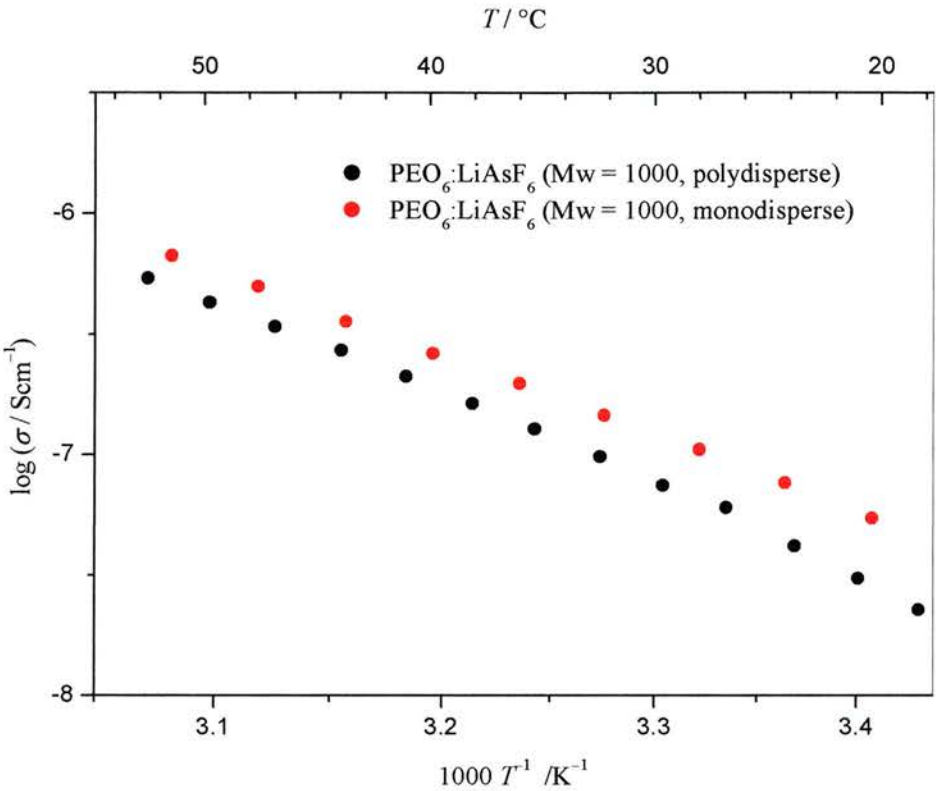

Figure 7.2.6. *Plot of log of conductivity vs reciprocal temperature for $P(EO)_6$:$LiAsF_6$ prepared from polydisperse PEO (black) and monodispersed PEO (red).*

---

[1] Seungja, M. Yu., Conticello, V.P., Zhang, G., Kayser, C., Fournier, M.J., Mason, M.L and Tirrell, D.A., *Nature*, **389**, 167, (1997)

[2] Le Fevere de Ten Hove, C., Penelle, J., Ivanov, D.A., Jonas, A.M., *Nature Materials*, **3**, 33, 2004

[3] MacGlashan G.S., Andreev Y.G. and Bruce P.G., *Nature*, **398**, 792-793, 1999

[4] Staunton E., Christie A.M., Andreev Y.G., Slawin A.M.Z. and Bruce P.G. *Chem. Commun.* 148-149, 2004

[5] Golodnitsky, D. and Peled, E., *Electrochimica Acta*, **45**, 1431-1436, 2000

[6] Golodnitsky, D., Livshits, E., Rosenberg, Yu., Peled, E., Chung, S.H., Wang, Y., Bajue, S., Greenbaum, S.G. *Journal of Electroanalytical Chemistry*, **491**, 203-210, 2000

[7] Golodnitsky, D., Livshits, E., Rosenberg, Yu., Lapides, I., Peled, E. *Solid State Ionics*, **147**, 265-273

Chapter 8

Structures of Glymes and Glycols Complexed with $LiXF_6$

Many hundreds of polymer electrolytes have been prepared but developing an understanding of their structural chemistry has proved especially difficult. The structure determination technique of choice, single crystal x-ray diffraction, is not generally applicable to these polymeric materials as it is difficult to grow single crystals of high molecular weight polymers and fibre diffraction gives rise to poor quality diffraction patterns. As a result, powder diffraction has been the main method by which the crystal structures of polymer electrolytes have been established[1,2,3,4].

However, Frech and co-workers accidentally discovered large single crystals during the preparation of a complex between diglyme ($CH_3O[CH_2CH_2O]_2CH_3$) and $LiSbF_6$[5]. The structure of the diglyme $LiSbF_6$ complex had a somewhat similar structural motif to the structure of $P(EO)_6$:$LiSbF_6$ solved from powder diffraction using *simulated annealing*[1]. With increasing molecular weight a point must be reached beyond which single crystals would not be formed. However, if single crystals complexes could be formed with chains of significant length to reproduce a 'continuous chain' then this might yield a route to crystal structures unobtainable from powder diffraction. It was thought that these materials could be suitable model complexes for their polymeric counterparts, sharing many of the same attributes and local interactions.

Attempts were made to prepare a number of salt glyme/glycol complexes using $LiPF_6$, $LiAsF_6$, $LiSbF_6$ and low molecular weight glymes.

Of the complexes prepared, crystals were grown of complexes between $LiAsF_6$ with triglyme, tetraglyme and hexaethylene glycol that were of sufficient volume for analysis by single crystal x-ray diffraction (see chapter 3.3.1).

Ligand/salt	Triglyme:$LiAsF_6$	Tetraglyme$_2$:$LiAsF_6$	Hexaethylene glycol:$LiAsF_6$
Empirical formula	$C_8 H_{18} O_4 Li F_6 As$	$C_{10} H_{22} O_5 Li F_6 As$	$C_{12} H_{26} O_7 Li F_6 As$
Crystal Size/mm	0.3 x 0.2 x 0.01	0.15 x 0.1 x 0.01	0.1 x 0.2 x 0.01
Formula Weight	374.05	418.14	476.17
Wavelength/ Å	0.71073	0.71073	0.71073
Crystal System	Monoclinic	Orthorhombic	Monoclinic
Space Group	$P2_1/n$	Pbcn	$P2_1/n$
Unit Cell Dimensions a, α (Å, °)	6.2042(17), 90	12.348(2), 90	11.591(3), 90
b, β(Å, °)	12.660(3), 95.546(5)	22.369(4), 90	15.384(3), 106.766(6)
c, γ(Å, °)	18.427(5), 90	12.314(2), 90	11.637(2), 90
Volume/ $Å^3$	1440.5(7)	3401.2(11)	1986.8(7)
Z	4	8	4
Calc. Density/mgm^{-3}	1.725	1.633	1.592
Abs. Coefficient/mm^{-1}	2.434	2.075	1.794
Temperature/K	125	125	125
Reflections Collected/Unique	8765/2570	20068/3063	11892/3533
Goodness-of-fit on F^2	1.011	1.017	1.047
R[I>2σ (I)]	0.0720	0.0315	0.0528
Rw	0.1616	0.0739	0.1357
R (all data)	0.1108	0.0542	0.0632
Rw	0.1811	0.0819	0.1440

Table 8.1 *Summary of crystallographic data for complexes between triglyme, tetraglyme, hexaethylene glycol and $LiAsF_6$. Single crystal diffraction data were collected using Mo K_α radiation on a Bruker SMART® diffractometer equipped with a fine-focus sealed tube, a graphite monochromatic and a CCD detector.*

Ligand/salt	Diglyme$_2$:Li SbF_6	Triglyme: $LiAsF_6$	Tetraglyme $_2$: $LiAsF_6$	Hexaethylene glycol:$LiAsF_6$
O to Li ratio	6	4	5	7
Ligand per Li	2	1	1	1
Li coordination No.	6	5	4	5
Li coordination geometry	Octahedral	Trigonal bipyramidal	Irregular	Square pyramidal
Anion Coordination ?	No	Yes	No	No

Table 8.2 *Summary of structural features of glyme/glycol:$LiXF_6$ complexes.*

8.1 Comparison of structures formed between glymes\glycols and $LiXF_6$.

8.1.1 Complex between diglyme and $LiSbF_6$

The first structure of a low molecular weight glyme and Li salt complex solved was $diglyme_2$:$LiSbF_6$ by Frech *et al*[5]. It exhibits a similar structural motif to that exhibited by the complex prepared from the polymeric, $P(EO)_6$:$LiSbF_6$ (see figure 8.1.1.1). There are two different chains co-ordinating the lithium ions.

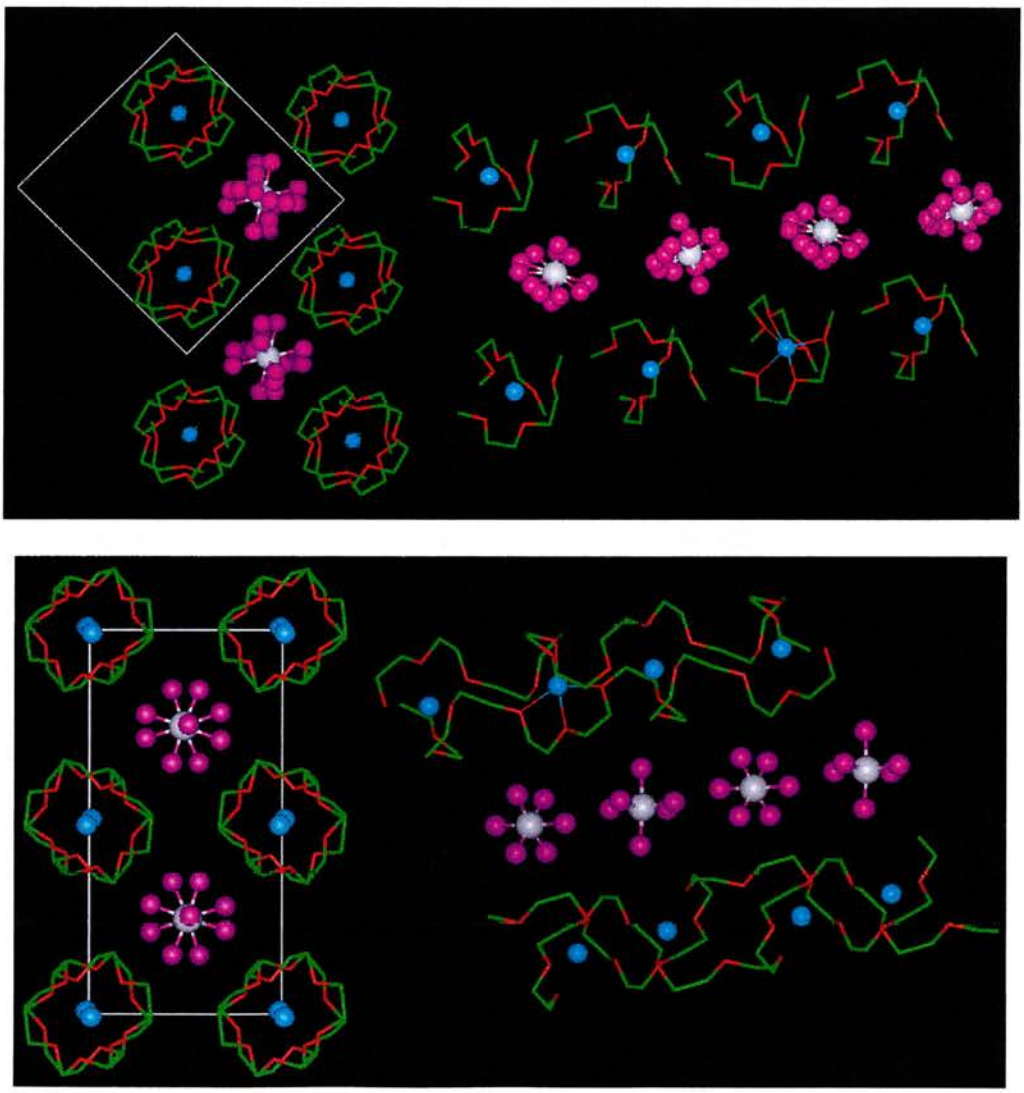

Figure 8.1.1.1. *Structure of diglyme:$LiSbF_6$, (top) and $P(EO)_6$:$LiSbF_6$, (bottom) showing similar structural attributes. Carbon (green), oxygen (red), lithium (light blue), anions (white and magenta)*

If the diglyme molecules were to be linked along the stacks they would describe two interlocking chains as does the complex with PEO. When viewed down the b axis the stacks of lithium:diglyme appear as tunnels. A completely dissociated anion is also present. However, because the diglyme chains are too short to provide a continuous interconnected tunnel, the lithium ions have no clear path to migrate from co-ordination site to co-ordination site, so this material is unlikely to conduct. Lithium is 6 co-ordinate in the glyme structure as opposed to 5 co-ordinate in the polymeric complex, in the polymeric structure the distance between the 6^{th} non-coordinating oxygen and lithium is over 3Å. Perhaps the continuous polymeric chain cannot fold sufficiently to allow coordination to all 6 oxygens available, unlike the discrete diglyme molecules. Coordination to a 6^{th} oxygen just outside the reach of the lithium ion makes ion-hopping energetically favourable by providing an intermediate co-ordination site.

The distance between adjacent lithium ions is 7.47 Å in the diglyme structure as opposed to the shortest distance of 4.97 Å in the polymeric structure. The lithium to oxygen distances are slightly different ranging from 2.07 to 2.17 Å in the glyme structure and are slightly longer in the polymeric structure, ranging from 2.15 to 2.19 for the 5 co-ordinating oxygens and 3.04 for the non-coordinating oxygen. Despite the disparity in chain lengths the diglyme $LiSbF_6$ structure acts as a good indication of what to expect with the polymeric complex.

8.1.2 Complex between Triglyme and $LiAsF_6$

Large single crystals of triglyme:$LiAsF_6$ were grown from an acetonitrile solution of triglyme and $LiAsF_6$ and their structures were determined by single crystal x-ray diffraction (unit cell a = 6.204, b = 12.660, c = 18.427, β = 95.546, R_p= 7.2%). This structure was also found by Henderson *et al* who published their results in 2003[6]. Crystals were grown from a solution where the ratio of ether oxygens to lithium was 6 to 1, despite this the crystals that formed had an ether oxygen to lithium ratio of 4 to 1. The structure of this complex is quite surprisingly different from the $diglyme_2$:$LiSbF_6$ structure (see figure 8.1.2.1, 8.1.2.2 and 8.1.2.3).

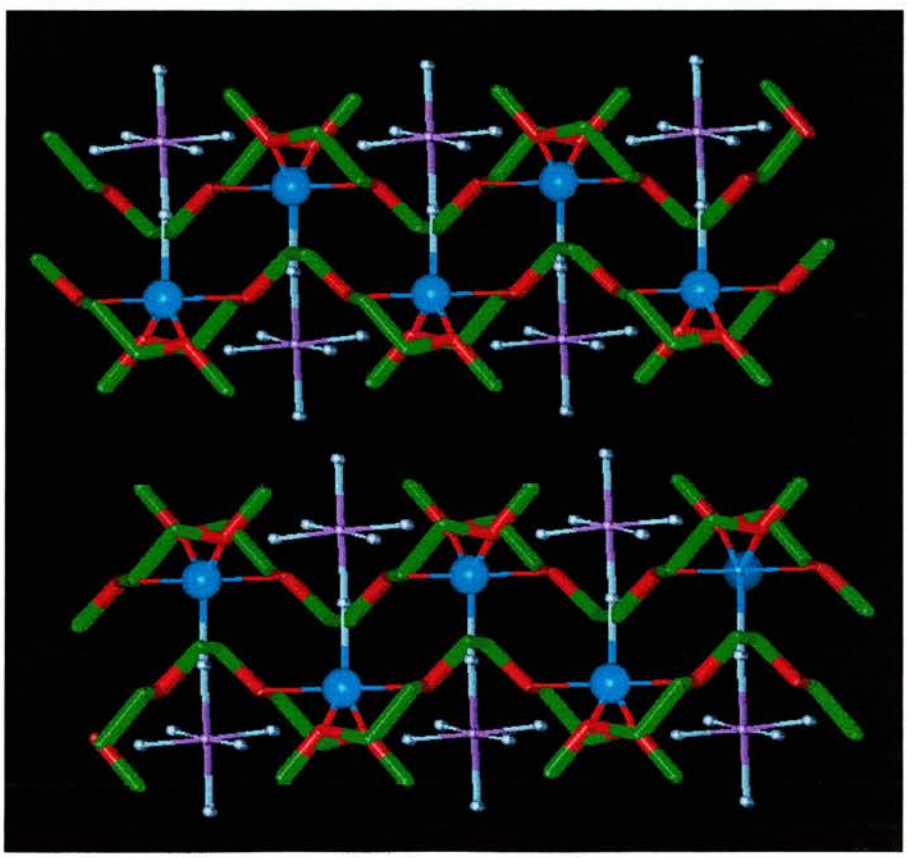

Figure 8.1.2.1. *Structure of triglyme:$LiAsF_6$, showing side view of the polymeric network of triglyme molecules and lithium (light blue) co-ordination to oxygen (red) and fluorine (white). Carbon, (green).*

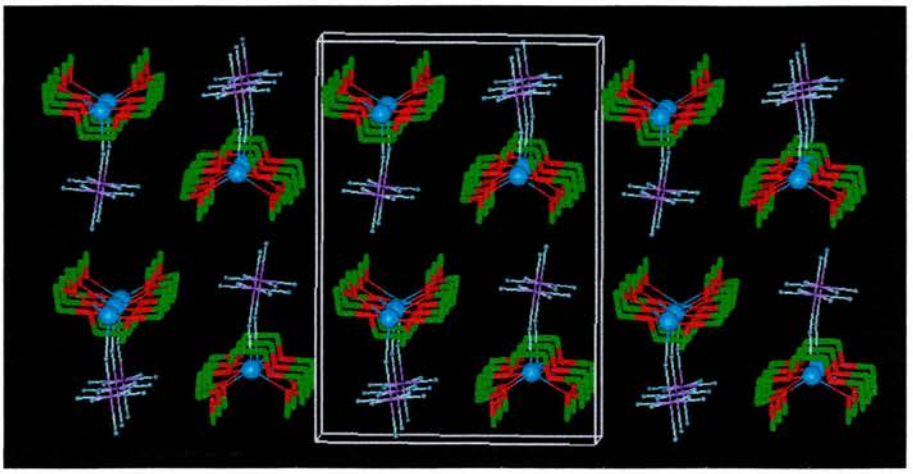

Figure 8.1.2.2. *Structure of triglyme:$LiAsF_6$, showing a section of the end on view of the polymeric network of triglyme molecules and lithium's (light blue) co-ordination to oxygen (red) and fluorine (white). Carbon, (green).*

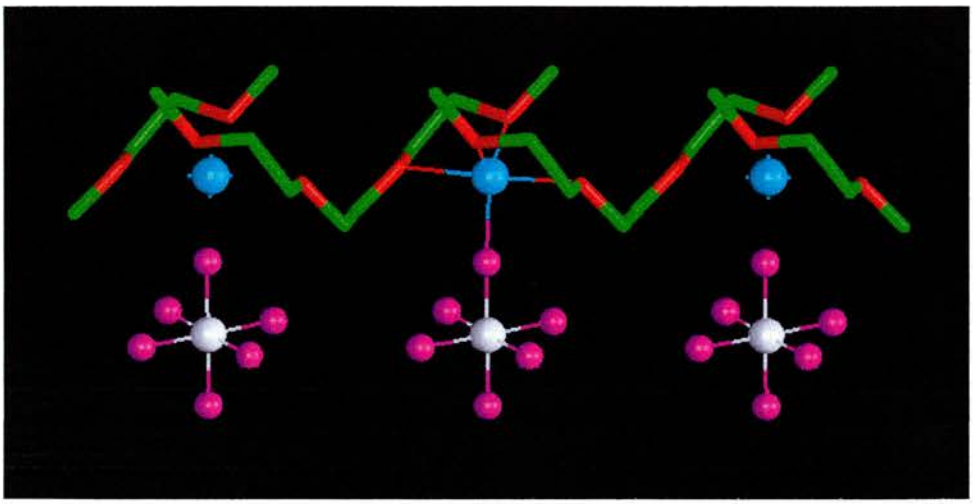

Figure 8.1.2.3. *Structure of triglyme:$LiAsF_6$, highlighting lithium's co-ordination environment . Lithium (light blue), oxygen (red) and fluorine (magenta). Carbon (green).*

The structure of triglyme:$LiAsF_6$ shows a 5 co-ordinate lithium in an trigonal-bypyramidal co-ordination geometry, it forms 4 bonds to ether oxygens provided by two different triglyme ligands. The ligands form an apparently continuous one dimensional chain. Lithium also makes bond to one fluorine in the hexafluoroarsenate

anion. The association with the anion is something not witnessed in the diglyme:$LiSbF_6$ complex or the $P(EO)_6$:$LiAsF_6$ complex. The structural motif is more similar to that of $P(EO)_3$:$LiAsF_6$[7] (see figure 8.1.2.4). There is no 4:1 structure formed between PEO and $LiAsF_6$

The structure of $P(EO)_3$:$LiAsF_6$ also shows co-ordination of the anion. The cation in this complex is co-ordinated trigonal-bipyramidally by three ether oxygens from the PEO chain and two fluorines from two anions.

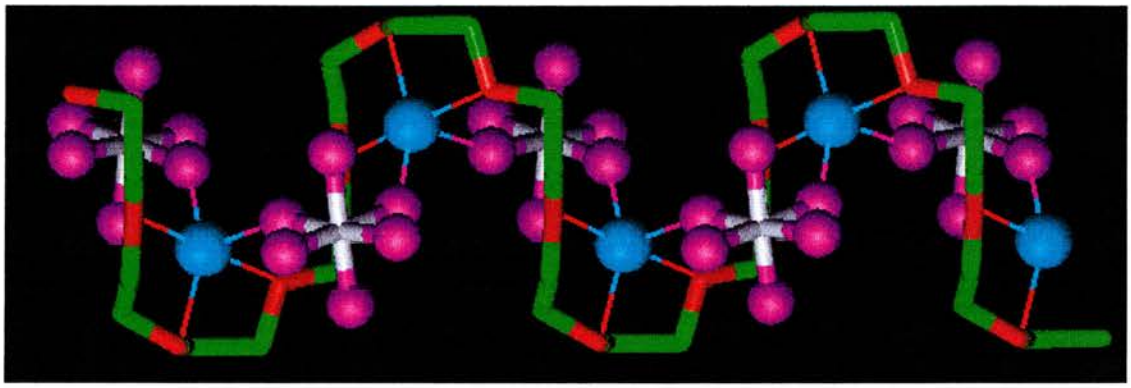

Figure 8.1.2.4. *Structure of $P(EO)_3$:$LiAsF_6$, highlighting lithium's co-ordination environment, making three bonds to oxygen and two bonds to the fluorine atoms of the anions . Lithium (light blue), oxygen (red) and fluorine (magenta). Carbon (green).*

Lithium forms a stronger bond with the terminal triglyme oxygens (bond lengths for these two bonds are 2.03Å and 1.95Å) compared to the bonds between lithium and the non-terminal oxygens (which are both 2.15 Å). The Li-F bond length is 1.94 Å.

8.1.3 Complex between Tetraglyme and $LiAsF_6$

The next complex in the series is that between tetraglyme and $LiAsF_6$. Single crystals of tetraglyme$_2$:$LiAsF_6$ were grown from an acetonitrile solution of tetraglyme and $LiAsF_6$ and their structures were determine by single crystal x-ray diffraction (unit cell, a = 12.348 b = 22.370 c = 12.314, $\alpha = \beta = \gamma = 90$, R_p= 3.15%). Some crystals of this material that were grown were extremely large, about 0.5cm x 0.5cm x 0.2cm. This structure was also found by Henderson *et al* who published their results in 2003[8]. This complex exhibits a unique dimeric structure (see figure 8.1.3.1 and 8.1.3.2). There is no bonding interaction between the cation and anion in this system. The anions exist between the lithium-tetraglyme dimers, negating any possibility of the chains linking up to form a tunnel (see figure 8.1.3.1). The two lithium ions in the complex are co-ordinationally identical but are crystallographically distinct. The lithium in this structure is bonded strongly by 4 oxygens, with bond distances from 1.99 to 2.07Å. The two ether oxygens that can be seen in the centre of figure 8.1.3.2 are both 2.5 Å away from each lithium position, too long for a lithium oxygen bond.

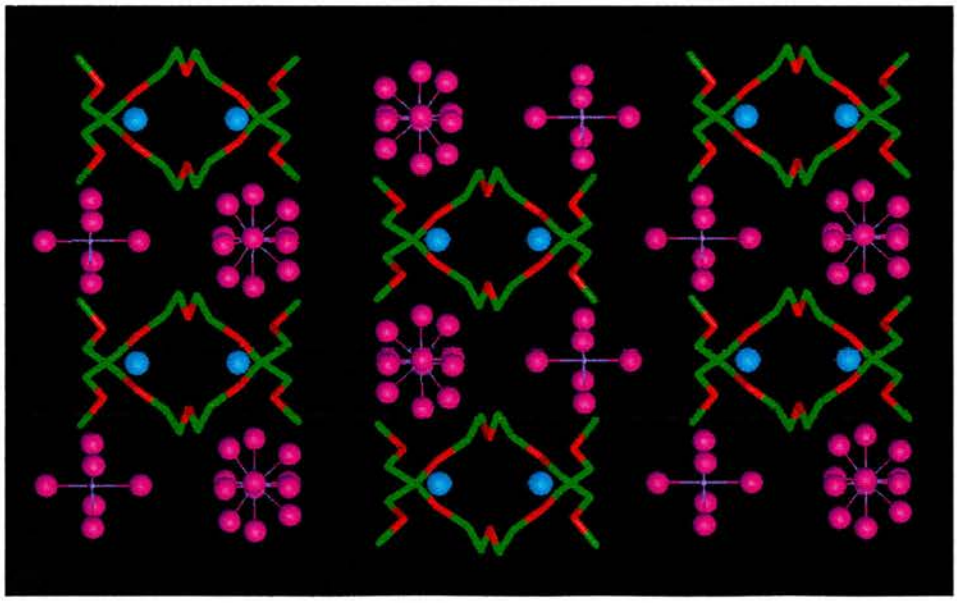

Figure 8.1.3.1. *Structure of tetraglyme$_2$:$LiAsF_6$, highlighting position of dimeric lithium:tetraglyme co-ordination relative to anion positions. Lithium (light blue), oxygen (red) and fluorine (magenta). Carbon (green).*

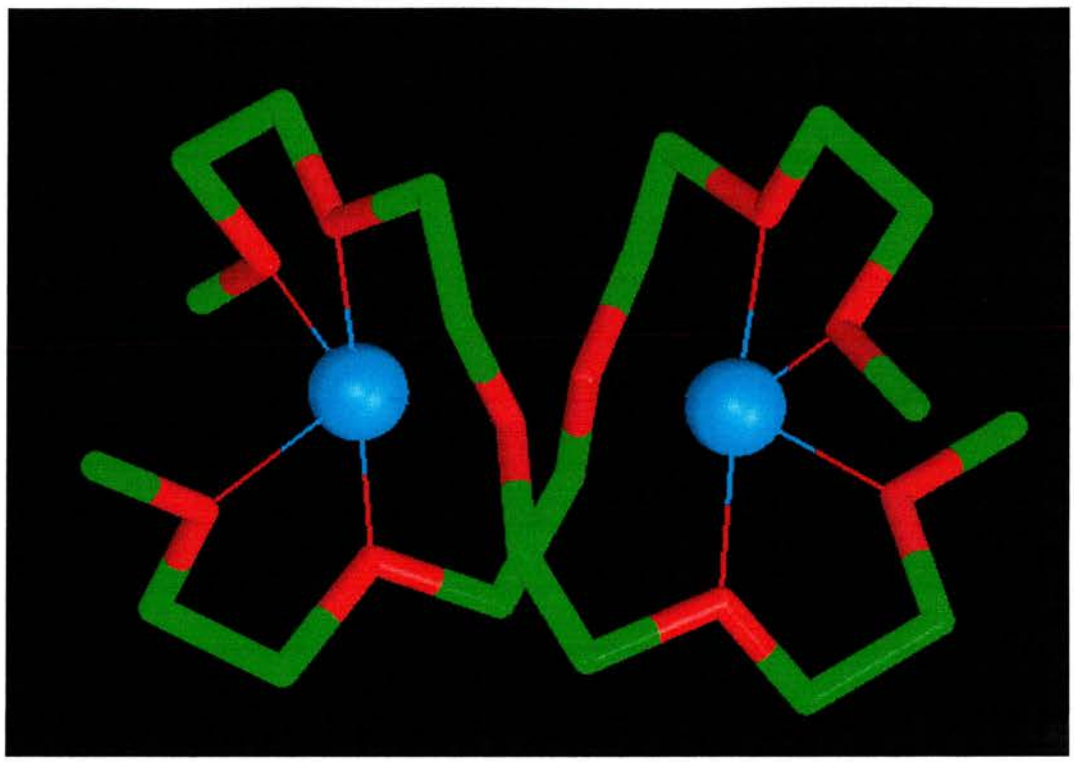

Figure 8.1.3.2. *Co-ordination sites of lithium:tetraglyme dimer. Each lithium is 2.5 Å from the two central oxygen atoms. Lithium (light blue), oxygen (red) and carbon (green).*

The co-ordination occurring in this complex is similar to that seen with the 6:1 complex of PEO and $LiAsF_6$, ie. that oxygens are provided for co-ordination to lithium by two separate chains. Lithium has a coordination number of 4 in this complex, which is the lowest we have seen in glyme or polymeric complexes. There are examples of these type of complexes that have 4 lithium to oxygen bonds but their complexation is also complemented by co-ordination to anions. The apparently non-coordinating oxygens in the middle of the complex maybe interact just enough with each lithium to allow this situation to exist.

This crystalline complex of $tetragyme_2$:$LiAsF_6$ has also been shown to ionically conduct (see figure 8.1.3.3). The plot of log conductivity vs. reciprocal temperature shows that the tetraglyme complex has a higher conductivity than that of the crystalline conductor $P(EO)_6$:$LiAsF_6$. The method by which these materials allow ion

transport has yet to be investigated, although initial observations of the structure suggest that an ion transport pathway through the material may be present.

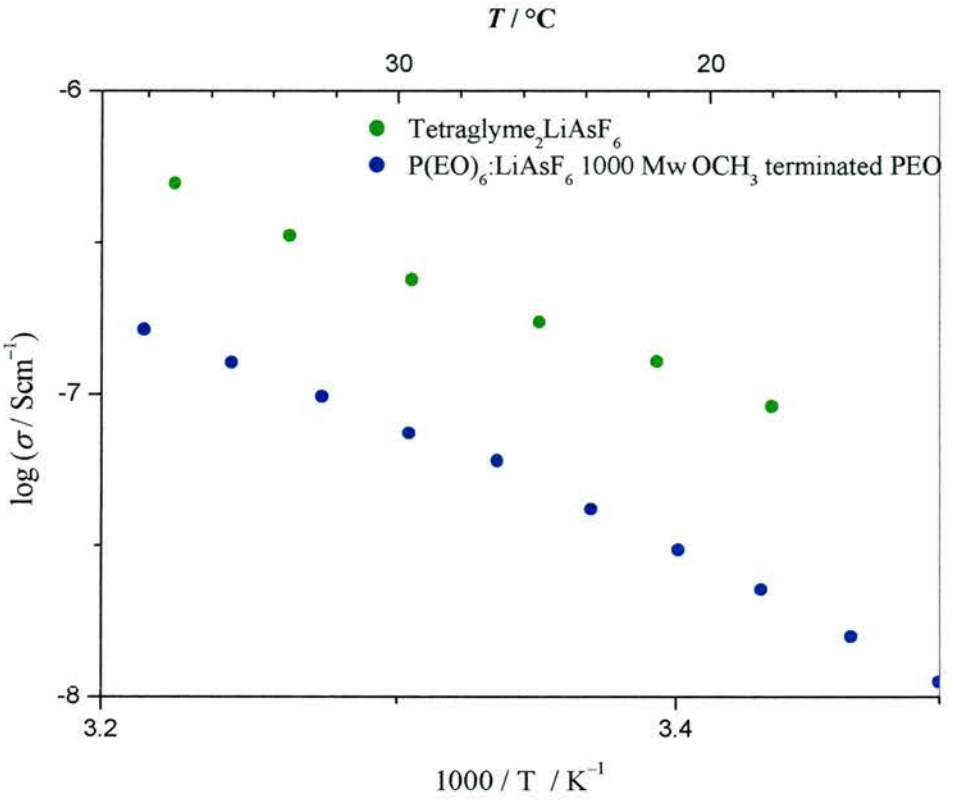

Figure 8.1.3.3. *Plot of log conductivity vs. reciprocal temperature for $Tetraglyme_2LiAsF_6$ (green) and $P(EO)_6$:$LiAsF_6$ (blue).*

8.1.4 Complex between Hexaethylene Glycol and $LiAsF_6$

The same method of growing crystals was applied to pentaglyme, pentaethylene glycol and hexaglyme with $LiAsF_6$ but unfortunately no crystals formed for these ligands on this attempt. A homologous series of ligands with $LiAsF_6$ would have been extremely interesting. However crystals could be grown for hexaglycol:$LiAsF_6$. The structure is shown in figure 8.1.4.1. (Unit cell a = 11.591, b = 15.384, c = 11.637, β = 106.77°, R_p = 5.28%). This structure is adopted to maximize the interaction between the –OH end groups and lithium. For this complex, 5 oxygens co-ordinate the lithium out of a possible seven and the cations are completely dissociated from the anions. The two ethylene oxide segments with non co-ordinating oxygens act essentially as spacers. The co-ordination with lithium gives a polymeric structure. The oxygens of the hydroxyl group at the chain ends of the hexaethylene glycol ligand bond in preference to the oxygen atoms in the chain, which makes chemical sense as the oxygen atoms of the hydroxyl groups are more electronegative than the oxygen atoms in the ether functionality. The lithium to oxygen bond lengths at the chain ends are 1.96Å and 1.97Å and the distances between the ether oxygens in the ligand and the lithium are 2.05Å for two and 2.24Å for the remaining bond. The lithium coordination adopts a distorted square pyramidal geometry. The lithium ions are separated by 7.1 Å from co-ordination site to co-ordination site, negating any possibility of ion transport along the chains.

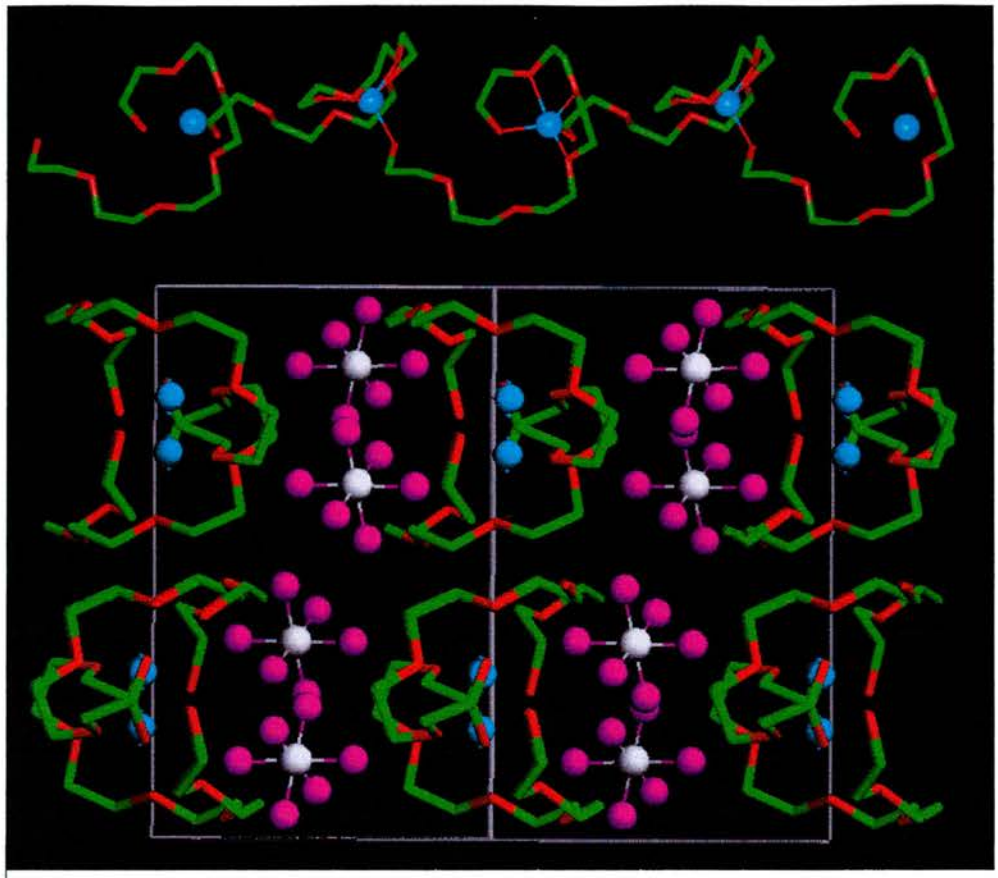

Figure 8.1.4.1. *Structure of hexaethylene glycol:$LiAsF_6$, showing view along the chain (top) and view perpendicular to the direction in which the chains project. Lithium (light blue), oxygen (red), fluorine (magenta), arsenic (white), carbon, (green).*

8.1.5 Conclusion

The structures exhibited by glymes/glycols and $LiXF_6$ anions present a number of different structural motifs and co—ordination environments/geometries for the cations in these systems. The ligand that has the smallest amount of structural constraint (diglyme) prefers to adopt a structure similar to that of the polymer electrolyte $P(EO)_6$:$LiAsF_6$. What is also apparent is that these complexes would prefer to adopt either a dimeric/ polymeric structure rather than a discrete crown-ether type complex despite the energetic advantages offered by the chelate effect. Complexes that adopt a low ethylene oxide to lithium ratio complement their bonding by interaction with

fluorine atoms provided by the anions, indicating that maintaining a polymeric structure is more of a driving force for complexation than co-ordination solely to oxygen. Complexes that have more than 4 oxygens available to them are not compelled to interact at all with the anions in the system. Also the functionality of the chain ends has an effect on the structures, as shown by the structure of hexaethylene glycol and $LiAsF_6$, where lithium bonds more strongly to the oxygen of the hydroxyl group in preference to the ether oxygens.. There are still a great number of glyme/lithium salt complexes left to examine. Advances in separation techniques are providing access to glymes of higher mass. Also, by synthetic methods a number of higher glymes, such as septaglyme octaglyme, nonaglyme, decaglyme, undecaglyme, dodecaglyme etc, are available.

It would be interesting to see the point at which the glymes adopt the same structure as the complex of $P(EO)_6$:$LiAsF_6$ and if there are any structural anomalies that could be exploited in the intermediate.

---

[1] MacGlashan, G. S., Andreev, Y. G. and Bruce, P. G. *Nature* **398**, 792-794 (1999).

[2] Lightfoot, P., Mehta, M. A. and Bruce, P. G. *Science* **262**, 883-885 (1993).

[3] Thomson, J. B., Lightfoot, P. and Bruce, P.G. *Solid State Ionics,* **85**, 203-208 (1996)

[4] Gadjourova, Z., Martin y Marero, D., Andersen, K. H., Andreev, Y. G. and Bruce, P. G. *Chem. Mater.* **13**, 1282-1285 (2001).

[5] Seneviratne V., Frech R. and Furneaux J.E., J. Phys. Chem. B **108,** 8124-8128 (2004)

[6] Henderson, W.A., Brooks, N.R., Brennessel, W.W. and Young, V.G. *Chem. Mater.*, **15**, 4679-4684 (2003)

[7] Martin-Litas I, Andreev Y.G., Bruce P.G., *Chem. Mater.* **14** (5): 2166-2170 (2002)

[8] Henderson, W.A., Brooks, N.R. and Young, V.G. *Chem. Mater.*, **15**, 4685-4690 (2003)

Chapter 9

Discovery, Structure Solution and Properties of the β Phase of $P(EO)_6:LiAsF_6$

Polymorphs (materials that possess exactly the same chemical constituents but vary structurally) offer valuable and rare insight into the effect that structure has on the properties of materials. In this chapter the discovery, structure and contrasting properties of a polymorph of $P(EO)_6:LiAsF_6$ (designated β–$P(EO)_6:LiAsF_6$) are detailed.

9.1 Discovery of β – $P(EO)_6:LiAsF_6$

On several occasions when trying to prepare samples of $P(EO)_6:LiAsF_6$ complex 'extra' peaks were observed in the powder diffraction pattern, the most prevalent one being at 15.6° in 2θ (see fig. 9.1.1). These peaks remained unaccounted for despite comparisons with the powder diffraction pattern of the salt and polymer used to make the complex and also the 3:1 complex of PEO and $LiAsF_6$. Further evidence for the presence of a new crystalline phase was observed from DSC measurements. A dual endothermic feature was seen on the first heating cycle but not on the second heating cycle (see fig. 9.1.3). The first peak on the first DSC heating trace was attributed to the phase change from the known $P(EO)_6:LiAsF_6$ phase (in future designated α-$P(EO)_6:LiAsF_6$) to a new β phase of the material and the second endothermic event to the melting of the β phase. The absence of the phase transition peak in the second heat shows that this transition is irreversible on the DSC timescale (10 degrees min^{-1}) and that the entire complex had converted to the β phase. PXRD carried out on a sample converted to the beta phase 2 months previous, shows only the pattern

associated with the beta phase indicating that the conversion from alpha to beta phase is irreversible. Previous VTXRD studies had also hinted at the presence of a phase transition at high temperature in these materials[1]. Recently Frech et al have also reported the existence of a polymorph of PEO_6:$LiSbF_6$[2] with a x-ray diffraction pattern that is very similar to our β - phase.

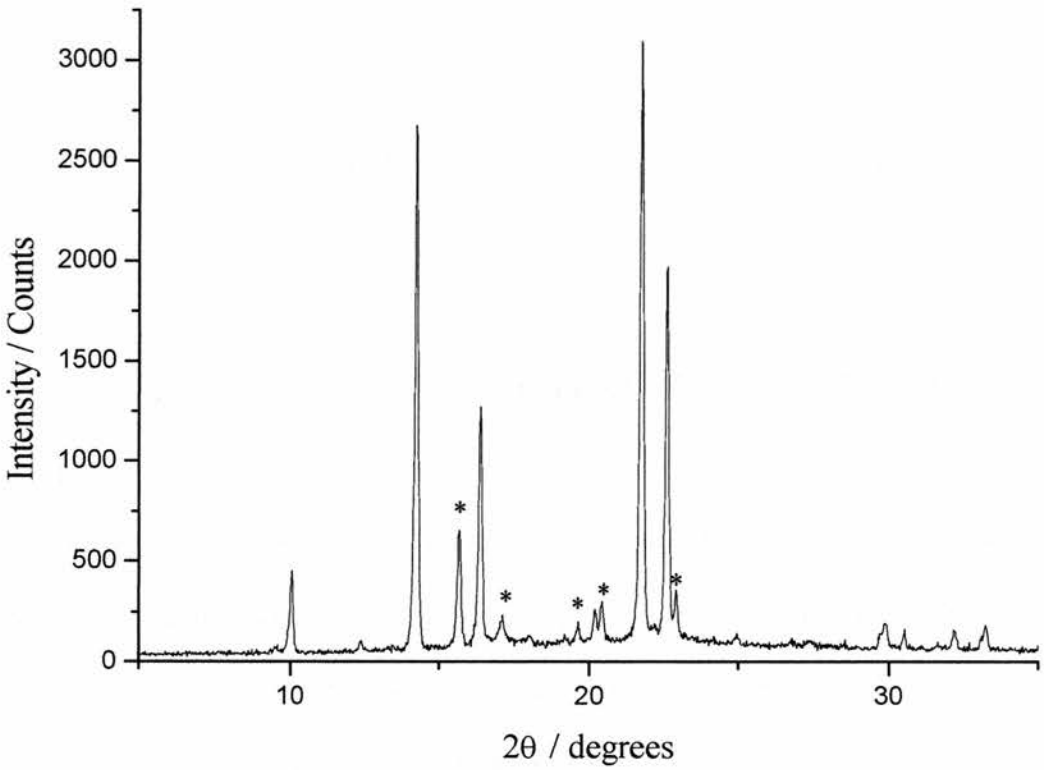

Figure 9.1.1 *PXRD pattern of mixed phase sample produced by solvent casting. Reflections from the β - phase are annotated by an asterix.*

A sample of composition $P(EO)_6LiAsF_6$ was melted and then cooled to room temperature (see section 3.1.3). Powder diffraction of this melt-cooled material yielded a completely different phase pure pattern to that of the usual α-phase $P(EO)_6$:$LiAsF_6$ structure and of excellent quality, the most intense reflection occurring at a 2 theta of 15.6° (see fig 9.1.2). There was no evidence of reactant peaks, 3 to 1 complex peaks or α phase 6 to 1 complex peaks. We had succeeded in preparing a pure phase of a new $P(EO)_6$:$LiAsF_6$ polymorph.

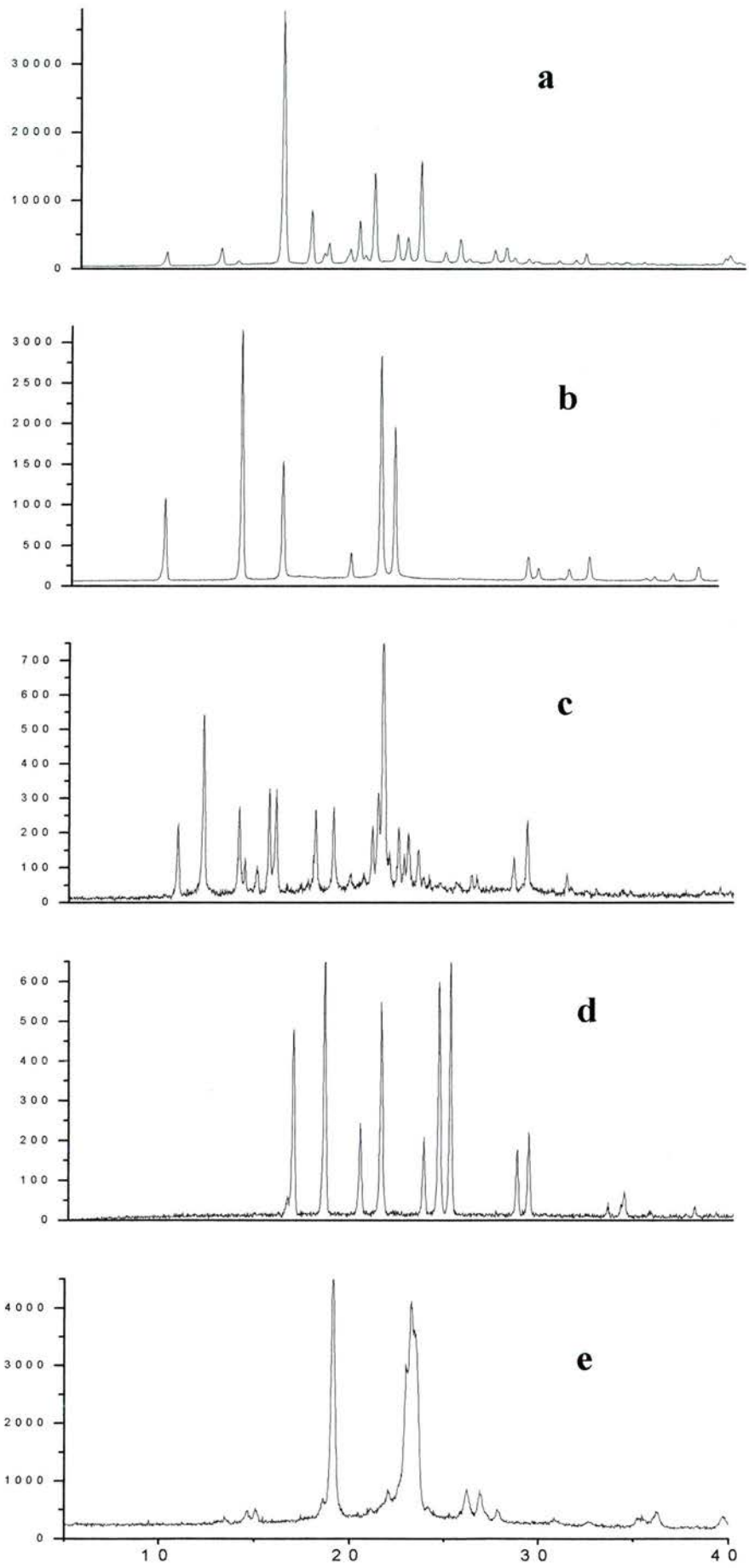

Figure 9.1.2. *PXRD patterns of (a) β – $P(EO)_6$:$LiAsF_6$, (b) α - $P(EO)_6$:$LiAsF_6$, (c) $P(EO)_3$:$LiAsF_6$, (d) $LiAsF_6$, (e) PEO Mw 1000*

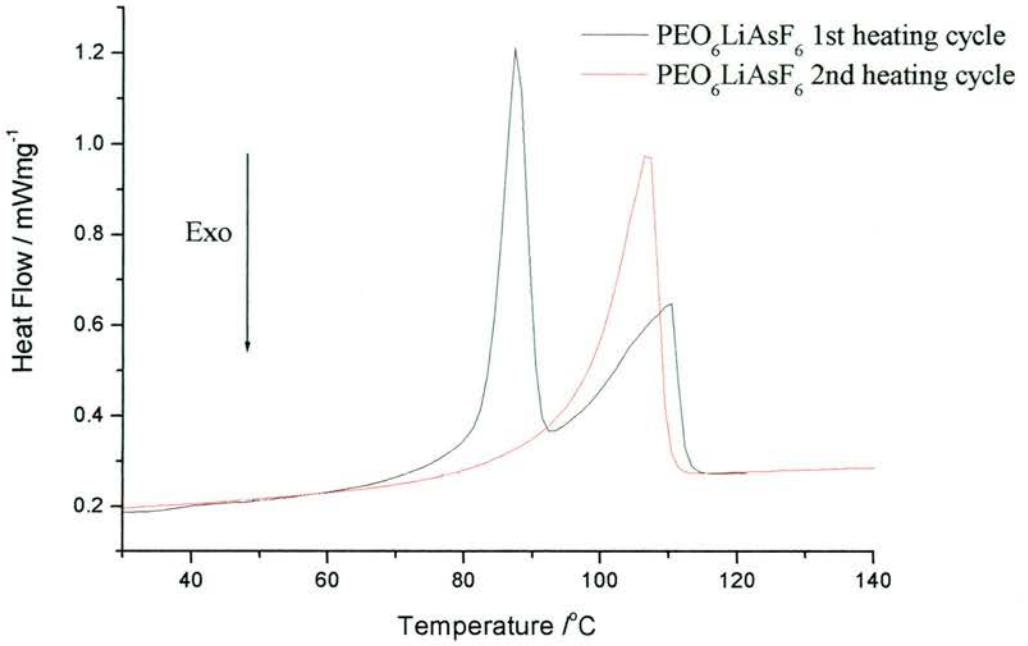

Figure 9.1.3. *DSC trace of $P(EO)_6$:$LiAsF_6$. First heating cycle: black line, second heating cycle: red line.*

9.2 Structure Solution of β – $P(EO)_6$:$LiAsF_6$

The powder diffraction pattern was indexed yielding an orthorhombic cell, a = 18.467(9) Å , b = 10.314(2) Å, c = 9.803(9) Å by six different powder indexing programs using the Crysfire program[3] and the first 20 peaks of the pattern. The best fit from TREOR yielding a figure of merit of 42 for the first 20 reflections. The space group was determined from a list of likely orthorhombic candidates (space groups with multiplicity four as dictated by the density of the material and by Le Bail fitting with GSAS), each possible space group was tried using the FOX code and only $P2_12_12$ gave a chemically feasible structure by this trial and error approach . Structure elucidation was carried out *ab-initio* using the FOX code[4]. Three structural fragments were placed within the unit cell: a Li^+ cation, a segment of PEO chain consisting of six ethylene oxide repeat units, and an AsF_6^- anion. The atomic positions were described in terms of internal stereochemical descriptors: bond lengths, bond angles

and torsion angles with respect to an atom chosen as an origin. Starting from randomly chosen positions 79 parameters including 23 bond lengths, 25 bond angles and 15 torsion angles in a Monte Carlo fashion to create trial structural models. Each model was used to calculate a powder pattern, which in turn was compared with the experimental powder diffraction data by means of an agreement factor (χ^2). FOX then located a global minimum in the agreement factor by parallel tempering producing a structural model with a continuous PEO chain (no assumption of chain continuity had been made *a priori*).

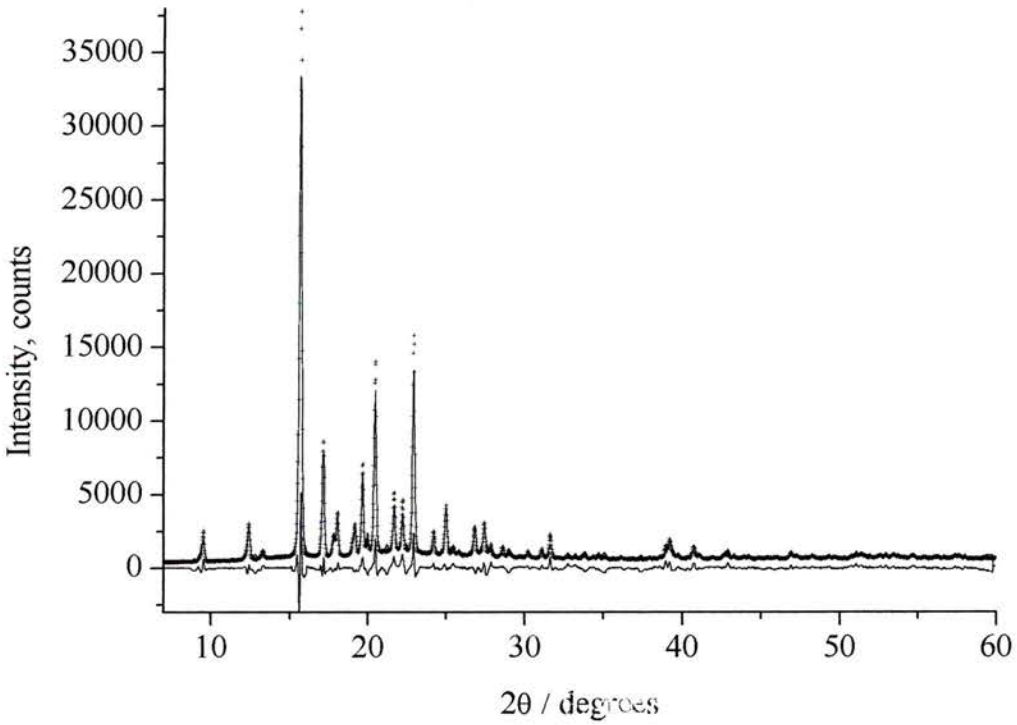

Figure 9.2.1. *Fitted X-ray powder diffraction pattern of β-PEO_6LiAsF_6. Crosses, observed profile; solid lines, calculated (upper). Lower: difference profile.*

The lithium ions were placed within the only two possible co-ordination sites provided by the geometry of the PEO chain, incidentally the locations afforded by the PEO chain for the lithium ions both corresponded to special positions within the unit cell. Given the structural complexity of this polymer electrolytes (79 degrees of freedom), the absence of a suitable structural starting model and the fact that there are

two distinct lithium ions in the unit cell both on 'special positions' this structure solution represents one of the most the most complex structures ever solved *ab initio* from powder diffraction data. The structural model was obtained using x-rays by means of Rietveld refinement using the GSAS package gave a good fit to the x-ray diffraction pattern (see figure 9.2.1) with Rp = 9.62%.

A sample of β-$P(EO)_6$:$LiAsF_6$ was prepared using deuterated PEO (see section 3.1.3) for the purposes of neutron diffraction. Neutron diffraction data were then collected on GEM at ISIS and the model obtained from the x-ray data was refined using this neutron diffraction data resulting in Rwp = 2.21% (see figures 9.2.2 and 9.2.3).

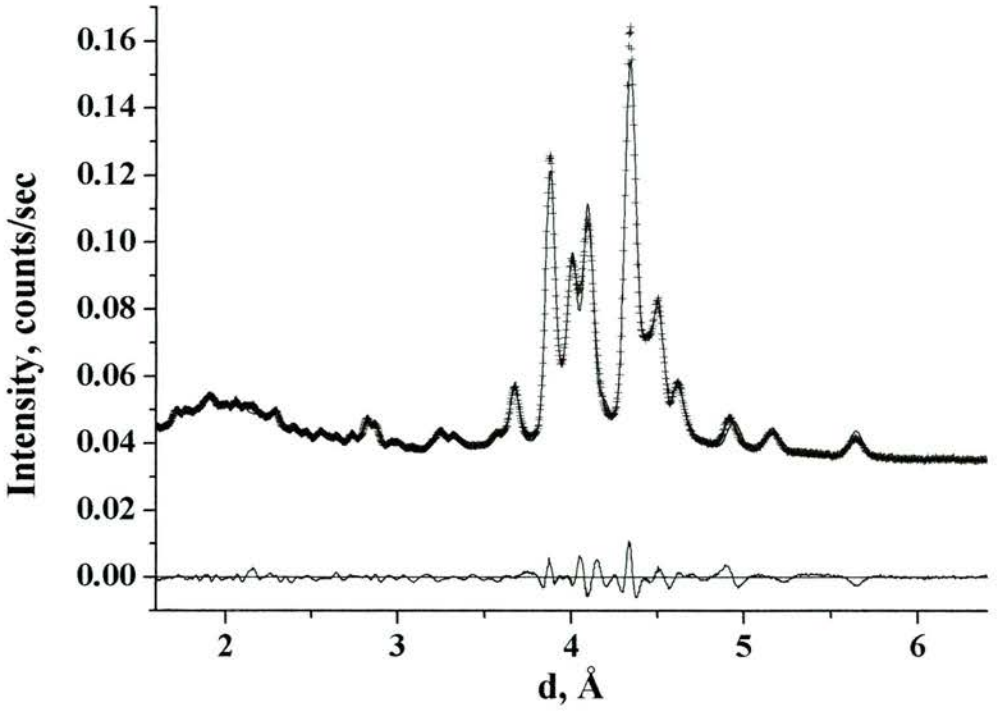

Figure 9.2.2. *Fitted powder neutron diffraction pattern of β-PEO_6LiAsF_6. Crosses, observed profile; solid lines, calculated (upper). Lower: difference profile.*

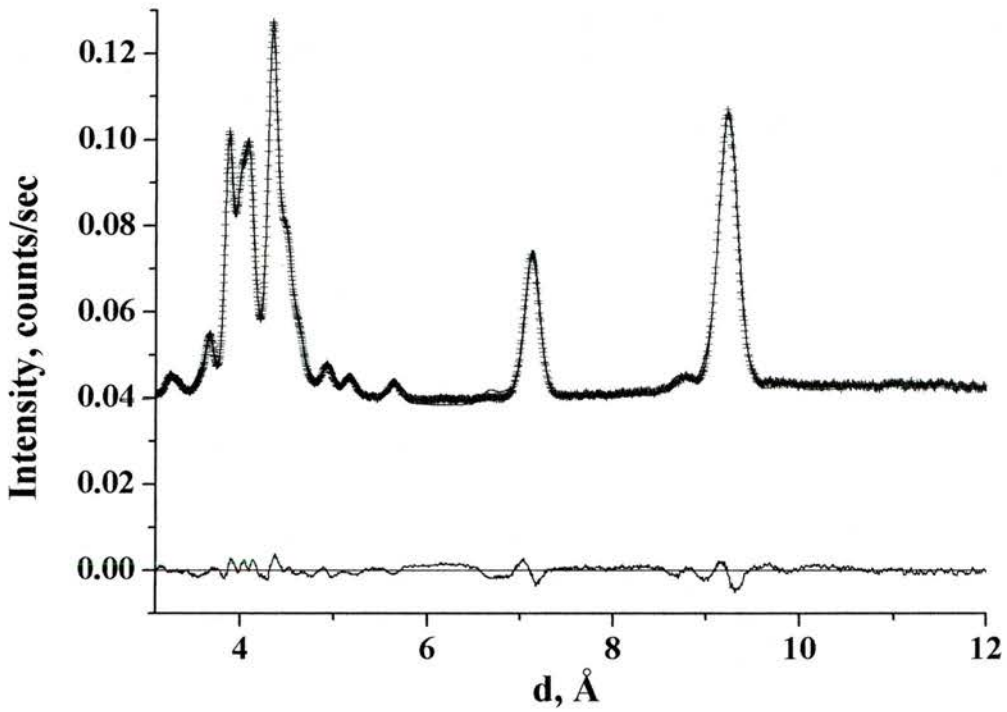

Figure 9.2.3. *Fitted powder neutron diffraction pattern of β-PEO_6LiAsF_6. Crosses, observed profile; solid lines, calculated (upper). Lower: difference profile.*

The structure of β–$P(EO)_6$:$LiAsF_6$ (see fig. 9.2.4) is different from all known crystal structures of PEO:salt complexes and most importantly it is quite distinct from the α-$P(EO)_6$:$LiAsF_6$ polymorph. Instead of the tunnels witnessed in the alpha phase of the material (see figure 1.3) we instead see a zig-zag chain arrangement (see figure 9.2.5) with two different lithium ion co-ordination sites (see figure 9.2.6).

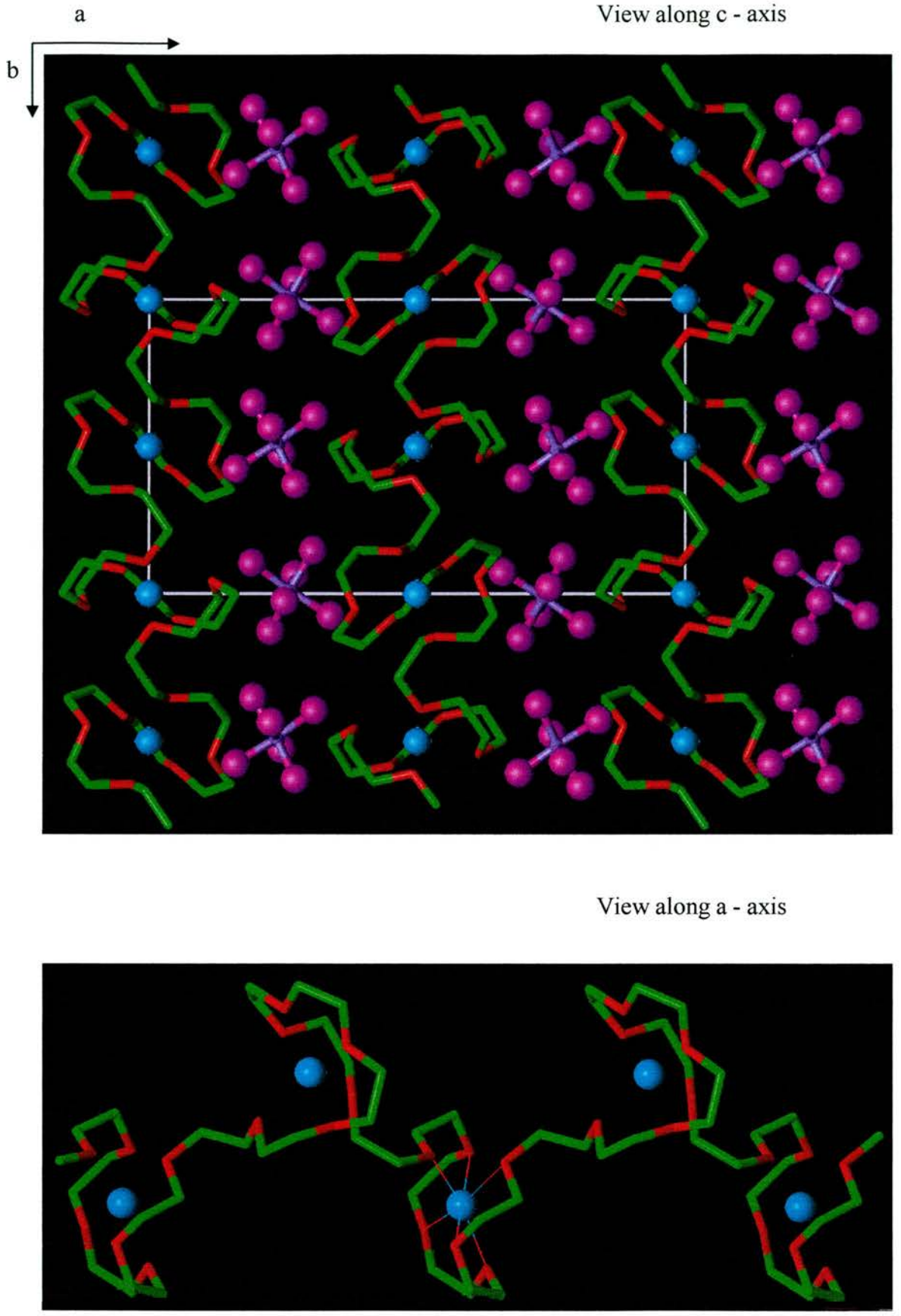

Figure 9.2.4. *Structure of β-P(EO)$_6$:LiAsF$_6$, refined from neutron diffraction data.*

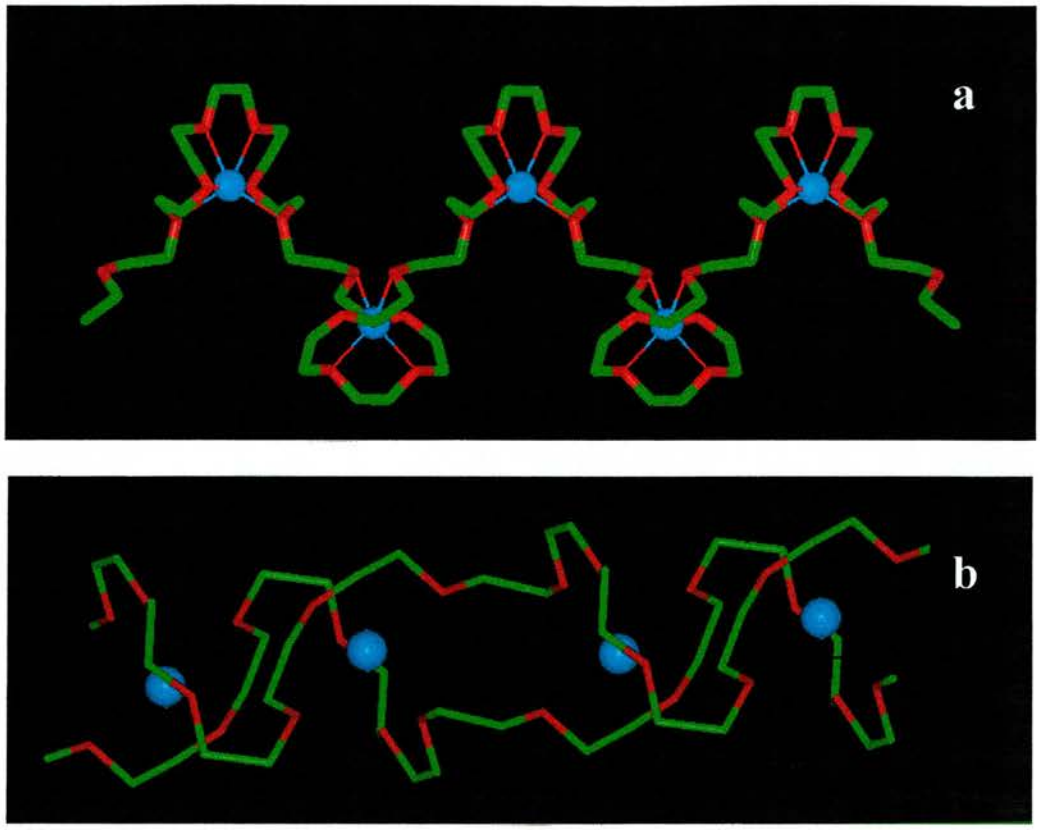

Figure 9.2.5. *Side projection of (a) β – $P(EO)_6$:$LiAsF_6$, and (b) α - $P(EO)_6$:$LiAsF_6$ showing that no clear pathway exists for lithium ion migration in the beta phase as it does in the alpha phase. Lithium: blue, carbon: green, oxygen: red.*

Both lithium ions are also 6 co-ordinate in the beta phase, where as in the alpha polymorph the lithium ions are only co-ordinated by 5 ether oxygens leaving one free oxygen per cation. In common with the alpha phase the cations are completely dissociated from the anion.

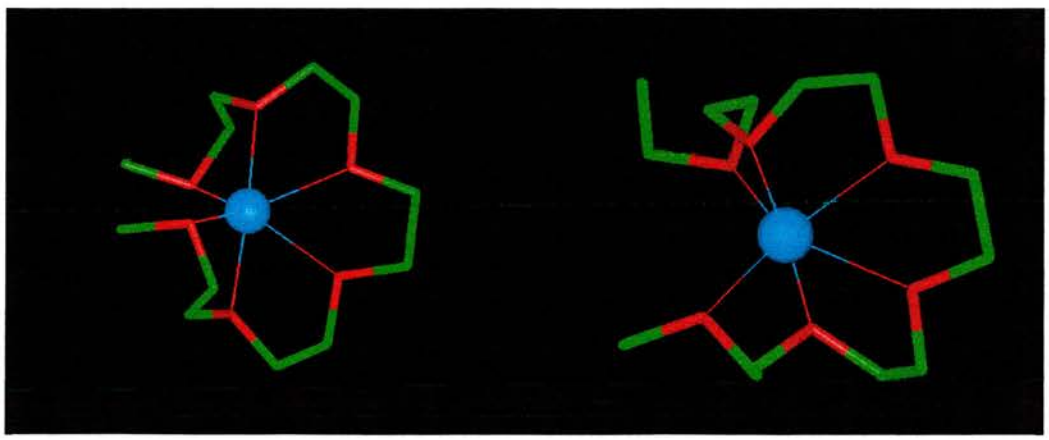

Figure 9.2.6. *Lithium co-ordination sites in β – $P(EO)_6LiAsF_6$*

The chain conformation for this complex is also unique. It describes both co-ordination sites that are created by the chain to accommodate the lithium ions.

$$(c\ t\ \bar{g}\ c\ \bar{g}\ g\ g\ g\ g\ \bar{g}\ c\ t\ c\ t\ \bar{g}\ c\ g\ t\ g^{*}\ t\ g\ c\ \bar{g}\ t\ c\ t\ c\ \bar{g}\ g\ g\ g\ g\ \bar{g}\ c\ \bar{g}\ tc)$$

The conformation is symmetrical around the torsional angle marked by the asterisk above, this corresponds to the angle that bridges the chain from the end of one unit cell to the beginning of the next.

9.3 Conductivity of β – $P(EO)_6$:$LiAsF_6$

In terms of conductivity, unsurprisingly, the conductivity of the beta phase of $P(EO)_6$:$LiAsF_6$ is substantially lower than the alpha phase, around three quarters of an order of magnitude lower at room temperature (see figure 9.3.1). The disparity in the conductivity between the alpha and beta phase can be attributed to the absence of a clear conduction pathway through the β-phase complex. The alpha phase provides tunnels through which the ions can travel in contrast to the beta phase where no clear ion migration channel exists. Also the alpha polymorph possesses one spare oxygen per cation that offers the possibility of an intermediate co-ordination site. Molecular dynamic simulations certainly suggest these spare oxygen play a part in the conduction mechanism of these materials[6] . This result offers compelling evidence that the bulk structure of these materials is at least an important factor in controlling their conductivity.

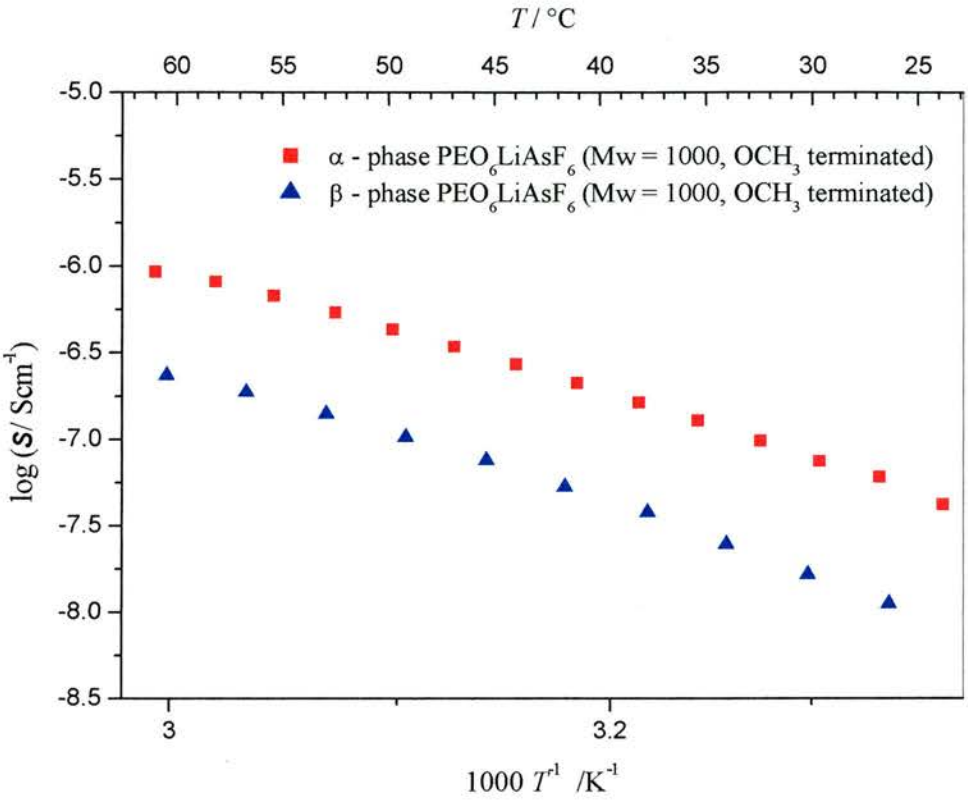

Fig. 9.3.1. *Log conductivity vs. reciprocal temperature for alpha (red squares) and beta (blue triangles) phases of $P(EO)_6$:$LiAsF_6$*

9.4 Thermal Analysis of β – $P(EO)_6$:$LiAsF_6$

The DSC analysis of the beta phase used for conductivity measurements yields only one sharp peak representing the endotherm associated with the phase transformation from solid to liquid (see figure 9.4.1 overleaf) Also present is a small hump indicating a small proportion (< 1%) of alpha phase present in the sample.

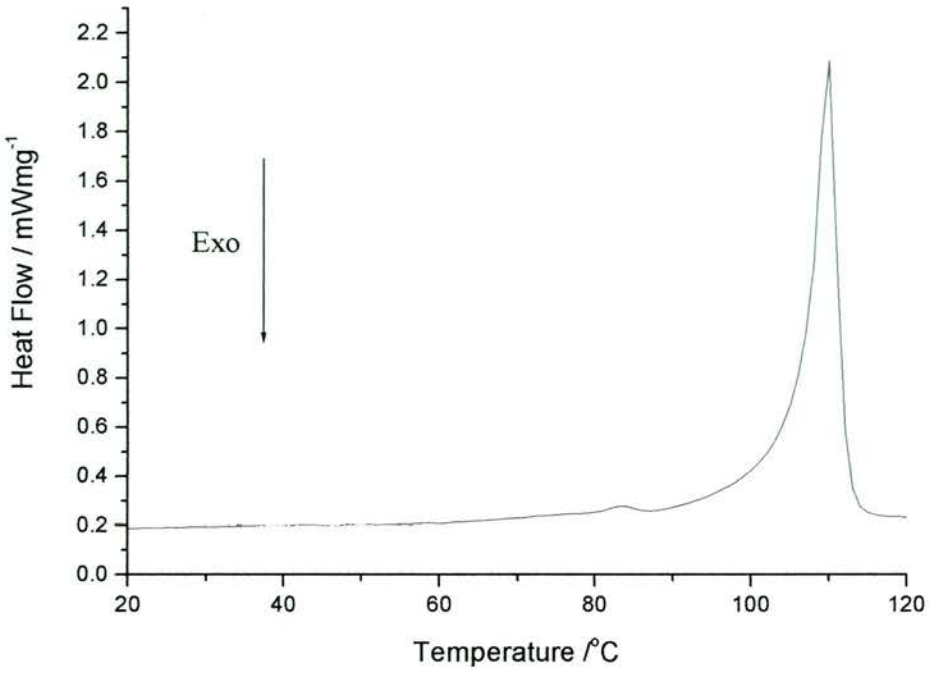

Fig. 9.4.1. *DSC trace of β-phase $P(EO)_6$:$LiAsF_6$ used for conductivity analysis.*

---

[1] Stoeva, Z., University of St. Andrews PhD. Thesis (2001)

[2] Seneviratne V., Frech R., Furneaux J.E., Electrochimica Acta, **48** 2221-2226 (2003)

[3] R. Shirley, "*The Crysfire 2002 System for Automatic Powder Indexing: User's Manual*", The Lattice Press, 41 Guildford Park Avenue, Guildford, Surrey GU2 7NL, England (2002)

[4] Favre-Nicolin, V. and Cerny, R. 'FOX' – Free Objects for Xtal Structures, version 1.6.0.2, (2001-2003)

[5]Larson, A. C. and Von Dreele, R. B. *GSAS, General Structure Analysis System* (Los Alamos National Laboratory rep. no. LA-UR-86-748, Los Alamos, 1987).

[6] Brandell, D. Conference proceedings *Molecular Scale Interations in Ion Conducting Polymers* (2001)

Chapter 10

Solving Structures of Polymer Electrolytes by Refinement of Oligomeric Single Crystal Models using Powder Diffraction Data of Polymeric Complexes

Elucidating the structure of any chemical compound is crucial to the understanding of how that compound behaves. Knowing the structure often acts as a catalyst to many further scientific discoveries. Two famous examples of structure-initiated research are the structure of Benzene proposed by Keuklé in 1865[1] and the discovery of the structure of DNA by Crick and Watson in 1953[2]. Both of these break-throughs led to a proliferation of work on aromatic compounds and nucleic acids respectively.

Many hundreds of polymer electrolytes have been prepared but developing an understanding of their structural chemistry has proved especially difficult. The structure determination technique of choice, single crystal x-ray diffraction, is not in general applicable to these polymeric materials as they have poor crystal growth characteristics; as such single crystals are not available. Also fibre diffraction has, in the past, proved unreliable leading to incorrect structural models being adopted[3]. As a result, powder diffraction has been the main method by which the crystal structures of polymer electrolytes have been established[4,5-8]. Where models of the structures are available they may be refined by fitting their calculated powder patterns to the observed powder diffraction data using the Rietveld method[5,8,9]. However, very few polymer electrolyte structures are known; this lack of structural information has severely restricted the availability of models and hence the potency of this approach for structure elucidation.

Recent years have seen substantial progress in the ability to solve crystal structures *ab initio* from powder diffraction data, i.e. without prior knowledge of the structure. One such method, which is based on generating random trial structures and then locating the global minimum in the goodness-of-fit between the observed and calculated powder diffraction data using simulated annealing, has proved especially powerful in the context of polymer electrolytes[4,7,10,11]. Using this method, the crystal structure of the 6:1 polymer electrolyte poly(ethylene oxide)$_6$:$LiAsF_6$ was solved, where other approaches had failed to elucidate a structure[8]. This structure solution was important because the 6:1 complex was the most dilute (in terms of salt) to be solved at that time, and presented a structure quite different from other known polymer electrolytes and most importantly proved to exhibit ionic conductivity[12].

The notion that crystalline polymer electrolytes conduct ions is contrary to the established view of some 30 years that such ordered materials were insulators! Other misconceptions that have been overturned by structural studies include the belief that ions larger than Na^+ could not be accommodated within a PEO helix; solution of the 4:1 complex, PEO_4:RbSCN, demonstrated that ions as large as Rb^+ could be so accommodated[6].

However powder diffraction techniques have their limitations, often when the number of variables far exceeds the number of observable reflections in the powder pattern it has to be conceded that the multi-dimensional (>90D) parameter space is too complex for the global optimisation algorithm to find the true minimum in the complex landscape of the figure of merit function. Therefore it is important to look beyond these methods alone in the pursuit of structural information.

Structure elucidation is always much simpler when access can be gained to the full three-dimensional diffraction pattern that single crystals provide. Several pointers indicating the possibility of growing suitable crystals presented themselves throughout the course of research carried out on crystalline polymer electrolytes.

It was observed that by decreasing the molecular weight of the polymer used to make $P(EO)_6$:$LiXF_6$ (X = P, As, Sb) an increase in crystallite size occurred[13]. It was conjectured that if the molecular weight of the polymer/oligomer was sufficiently small, crystals could be grown that were suitable for single crystal x-ray diffraction. This information coupled with the fact that PEO of around M_w = 500 is a viscous liquid (crystal growth is known to be favoured when occurring in a medium that can slow diffusion of molecules to the growing crystal[14]) yielded the idea that suitable crystals may be able to be grown. It was also known that at the opposite extreme of molecular weight ie. glymes, it had been observed that single crystals could be grown of the complexes these low molecular weight species form with salts[15].

Crystals of $P(EO)_8$:$NaBPh_4$, $P(EO)_4$:$ZnCl_2$ and $P(EO)_4ZnBr_2$ were grown that had sufficient volume for analysis by single crystal x-ray diffraction.

Using an oligomer with a weight average molecular mass of 500 (11 ethylene oxide repeat units) proved to be sufficiently long to ensure that the structure adopted would be similar to that of the high molecular mass polymeric analogue, rather than the glyme:salt complexes, whose structures although of course related, are rather different.

Although structures of the above complexes were observed from the single crystal, examination of the bond lengths and angles revealed some unrealistic values. This remained so despite collecting data on several different crystals of each complex and attempts to improve the refinement, including modelling the disorder by introducing multiple chains with partial occupancies. The origin of the problem lies in the short ethylene oxide chains of the oligomer, chains are distributed in length about a mean of 11 repeat units (see fig. 10.1), resulting in the chain ends being randomly distributed throughout the crystal. The structure determined by single crystal diffraction does not identify discrete chains; instead the chains appear continuously. Where two chain ends meet two CH_3 groups are adjacent to each other instead of a C-C bond. The separation of two covalently bonded carbons and two adjacent CH_3 groups are of course different. This introduces disorder along the chains within the average crystal

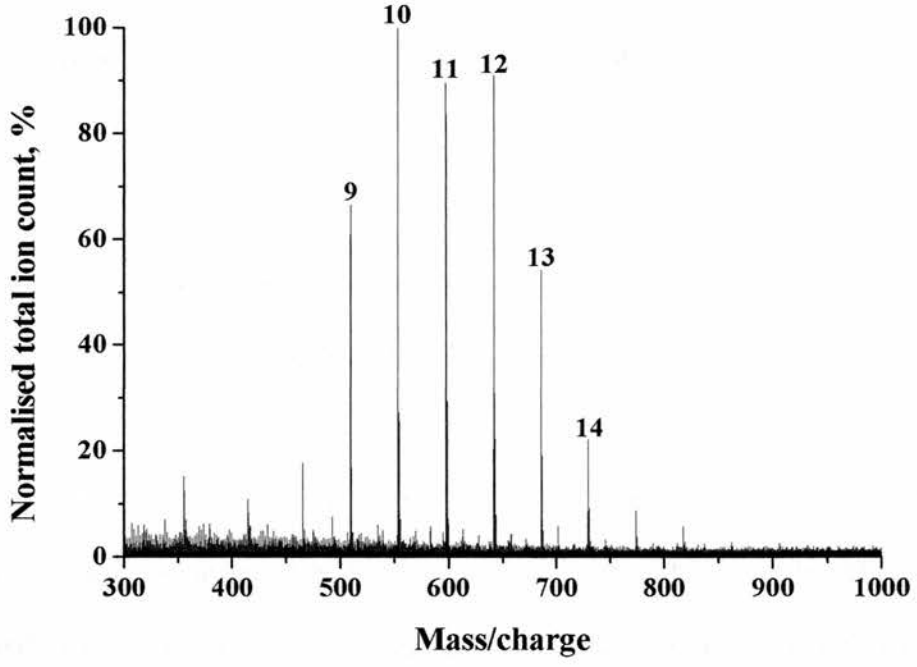

Fig.10.1. *Mass spectrum of a single crystal of PEO_8:$NaBPh_4$, average molar mass 500. As sodium formate was used as calibrant, all masses correspond to the ethylene oxide chain and one Na. Numbers above the peaks represent the number of EO units in the corresponding chains.*

structure hence the abnormalities observed from the single crystal diffraction data. Of course, the effect of the chain ends may be reduced by using longer chains but then single crystals can not be grown.

However powder diffraction data of excellent quality may be obtained even using high molar mass polymers, while the oligomer structure can serve as an adequate starting model for elucidation of the polymer electrolyte structure by refinement.

This approach to structure solution described herein opens the door to the establishment of many polymer electrolyte structures that were too complex to access by other means. The approach is applicable to other crystalline polymers and has potential impact beyond the field of polymer electrolytes, especially to other polymeric solids.

10.1 Structure of poly(ethylene oxide)$_8$:NaBPh$_4$

A single crystal of size 0.1x0.1x0.1mm of the oligomeric 8:1 complex made from PEO of average molar mass equal to 500, was selected for examination by single crystal X-ray diffraction, see section 3.3.2. The structure was solved by Direct Methods and subsequently refined using the SHELXL-97 code[16]. 2699 independently observed reflections with $I > 2\sigma(I)$ were included with 50 non-hydrogen atoms in the asymmetric unit of the cell, which contained one formula unit (8 ethylene oxides and one $NaBPh_4$). The refinement converged to an R factor of 10%. The basic structure was evident from the single crystal solution, examination of the bond lengths and angles revealed some unrealistic values; for example, C-O distances as high as 1.72 Å and C-C distances as low as 1.14 Å were seen for some of the bonds, compared with typical values for PEO of 1.41-1.46 Å (C-O) and 1.52 -1.56 Å (C-C). Excellent

quality powder diffraction data were obtained using a high molar mass polymer (PEO M_w = 100,000). The single crystal structure of the oligomer provided a structural model with which to carry out refinement using the powder diffraction data. The GSAS program package was used for refinement[17]. The powder pattern consisted of 2869 points and contained 1159 reflections. The refinement involved 164 variables with 121 bond length and bond angle slack restraints. In the final stages of the refinement all the constraints were removed and the refinement remained stable. The final R_{wp} was 7% and corresponded to a good fit as seen in Fig 10.1.1.

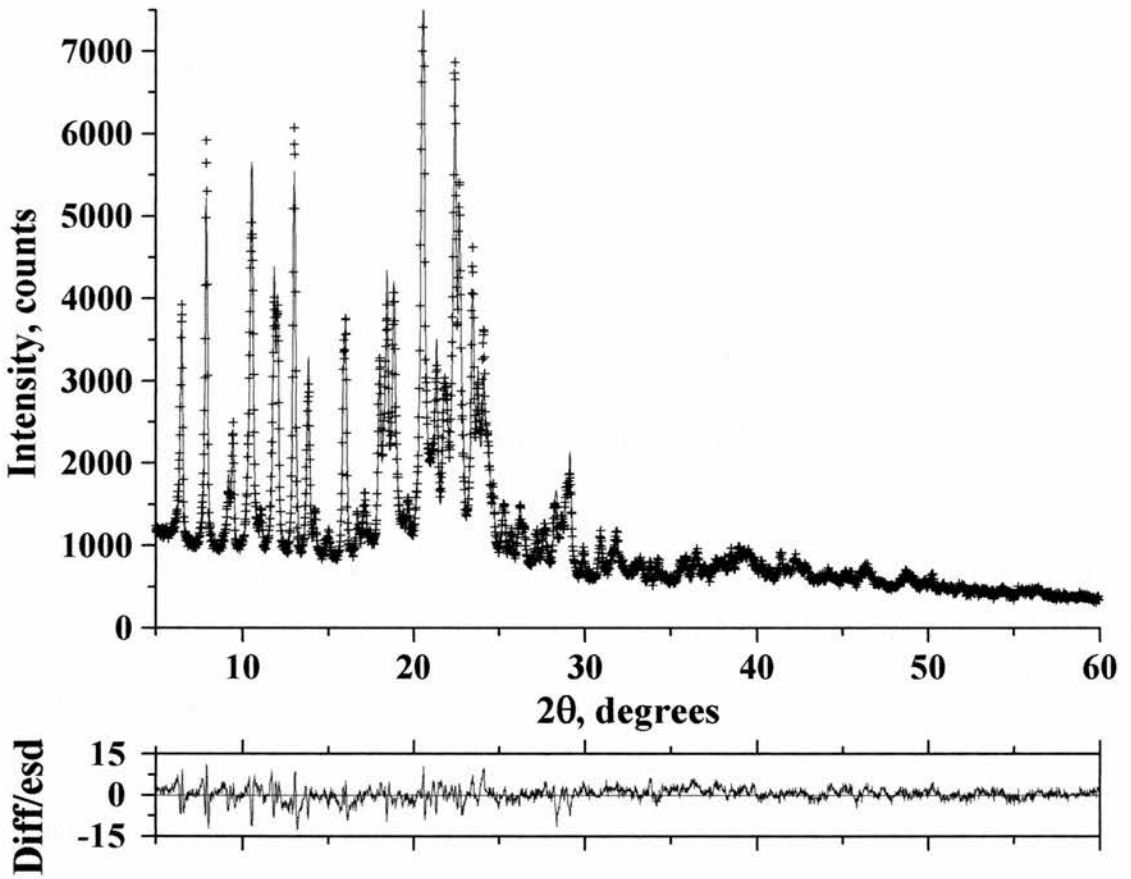

Fig.10.1.1. *Fitted X-ray powder diffraction pattern of PEO_8:$NaBPh_4$, average molar mass 100,000. Crosses, observed profile; solid lines, calculated (upper) and difference (lower) profiles. The unit cell is monoclinic with refined lattice parameters a = 22.737(2) Å, b = 17.117(1) Å, c = 9.8903(8) Å, β = 101.286(7)°. The space group is $P2_1/n$.*

The final structure obtained by refinement using the powder diffraction data is shown in figures 10.1.2 and 10.1.3. Each poly (ethylene oxide) chain folds such as to present a ring of 5 ether oxygens with one ether oxygen above and another below the plane of the ring. The Na^+ ions are located within this ring and are therefore coordinated by 7 ether oxygens. All the sodium-ether oxygen distances lie within the range 2.45-2.50 Å, which is typical for such distances in other complexes. There exists one ethylene oxide unit linking neighbouring rings along the chain (fig. 10.1.2.). The tetraphenyl borate anions are located between the chains and do not coordinate to the cations. Although located between the chains, each BPh_4^- anion is slightly closer to one PEO chain with one Ph moiety situated opposite an ethylene oxide link between two rings that coordinate Na^+ ions (fig.10.1.3).

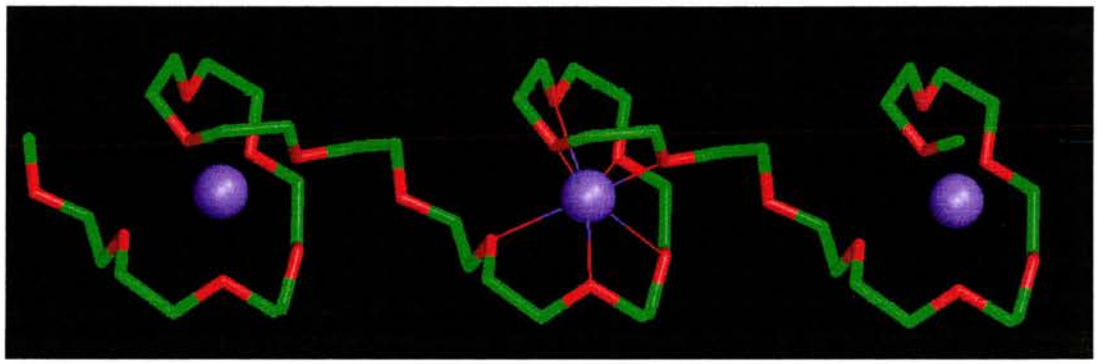

Fig.10.1.2. *View of the structure of PEO_8:$NaBPh_4$ showing the conformation of the PEO chain and the coordination around the Na^+ cation (thin lines) (hydrogens not shown). Purple, sodium: green, carbon: red, oxygen.*

The structure is quite different from all previously known polymer electrolyte crystal structures. Only one chain is involved in coordinating the cations whereas in the 6:1 structures each PEO chain folds to form a half cylinder with pairs of chains interlocking to generate tunnels within which the Li^+ anions reside; there is no coordination of the cations by the anions.

chain confirmations. Also for the first time we observe a chain that describes two conformations which repeat alternately along its length.

$$(t\,g\,g\,\bar{g}\,\bar{g}\,t\,\bar{g}\,\bar{g}\,t\,\bar{g}\,g\,t\,t\,\bar{g}\,\bar{g}\,t\,\bar{g}\,\bar{g}\,t) \text{ and } (c\,t\,\bar{g}\,\bar{g}\,\bar{g}).$$

One involves chain folding to form a coordination site for the cation and the other links these coordination sites along the chain. This is in contrast to structures determined previously which exhibit the same single repeating conformation throughout the structure.

10.2 Structure of poly(ethylene)$_4$:ZnCl$_2$

Many polymer electrolytes containing multivalent cations (including transitional metals, lanthanides and actinides) have been prepared[18,19]. Such materials have potentially important optical, magnetic and electrical properties in a flexible solid, yet it has proved impossible to solve their structures. This section describes the solution of the first polymer electrolyte structure containing multivalent cations, poly(ethylene oxide)$_4$:ZnCl$_2$. This result opens the way to accessing the structures of many other polymer electrolytes containing multivalent cations, something that is essential if their potentially important properties are to be explored, and ultimately exploited.

Some previous work has been carried out on PEO$_4$:ZnCl$_2$ prepared with PEO Mw = 5x10^6 by Sequeira et al[20]. The results of which shows that the material has a room temperature conductivity of around 10^{-6} S cm^{-1} and that it is a mixed ion conductor with a $t+$ of 0.47.

A single crystal of size 0.1 x 0.1 x 0.1mm of the oligomeric 4:1 complex was selected for examination by single crystal x-ray diffraction (see section 3.3.2 for single crystal preparation method). The structure was solved by Direct Methods and subsequently refined using the SHELXL-97 code[16]. 1196 independently observed reflections with I > 2σ(I) were included with 6 non-hydrogen atoms in the asymmetric unit of the cell, which contained 2 ethylene oxides, one Zn^+ and one Cl^- ions. Examination of the structure revealed some unrealistic bond lengths. For example, C-O and C-C distances as short as 1.29Å and 1.35Å respectively. The single crystal solved did however provided a suitable model with which to refine the structure of polymeric

poly(ethylene oxide)$_4$:$ZnCl_2$ complex using powder diffraction data collected from the latter material. It is clear that the crystallite size is generally larger in polymer electrolytes prepared with materials of molar mass close to 1000[13]. This results in narrower powder x-ray peak widths and hence peaks that are better resolved in the powder diffraction patterns, providing data of better quality for refinement. The structure of PEO_4:$ZnCl_2$ was refined using PEO of average molar mass 2000 which offers a good compromise between the resolution of the powder pattern and the proportion of chain ends.

PEO_4:$ZnCl_2$ of average molar mass 2000 was prepared as described in section 3.1.6. Refinement of powder diffraction data was carried out starting from the model obtained from the single crystal diffraction of the oligomeric complex. The GSAS program package was used for refinement[17]. The powder pattern consisted of 2498 points and contained 194 reflections. The refinement involved 30 variables with 15 bond length and bond angle slack restraints. The final χ^2 was 2.6 and corresponded to a good fit as seen in Fig 10.2.1 overleaf.

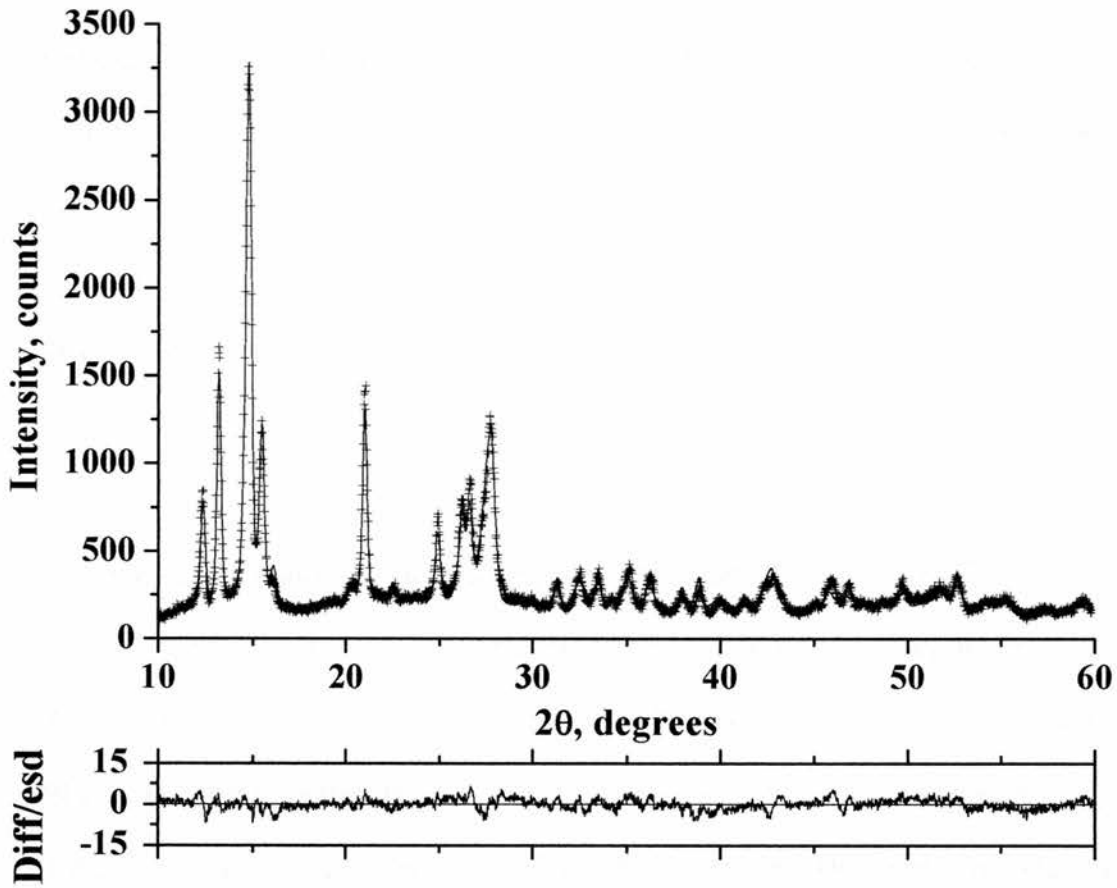

Fig.10.2.1. *Fitted X-ray powder diffraction pattern of PEO_4:$ZnCl_2$, average molar mass 2,000. Crosses, observed profile; solid lines, calculated (upper) and difference (lower) profiles. The unit cell is monoclinic with refined lattice parameters a = 8.4540(8) Å, b = 13.388(2) Å, c = 11.007(2) Å, β = 89.84(3)°. The space group is C2/c.*

The structure of PEO_4:$ZnCl_2$ is shown in Fig. 10.2.2. The PEO chains are located in sets of planes parallel to the *bc* plane of the unit cell, with the chains running along *b*. As can be seen in Fig. 10.2.2 the chains are remarkably flat within these planes. The single chain possesses large loops; within each a Zn^{2+} ion is located. Each Zn^{2+} ion is coordinated by two neighbouring ether oxygens along the chain and two Cl^- ions, each Zn^{2+} is four co-ordinate forming a slightly distorted tetrahedron with the

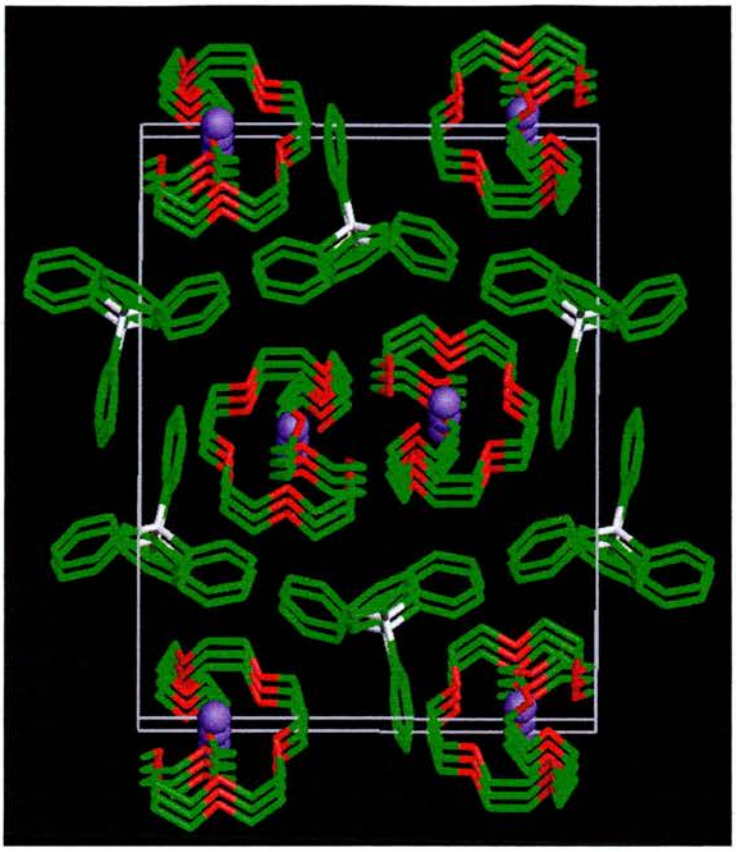

Fig.10.1.3. *View of the structure of PEO_8:$NaBPh_4$ showing the location of the tetraphenyl borate anions relative to the PEO chains and Sodium ions (hydrogens not shown). Purple, sodium; white, boron; green, carbon; red, oxygen.*

As the salt content is increased and we reach the 4:1 and 3:1 complexes, each chain folds to form a helix with a cation being located in each loop of the helix. At these salt concentrations the anions also coordinate the cations unlike the situation in the 6:1 or 8:1 complexes[4]. In the case of the even more concentrated 1:1 complexes the PEO chains adopt a zig-zag confirmation with the cations being coordinated by only 2 ether oxygens and either 4 or 5 anions depending on the particular salt, the anions bridge two cations associated with neighbouring chains thus generating a 3-dimensional network. It can see that extending the boundaries of our polymer electrolyte structure to include the 8:1 complexes has revealed quite new polymer

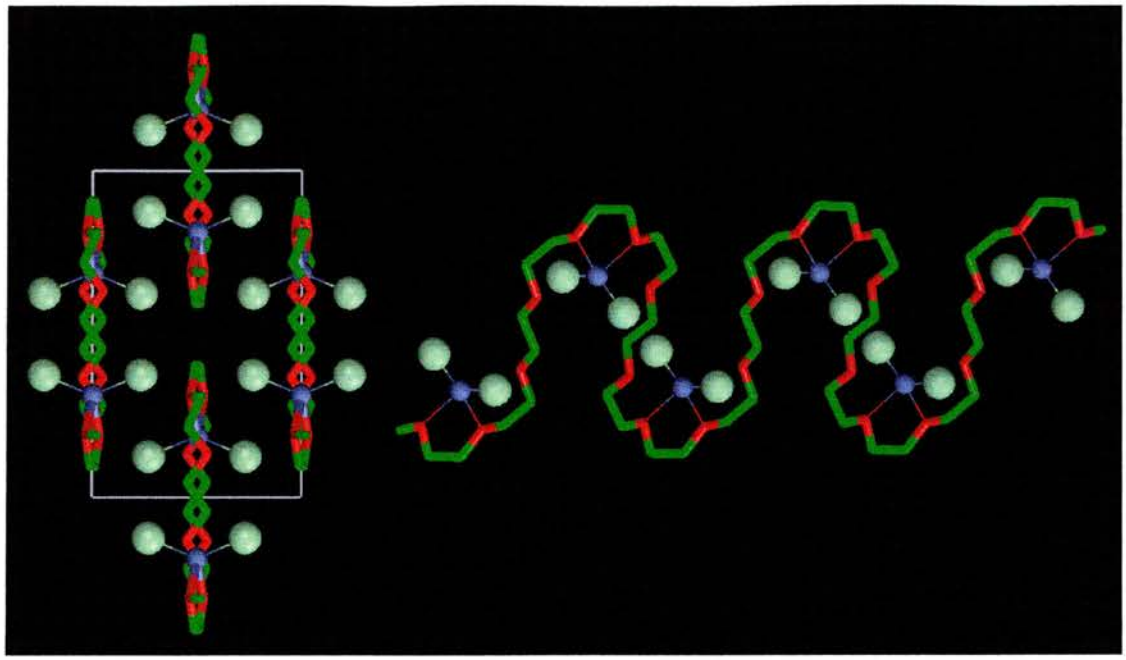

Fig.10.2.2 *(Left) View of the structure of PEO_4:$ZnCl_2$ showing the stacking of 4 PEO chains in the unit cell. The chains are located within the bc plane and run along b. (Right) The conformation of an individual chain and the coordination around the Zn^{2+} cation (thin lines) (hydrogens not shown). Purple, zinc; pale grey, chlorine; green, carbon; red, oxygen.*

surrounding oxygens. There are two non-coordinating ether oxygens between each Zn^{2+} along the chain. Each chain is isolated from its neighbours. The Cl^- ions protrude from each chain but are more than 2.5Å from the atoms of the neighbouring chains, therefore there is no evidence of interaction between the Cl^- ions, or indeed any other parts of the chain, with neighbouring chains. The chains are held together in the solid state by only Van der Waals forces.

As might have been anticipated for the first structure of a polymer electrolyte containing divalent cations, the structure is completely different from any of the previously known polymer electrolytes containing monovalent cations. It would not have been possible to establish the structure of the present material starting from any known monovalent structure.

The structure of a 4:1 complex between PEO and $HgCl_2$ has been solved previously by fibre diffraction[20] (one of the few successful determinations by this method). This complex also contains flat PEO chains however there is no significant bonding between the metal centre and the PEO chain. The mercury atoms are over 2.6 Å from the nearest oxygens in the PEO chain. Also the Hg-Cl bond lengths and angles remain unperturbed compared with their values in the vapor phase eg. Hg-Cl of 2.28 Å [21], indicating that there is no interaction between the chain and the $HgCl_2$ molecules. The PEO chains in $P(EO)_4HgCl_2$ adopt a zig-zag conformation whereas the zinc chloride complex a square-wave like assembly.

The combination of single crystal growth using an oligomer, single crystal diffraction methods and the use of the single crystal structure as a model for refining the structure of the higher molecular weight material using powder diffraction data, provides a powerful tool with which to access polymer electrolyte crystal structures that cannot be solved from powder data alone. In particular, by solving the first crystal structure of a multivalent cation polymer electrolyte it has been demonstrated that it is possible to establish such structures and this opens the way to investigate other multivalent cation polymer electrolytes, not only in terms of their structure but also their potentially important properties and applications.

---

[1] Kekulé, A. *Bulletin de la Société Chimique de France*, **3**, 98 (1865).

[2] Watson, J. D. and Crick, F. H. C., *Nature*, **171**, 737-738 (1953).

[3] Hibma, T., *Solid State Ionics* **9/10**, 1101 (1983).

[4] MacGlashan, G. S., Andreev, Y. G. and Bruce, P. G. *Nature* **398**, 792-794 (1999).

[5] Lightfoot, P., Mehta, M. A. and Bruce, P. G. *Science* **262**, 883-885 (1993).

[6] Thomson, J. B., Lightfoot, P. and Bruce, P.G. *Solid State Ionics,* **85**, 203-208 (1996).

[7] Andreev, Y. G., Lightfoot P. and Bruce, P. G. *Chem. Commun.*, 2169-2170 (1996).

[8] Gadjourova, Z., Martin y Marero, D., Andersen, K. H., Andreev, Y. G. and Bruce, P. G. *Chem. Mater.* **13**, 1282-1285 (2001).

[9]Rietveld, H. M. *J. Appl. Crystallogr.* **2**, 65-71 (1969).

[10]Andreev, Y. G., MacGlashan G. S. and Bruce, P. G. *Phys. Rev. B.* **55**., 12011-12017 (1997).

[11]Martin-Litas, I., Andreev, Y. G. and Bruce, P. G. *Chem. Mater.* **14**, 2166-2170 (2002).

[12]Gadjourova, Z., Andreev, Y. G., Tunstall, D. P. and Bruce, P. G. *Nature* **412**, 520-523 (2001).

[13]Stoeva, Z., Martin-Litas, I., Staunton, E., Andreev, Y.G. and Bruce P.G. *JACS* **125**, 4619-4625 (2003)

[14] Henisch, H.K., Crystal Growth in Gels, Dover Publications (1996)

[15] Seneviratne V., Frech R. and Furneaux J.E., J. Phys. Chem. B **108,** 8124-8128 (2004)

[16]Sheldrick, G. M. and Schneider, T. R. *Method. Enzymol.* **277**, 319-343 (1997).

[17]Larson, A. C. and Von Dreele, R. B. *GSAS, General Structure Analysis System* (Los Alamos National Laboratory rep. no. LA-UR-86-748, Los Alamos (1987).

[18]Farrington, G. C. and Linford, R. G. Poly(ethylene oxide) electrolytes containing divalent cations. In *Polymer Electrolyte Reviews*: edited by J. R. MacCallum and C. A. Vincent, pp. 255-284. Elsevier Science Publishers Ltd, Barking (1989).

[19]Armand, M. and Gauthier, M. Polymeric Solid Ion Conductors. In *High Conductivity Solid Ionic Conductors – recent trends and applications*: edited by T. Takahashi, pp. 114-145. World Scientific Publishing Co. Pte. Ltd, Singapore (1989).

[20]Plancha, M. J., Rangel, C.M., Sequeira C.A.C., *J. Electroanalytical Chem.* **442**, 91-97 (1998)

[21]Cotton, F.A. and Wilkinson G., Advanced Inorganic Chemistry, 5th Edition, 611

Chapter 11

Confirmation of a Structure Solved *Ab-Initio* from Powder Diffraction Data using 'Simulated Annealing' by Single Crystal X-ray Diffraction.

Methods of solving structures from PXRD data have yielded many polymer electrolyte structures[1]. For the first time, one of these structures, solved from powder diffraction data, $P(EO)_3$:$LiAsF_6$, has been confirmed by analysis of a single crystal of the same complex. This confirms the potency of the '*Simulated Annealing*' method of structure solution when single crystals cannot be grown.

11.1 Solution from PXRD Data

The structure of $P(EO)_3$:$LiAsF_6$ was first solved *ab-initio* using powder diffraction data (both x-ray and neutron) by Martin-Litas, Andreev and Bruce in 2002[2]. The sample produced a powder diffraction pattern of excellent quality. It consisted of around 351 Bragg reflections, 2749 data points in the range of 2 theta from 5 to 60 with 0.02° steps. The powder pattern was used to index a unit cell by analysis of systematic absences as a monoclinic cell of dimensions a = 16.690 Å, b = 8.5912 Å, c = 9.3945 Å and β = 119.175 with space group $P2_1/a$. An assumption was made that there was 1 formula unit ie. 3 ethylene oxide repeats and one $LiAsF_6$ molecule, in the asymmetric units of the unit cell based on the expected density of the complex. The 'Simulated Annealing' method of structure elucidation was carried out using powder diffraction data, see section 2.1.1 for details. In total 37 parameters were varied simultaneously during the global optimisation. Over 1 million trial structures were tested against the whole powder pattern, converging to give a model that gave a

reasonably good fit to the PXRD data (χ^2 = 14, R_{wp} = 13%). The model consisted of all the $(CH_2\text{-}CH_2\text{-}O)_3$ units linked at the junctions of the neighbouring asymmetric units, thus forming a continuous PEO chain, no assumption of chain continuity had been made *a priori*. This served as a useful independent test of the structural model. The positions of the lithium ions in the structural model obtained from 'Simulated Annealing' using the powder x-ray diffraction data were physically unreasonable, located outside the PEO helices and bonding to neither the PEO chain nor the anions. Lithium is a weak scatterer of x-rays, as such, its position within the asymmetric unit causes very little difference to the calculated diffraction pattern of the model or the experimentally obtained pattern. To determine the positions of the lithium ions, neutron diffraction was carried out on a deuterated complex. Lithium is a stronger scatterer of neutrons than it is of x-rays relative to other atoms. Structural refinement using GSAS[3], of the structural model using neutron data (64 variables and 41 soft constraints) was carried out. At the start of the refinement the lithium ion was placed within the helix. A much better fit to experimental data was achieved from the refinement (χ^2 = 6, R_{wp} = 8.6%). The location of the lithium ions made physical sense and the conformation pattern of the chain was the same as with all other known 3:1 complexes.

11.2 Solution from Single Crystal X-ray Diffraction.

Single crystals of $P(EO)_3$:$LiAsF_6$ were grown by slow evaporation of acetonitrile from a solution of PEO Mw 1000 and $LiAsF_6$, the relative amount of PEO to salt in the solvent gave a ethylene oxide to salt ratio of 3 to 1. These crystals were subsequently used in structure determination by single crystal x-ray diffraction. The details are shown below in table 11.2.1. Single crystal diffraction data were collected using Mo K_α radiation on a Bruker SMART® diffractometer equipped with a fine-focus sealed tube, a graphite monochromatic and a CCD detector.

Complex	PEO_3LiAsF_6
Empirical formula	$C_6 H_{12} O_3 Li F_6 As$
Crystal Size/mm	0.2 x 0.1 x 0.05
Formula Weight	328.05
Crystal System	Monoclinic
Space Group	P2(1)/n
Unit Cell Dimensions a, α (Å, °)	9.304(3), 90
b, β(Å, °)	8.535(2), 97.444(9)
c, γ(Å, °)	14.514(4), 90
Volume/$Å^3$	1142.7(5)
Z	4
Calc. Density/mgm^{-3}	1.907
Abs. Coefficient/mm^{-1}	3.047
Temperature/K	125
Wavelength/ Å	0.71073
Reflections Collected/Unique	6522/2008
Goodness-of-fit on F^2	1.059
R[I>2σ (I)]	0.0274
Rw	0.0679
R (all data)	0.0314
Rw	0.0703

Table 11.2.1. *Details of structure determination from single crystal x-ray diffraction of $P(EO)_3$:$LiAsF_6$.*

11.3 Comparison of Solution from PXRD Data and Single Crystal Data.

Each structure solutions employs a different but equally valid unit cell and space group. The basic structural features of the solutions from powder data and the solution from single crystal data are very similar (see figure 11.3.1 and 11.3.2). Each PEO chain adopts the conformation of a 6(1) helix. Lithium ions are located within each coil of the helix with each lithium ion being co-ordinated by three ether oxygens and one fluorine from each of two AsF_6^- ions. The anions are located near the edge of the PEO chains with each bridging between two Li^+ ions along the chain by donating one F to each of two neighboring Li^+ ions. The anions do not coordinate cations on

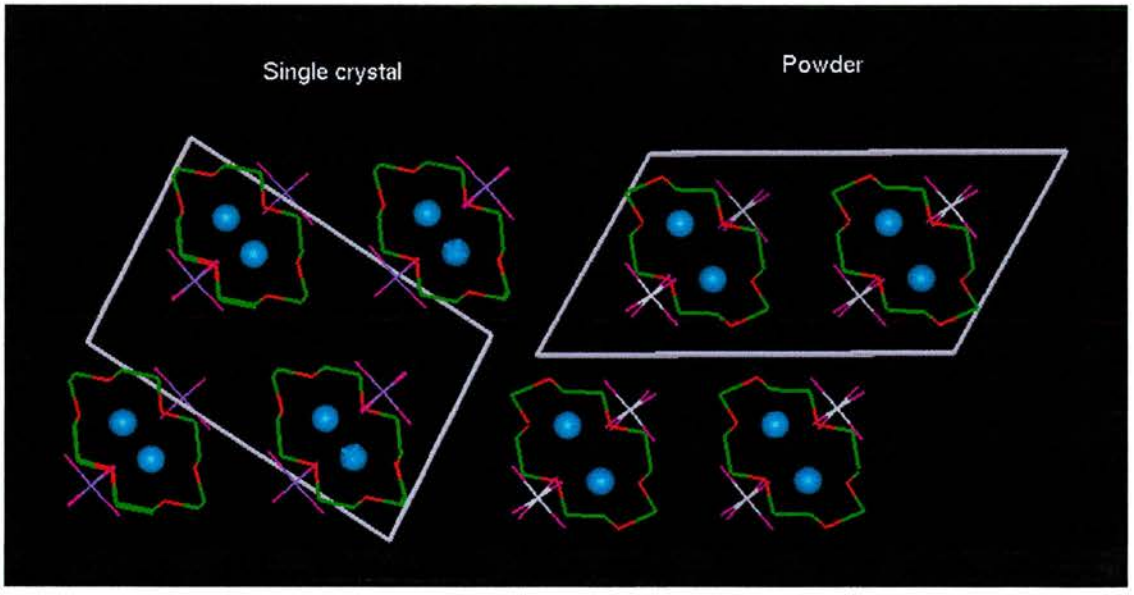

Figure 11.3.1. *Comparison of $P(EO)_3$:$LiAsF_6$ structure from single crystal diffraction data (left) and powder diffraction data (right), looking along 'b' axis. Carbon (green), oxygen (red), lithium (blue), anions (magenta and white)*

neighboring chains; hence, there is no ionic crosslinking. Each PEO chain is associated with a dedicated set of Li^+ and AsF_6^- ions. However there are slight

differences in the structures obtained from single crystal data and from powder diffraction data (see table 11.3.1).

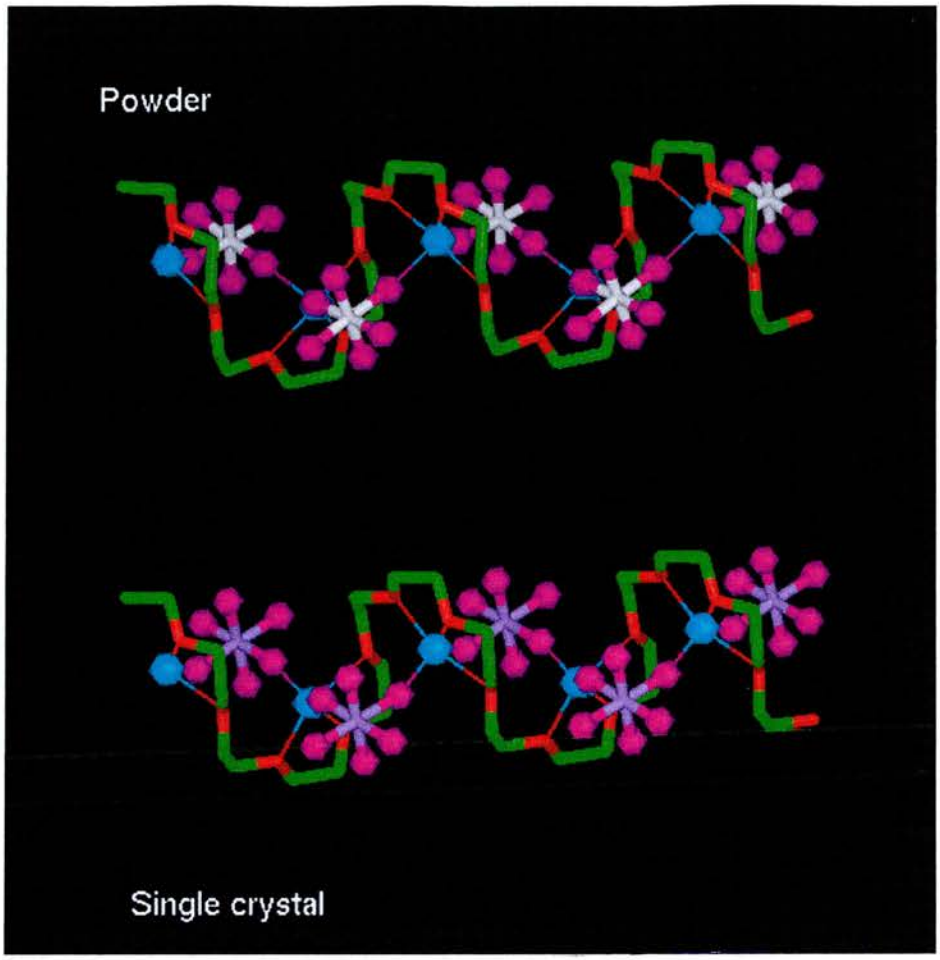

Figure 11.3.2. *Comparison of $P(EO)_3$:$LiAsF_6$ structure from single crystal diffraction data (bottom) and powder diffraction data (top). Carbon (green), oxygen (red), lithium (blue), anions (magenta and white)*

These differences are not surprising when you consider that single crystals give access to around 100 times more observable reflections than their microcrystalline counterparts. There most significant difference in the two structural models are the difference in the conformation of the PEO chains.

The model from single crystal diffraction gives the chain conformation as:

$$t\,t\,g\,t\,t\,g\,t\,t\,\bar{g}$$

Whereas the chain conformation from PXRD data is:

$ttgtt\bar{g}tt\bar{g}$

The difference that the different torsional angle makes in terms of structure is highlighted below in figure 11.3.3.

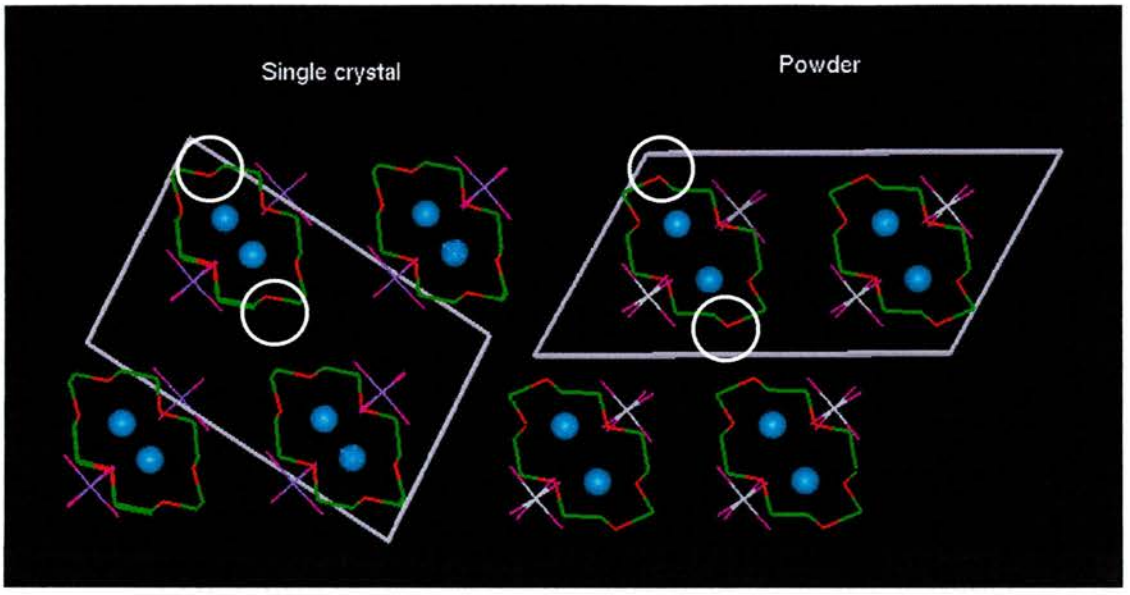

Figure 11.3.3. *Comparison of structures highlighting the effect of the different torsional angle in both models.*

There are also small differences in the Li-O\F bond lengths. Li – O bond lengths in the solution from powder data are 2.10(2) Å to 2.22(2) Å and Li-F bond lengths are 2.13 Å and 2.20 Å. From the single crystal solution Li – O bond lengths are 2.10 Å, 2.41 Å and 1.95 Å and Li – F bond lengths are shown to be 1.89 Å and 1.92 Å. The geometry of the AsF_6^- anion shows good agreement in both models.

	Powder Diffraction	**Single Crystal**
Li – O1	2.22(2) Å	2.103(5) Å
Li – O2	2.22(2) Å	2.410(4) Å
Li – O3	2.10(2) Å	1.950(5) Å

Li – F3	2.13(2) Å	1.892(5) Å
Li – F4	2.20(2) Å	1.924(4) Å
O1 – C1	1.43(5) Å	1.430(3) Å
C1 – C2	1.56(2) Å	1.496(4) Å
C2 – O2	1.44 (2) Å	1.428(3) Å
O2 – C3	1.42(2) Å	1.428(3) Å
C3 – C4	1.57(2) Å	1.477(4) Å
C4 – O3	1.42(2) Å	1.436(3) Å
O3 – C5	1.41(2) Å	1.412(3) Å
C5 – C6	1.53(2)Å	1.499(4) Å
O1 – C6	1.41(2) Å	1.433(3) Å
C1 – O1 – C6	114(2)°	112.35(19)°
O1 – C1 – C2	110(2)°	109.5(2)°
C1 – C2 – O2	105(2)°	110.3(2)°
C2 – O2 – C3	110(2)°	110.5(2)°
O2 – C3 – C4	104(2)°	106.8(2)°
C3 – C4 – O3	106(2)°	106.2(2)°
C4 – O3 – C5	108(2)°	116.2(2)°
O3 – C5 – C6	110(2)°	105.2(2)°
O1 – C6 – C5	106(2)°	106.8(2)°
C1 – C2 – O2 – C3	-153 (*t*)	-178.63 (*t*)

C2 – O2 – C3 – C4	160 (*t*)	169.1 (*t*)
O2 – C3 – C4 – O3	81 (*g*)	74.5 (*g*)
C3 – C4 – O3 – C5	-149 (*t*)	-168.2 (*t*)
C4 – O3 – C5 – C6	150 (*t*)	-176.1 (*t*)
O3 – C5 – C6 – O1	-108 ($\bar{g}$)	60.6 (*g*)
C5 – C6 – O1 – C1	-173 (*t*)	175.5 (*t*)
C6 – O1 – C1 – C2	175 (*t*)	-171.3 (*t*)
O1 – C1 – C2 – O2	-66 ($\bar{g}$)	-57.3 ($\bar{g}$)

Table 11.3.1. *Comparison of selected bond lengths, bond angles and torsion angles of $P(EO)_3$:$LiAsF_6$ solved from single crystal diffraction and powder x-ray diffraction.*

---

[1] MacGlashan, G. S., Andreev, Y. G. and Bruce, P. G. *Nature* **398**, 792-794 (1999).

Lightfoot, P., Mehta, M. A. and Bruce, P. G. *Science* **262**, 883-885 (1993).

Thomson, J. B., Lightfoot, P. and Bruce, P.G. *Solid State Ionics,* **85**, 203-208 (1996).

Andreev, Y. G., Lightfoot P. and Bruce, P. G. *Chem. Commun.*, 2169-2170 (1996).

Gadjourova, Z., Martin y Marero, D., Andersen, K. H., Andreev, Y. G. and Bruce, P. G. *Chem. Mater.* **13**, 1282-1285 (2001).

[2] Martin-Litas, I., Andreev, Y.G. and Bruce, P. G. *Chem. Mater.* **14**(5), 2167 (2002)

[3] Larson, A. C. and Von Dreele, R. B. *GSAS, General Structure Analysis System* (Los Alamos National Laboratory rep. no. LA-UR-86-748, Los Alamos (1987).

Chapter 12

Conclusion

The work presented in this thesis can be divided into two distinct themes. Investigation and manipulation of the crystalline polymer electrolytes, $P(EO)_6$:$LiXF_6$, X = P, As, Sb, and exploration of new crystal structures of polymer electrolyte materials.

Regarding the former theme, these materials have been modified to increase their conductivities, by doping, and by altering the polymer chains of these materials. These techniques have given rise to materials that are on the verge of being commercially exploitable.

Also to gain a better understanding of these systems, monodispersed polymers have been used to probe the relationship between chain length, crystal structure and conduction mechanism, which have led to interesting and unexpected results.

The structure-property relationship of these crystalline materials were further explored when the structure of the beta phase of $P(EO)_6$:$LiXF_6$, X = P, As, Sb was elucidated. It was shown that by virtue of its structure, it exhibited inferior conductivity compared to the alpha phase. This is direct evidence that the structure of crystalline polymer electrolytes plays a role in determining conductivity.

The second theme covered by this thesis is the exploration of new polymer electrolyte crystal structures. With glymes and glycols, (low molecular weight analogues of PEO) it has been shown that an array of structures are adopted when complexed with

$LiXF_6$. It has been shown that structural motifs are dependant on the chain length of the glyme or glycol used and also the functionality of the chain ends. They exhibit different structures from their polymeric counterparts.

A new method to solve crystal structures of polymer electrolytes was developed and presented in this thesis. This new method involves growing single crystals of polymer electrolyte complexes, using low molecular weight polymers and then refinement of the structural model gained from this, using the powder diffraction data obtained from high molecular weight PEO complexes. This method proved successful in solving the crystal structures of $P(EO)_8$:$NaBPh_4$ and $P(EO)_4$:$ZnCl_2$, the latter the first polymer electrolyte structure elucidated that contains a divalent cation.

In summary, this thesis has further explored the area of crystalline polymer electrolytes and proved that these materials are viable candidates in the search for a suitable electrolyte for the all-solid-state lithium ion battery. It has offered compelling evidence that the structures of crystalline polymer electrolytes affect their conductivity. Also, crystallite size of crystalline polymer electrolytes can be correlated with the conductivity of these materials. Finally, it has added to the current structural knowledge of crystalline polymer electrolyte materials by presenting two new polymer electrolyte structures and a number of analogous glyme and glycol structures.